UCRL-19644

c.2

DIFFUSION STUDIES IN THE ALUMINA-SILICA SYSTEM

Robert Foster Davis
(Ph. D. Thesis)

July 1970

AEC Contract No. W-7405-eng-48

LAWRENCE RADIATION LABORATORY
UNIVERSITY of CALIFORNIA BERKELEY

UCRL-19644

c.2

DISCLAIMER

DIFFUSION STUDIES IN THE ALUMINA-SILICA SYSTEM

Contents

DIFFUSION STUDIES IN THE ALUMINA-SILICA SYSTEM

Robert Foster Davis

Inorganic Materials Research Division, Lawrence Radiation Laboratory,
and Department of Materials Science and Engineering,
College of Engineering, University of California,
Berkeley, California

ABSTRACT

July 1970

The diffusion kinetics and phase equilibria between silica and sapphire or mullite couples annealed in helium and air were investigated with particular emphasis placed on the relationships between atomistic mechanisms and structural changes. Dissolution occurred in the SiO_2-rich liquid accompanied by the formation of a detectable mullite solid solution (sapphire-silica couples) above 1634°C. The mullite liquid interfacial compositions formed a revised liquidus curve between the melting point of mullite and the mullite-silica eutectic. This curve was extended below the eutectic temperature due to the appearance of a metastable amorphous phase at the sapphire-cristobalite couple interface. The presence of a liquid phase is thought to be an initial step in the nucleation of mullite at the sapphire interface. The growth of mullite is dependent upon the relative dissolution rates of mullite in the liquid.

The diffusivities of the aluminum ion vary greatly with concentration and temperature. As a result, Q and D_o values are very high at low aluminum concentrations and decrease as Al_2O_3 is taken into the glass as shown by the following equations:

at 4.30 w/o Al_2O_3 $D = 3.47 \times 10^{23} \exp(-307.5 \text{ Kcal/RT})$

at 7.60 w/o Al_2O_3 $D = 1.64 \times 10^{19} \exp(-264.8 \text{ Kcal/RT})$

at 12.40 w/o Al_2O_3 $D = 9.93 \times 10^{12} \exp(-203.3 \text{ Kcal/RT})$

at 20.10 w/o Al_2O_3 $D = 3.38 \times 10^{2} \exp(-99.6 \text{ Kcal/RT})$

Aluminum coordination measurements and physical property data from the literature suggest that low Al_2O_3 concentrations are incorporated into the silica structure through the formation of "triclusters" composed of one AlO_4 and two SiO_4 groups. Higher concentrations of Al_2O_3 allows the formation of AlO_6 octahedra as well as normal AlO_4 tetrahedra; however, the AlO_6 octahedra do not form as readily with an increase in temperature.

The diffusion process in the liquid is thought to be a cooperative movement of large oxygen-containing aluminum and silicon complexes in a type of ring mechanism. The decrease in activation energy and viscosity suggests a gradual decrease in size of the diffusing unit with an increase in Al_2O_3 concentration at a given temperature and a change in size with an increase of temperature at a given concentration.

DIFFUSION STUDIES IN THE ALUMINA-SILICA SYSTEM

I. INTRODUCTION

The studies of ionic self-diffusion in glasses and the interdiffusion or dissolution processes which occur between refractory oxides and glasses have been receiving increased attention from many of the disciplines of physical science as shown by the reviews of Williams[1] and Doremus.[2] There are two primary reasons. First, a knowledge of these processes is necessary in order to understand the reactions that occur in these materials and, secondly, it is instructive in the determination of the mechanism by which the particular atoms or groups of atoms move at high temperature.

Paladino and Kingery[3] and Oishi and Kingery[4] have studied the self-diffusion of aluminum and oxygen, respectively, in Al_2O_3 while Sucov[5] has studied the movement of oxygen in vitreous SiO_2. A dearth of information exists, however, on interdiffusion in the Al_2O_3-SiO_2 system even though it is one of the most important and most studied binary systems in refractory technology. A phenomenological approach to this problem was undertaken by de Keyser[6] who studied reactions between polycrystalline alumina and cristobalite at 1600°C for two hours. He found that as a result of the diffusion of Al_2O_3 into the SiO_2, a glass phase formed surrounding the cristobalite grains. In comparison, the diffusion of a SiO_2-rich glass into the Al_2O_3 initiated the formation of mullite crystals which tended to grow along its C axis parallel to the direction of the diffusion of SiO_2.

Staley[7] has conducted a more enlightening study of the subsolidus reactions between these phases using pressed pellets or single crystals of the individual oxides in contact as well as mixed powders. His findings were similar to those of de Keyser.[6] No mullite was observed when the polycrystalline alumina pellet was replaced by an alumina single crystal. A kinetic analysis at 1500°C indicated that the dissolution of the corundum grains is primarily a diffusion process with an effective diffusion coefficient of approximately 2.5×10^{-13} cm^2/sec. The rate of dissolution of cristobalite, on the other hand, appeared to be controlled by the reaction at the cristobalite-glass interface leading to a constant phase boundary velocity of 1.6×10^{-9} cm/sec.

The purposes of this study were to determine definitely the nature of the dissolution of alumina by silica, to describe the kinetics of dissolution in technologically useful terms, and to relate the latter to possible operative mechanisms.

II. EXPERIMENTAL PROCEDURE

A. Materials and Sample Preparation

Several types of diffusion couples were prepared using alumina, silica, and mullite. Highly polished 11/32 in. dia. by 1/16 in. high single crystals of alumina (sapphire) cut with the C axis oriented approximately 30° from the vertical were purchased from the Union Carbide Corporation, Torrance, California. High purity air and water-free 3/8 in. diameter vitreous silica rod, sold under the trade name "Amersil," was obtained from the Englehard Company, San Francisco, California. The cristobalite phase was prepared by crystallization of fused silica rod by the Georgia Institute of Technology Experimental Station, Atlanta, Georgia. The mullite used in the diffusion studies (provided by the Carborundum Corporation, Niagara Falls, New York) was from the center of a much larger ingot cooled from the melt. A chemical analysis* revealed a molar composition of approximately 2 $Al_2O_3 \cdot SiO_2$ (77.3 wt % Al_2O_3) plus unreacted Al_2O_3.

Also, a 15 wt % Al_2O_3-85 wt % SiO_2 glass was prepared from powders of high purity -325 mesh Corning 7940 fused silica and Alcoa XA-16 reactive alumina. These were intimately mixed in isopropyl alcohol, dried at 110°C, and vacuum melted at 1800°C for thirty minutes in thin-walled molybdenum containers which could be separated from the glass. This glass was subsequently used in a diffusion couple with sapphire to determine the rate of growth of mullite and the rate of aluminum ion diffusion in the mullite.

---

* See Appendix I for the analysis of all diffusion couple materials.

The silica, mullite, and 15% alumina glass were cut into appropriate sizes, polished to optical smoothness, and checked for flatness against their diffusion couple counterpart. This last operation was performed to effect not only good bonding between the materials[8] composing the couple, but also to prohibit the entrapment of He or air in the irregular surfaces of the unpolished silica.

B. Diffusion Experiments

The materials to be used for the runs were washed in ethyl alcohol to remove any foreign matter, and placed into 13/32 in. dia. by 5/16 in. high spun molybdenum or Coors CN-2 99.8% alumina crucibles in the manner showns in Figs. 1 and 2.

The molybdenum crucibles were placed into the center of an 8 in. long by 4 in. diameter tantalum resistance heating element of a model 466S-4 Brew Furnace. The arrangement, as shown in Fig. 1, consisted of two layers of four crucibles each, covered by a molybdenum disk. The bottom four crucibles contained couples of sapphire and silica while the top section held three mullite-silica couples and one of the 15% Al_2O_3 glass-sapphire type. The total assembly was covered by a large 1-1/8 in. I.D. molybdenum crucible to equalize the heat distribution and to reduce the vaporization of SiO_2 during heating. This arrangement was modified for all temperatures below 1650° by placing the couples topped by 1000 gram platinum weights into 7/8 in. I.D. Al_2O_3 crucibles. In this case, only four samples could be run at one time.

The tantalum chamber was then heated to 1200°C under a pressure of 10^{-6} torr. This was found necessary to remove organic and reported[9,10] hydroxide films from the sapphire surface. The chamber was then isolated

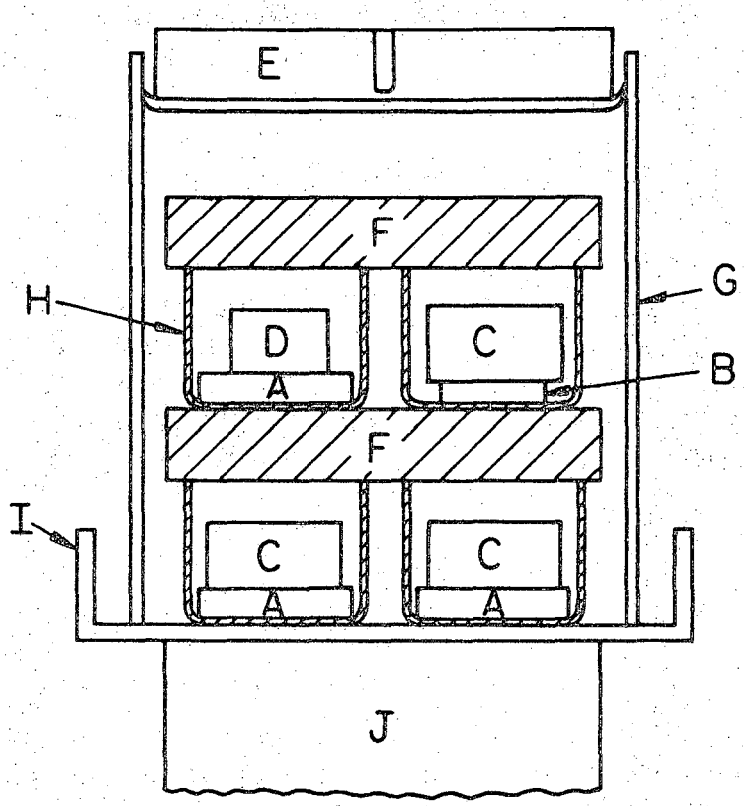

A - Sapphire
B - Mullite
C - Silica
D - 15% Al_2O_3 Glass
E - Black Body
F - Spacers
G - Sample Cover
H - Sample Container
I - Sample Holder
J - Support Stand

XBL 707-1404

Fig. 1. Schematic diagram of diffusion couple arrangement in helium. Parts E-J are of molybdenum.

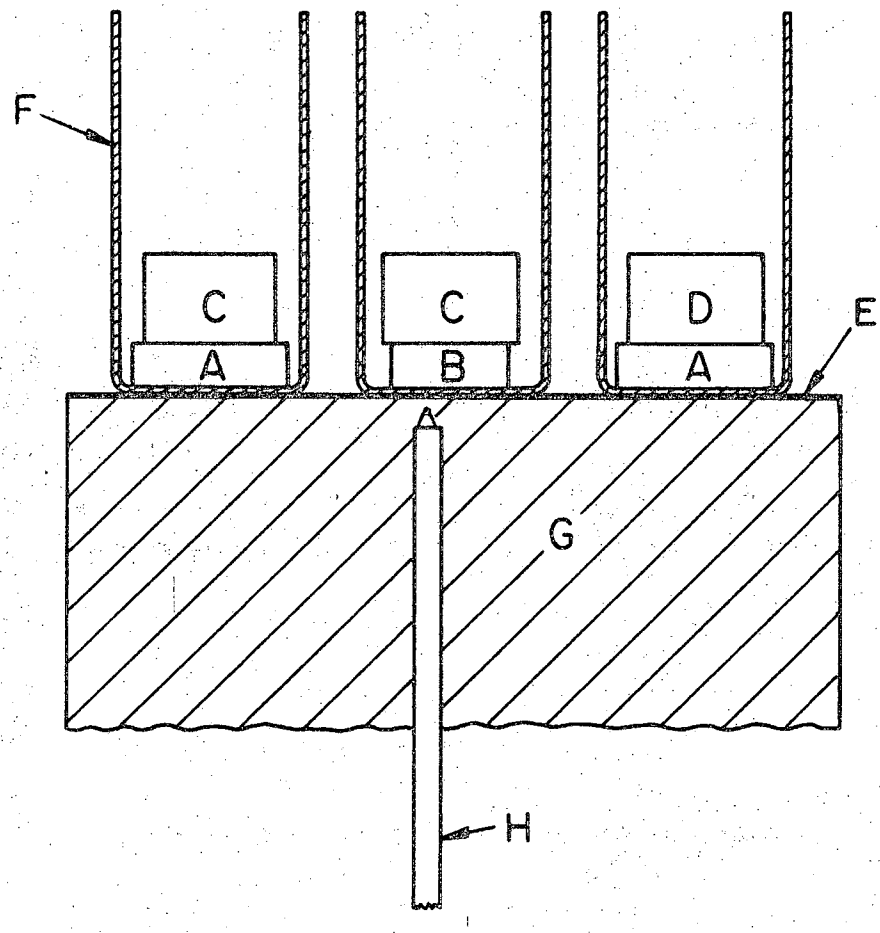

Code

A – Sapphire
B – Mullite
C – Silica
D – 15% Al_2O_3 Glass
E – Platinum Sheet
F – Al_2O_3 Crucible
G – Al_2O_3 Pedestal
H – Thermocouple Lead

XBL 707-1405

Fig. 2. Schematic diagram of diffusion couple arrangement in air.

and high purity He allowed to enter at a rate slow enough to permit the controller to hold the temperature constant. Having obtained atmospheric pressure within the furnace chamber, the temperature was rapidly (approximately 10 minutes) raised to the working point to avoid reaction at low temperatures and subsequent cracking of the sapphire at higher temperatures due to the difference in thermal expansion between it and the fused silica.

The principal temperature range of interest using the He atmosphere was 1650° to 1800°C in 50° intervals for times ranging from hours to days, depending on the temperature (see Table II, Section IV). Couples of sapphire-silica and mullite-silica were also run at subsolidus temperatures, as mentioned above, to determine the interfacial concentration of Al. The cristobalite-sapphire couples were fired at 1550° and 1580°C and the 15% Al_2O_3 glass-sapphire couples at 1650°, 1700°, and 1750°C.

The temperature of the He fired samples was measured by a W-5 Re/W-26 Re thermocouple (accuracy ± 7° at 1800°C) connected to a Leeds and Northrup Speedomax H Recorder-Controller and cross checked with a Leeds and Northrup optical pyrometer utilizing black-body conditions.

By comparison, the Al_2O_3 crucibles were placed in a Kanthal Super 33 element air atmosphere furnace preheated to a temperature of 1200°C. The specimens remained at this temperature for one hour, as before, and again were rapidly (approximately 45 minutes) heated to 1650°C--the only temperature comparable to the He runs that could be safely maintained for a long period of time with these elements. There were eight specimens in all containing the various couple types discussed in connection with the He runs. The temperature was measured by a Pt-6Rh/Pt-30Rh thermocouple

(accuracy ± 5° at 1650°C) and monitored by a Leeds and Northrup Speedomax H recorder.

A very slow (48-96 hours) and very carefully controlled cooling rate was employed for all runs in order to avoid the loss of integrity at the interface due to the difference in thermal expansion. The specimens were then removed from the furnace, mounted in polyester casting resin, sectioned in half parallel to the direction of diffusion, and remounted for polishing* in such a way that each mount contained two halves of two different specimens. This last procedure was both necessary and time saving in that it prevented faceting of the polished faces, and fewer mounts were required for the electron microprobe analysis.

C. Electron Microprobe

The highly polished surfaces of the specimens were made electrically conductive by the vapor deposition of carbon and by painting the mounting material and extremities of the diffusion couple with a slurry of carbon in ethanol.

A Materials Analysis Company Model 400 electron microprobe analyzer was used to determine the profiles of Al concentration versus distance. In this type of instrument, a monoenergetic beam of electrons is produced by a heated tungsten filament and focused onto the specimen. The resulting excitation of the electrons of the atoms in the material produces characteristic X-radiation which is monitored, reproduced as a number on logic circuit counters, and punched on IBM cards for computer data

---

* The polishing procedure consisted of 2 min each on a 240μ and 15μ metal bonded diamond lap, 24 hrs on 6μ diamond lap, 24 hrs on 1μ diamond lap, and 6 hrs in a syntron vibrated, Linde A (0.3μ Al_2O_3)-water slurry.

correction and evaluation.

All data from the various diffusion couples discussed previously was measured at an electron beam potential of 15 KV and a sample current of .025μ amps. in order that they could be compared. Two spectrometers operated in vacuum with incorporated Rowland Circle optics of 5.6 in. radius and equipped with KAP (potassium acid phthalate) curved crystals bent and ground in the Johansson mode were used to view the specimen simultaneously. Detectors were of the sealed flow proportional type containing 93% argon and 7% methane and utilizing 2500 Å polypropylene windows. In normal use the beam diameter is 1μ; however, the resolution for light elements may be 3-5μ.[11]

Crystallization of mullite occurred in the glass on cooling at temperatures above 1650°C. As a result, the measured diffusion profile perpendicular to the interface was very irregular in shape (Fig. 3a) and, thus, difficult to measure quantitatively. To overcome this difficulty, the point beam was tuned so that it very rapidly scanned a line 100μ long in a direction parallel to the interface of the couple. After ten seconds of counting, the data was recorded as discussed above, and the scanning beam moved toward the interface in 1μ steps. This averaging procedure greatly enhanced the smoothness and, thus, the interpretation of the diffusion profile as seen in Fig. 3b. It should be noted that while the measured X-ray intensity decreases as the beam deviates from the center position (see Fig. 4), it does not cause inaccuracies in the concentration data since the Al_2O_3 and SiO_2 standards are measured in the same manner.

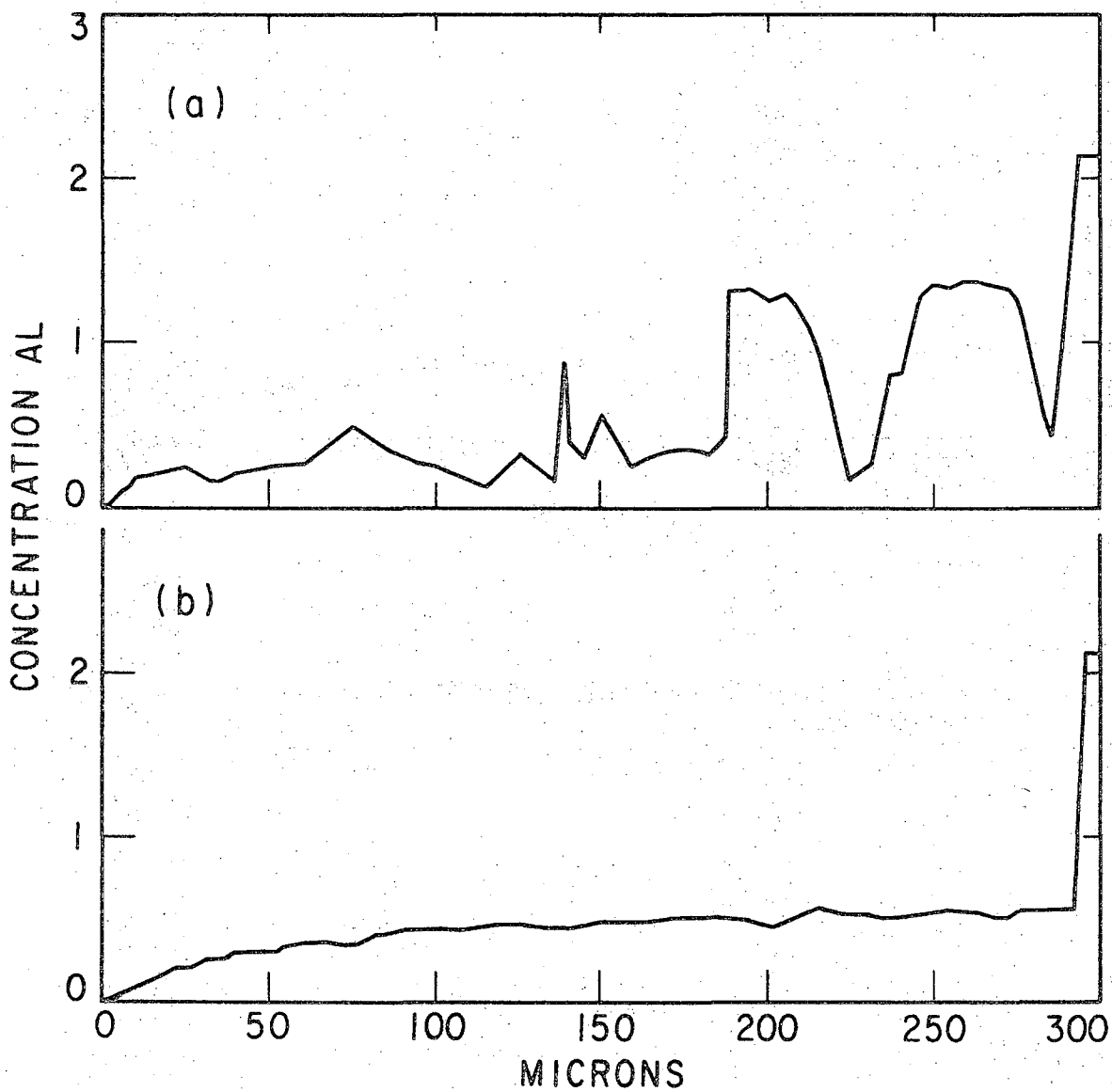

Fig. 3. Concentration Al versus distance diffusion profile at 1800°C for (a) point beam analysis (b) scanning beam analysis.

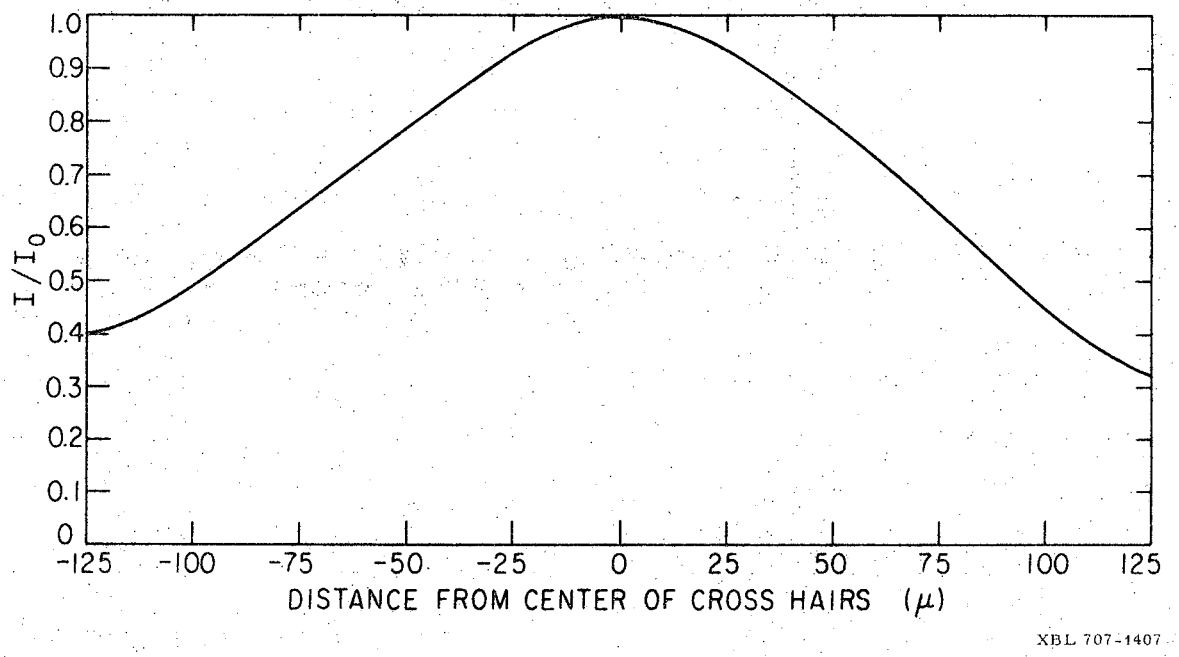

Fig. 4. Drop of intensity of X-radiation with deviation of electron beam from center of microprobe cross hairs.

D. Computer Analysis and Density Measurements

Frazier, et al.[12] have written computer programs which correct the raw microprobe data for dead time, drift, background, absorption, and fluorescence and record the composition of each data point in weight per cent of the elements or their oxides.

Diffusion equations are, however, formulated in terms of concentration (i.e. grams/cubic centimeter) and not weight or mole per cent. If there is a significant change in the density of the solvent with the introduction of the solute atoms, as is the case when Al_2O_3 diffuses into SiO_2, this change must be accounted for in the calculation of the diffusion coefficient.

Density determinations were made on glasses containing 5-40 wt % Al_2O_3 in 5% intervals. Higher Al_2O_3 contents resulted in extensive crystallization of the cooled melt. The preparation and vacuum firing of the samples followed the procedure outlined in part A for the 15% Al_2O_3· 85% SiO_2 glass. All specimens were quenched by turning off the power to the furnace and allowing He to flow rapidly through the furnace when the temperature dropped to 1500°C. The glasses were cooled to 500°C within three minutes. Regions along the edges showing crystallization, heterogeneously nucleated by the walls of the container, were removed in order to obtain the true density of the glasses. The composition of Al_2O_3 in the glass was checked by microprobe analysis and found to be within 1 wt % of the starting value.

The densities were determined using the displacement technique. Two hundred proof ethyl alcohol was selected as the displacement medium, and an account was made for the change in its density with a change in room

temperature. The measurements are given in Table I.

Table I. Measured density value of aluminosilicate glasses having 0-40 wt% Al_2O_3.

Wt% Al_2O_3	Density (g/cc)
0	2.207
5	2.234
10	2.297
15	2.326
20	2.340
25	2.381
30	2.443
35	2.474
40	2.535

The resulting graph of density versus wt% Al_2O_3, determined from a least squares fit of the measured values, is shown in Fig. 5 and compared with a curve calculated from the theoretical data of Huggins and Sun[13] for quickly cooled glass of the same composition. The deviation of the measured data from theory is thought to be caused by the formation of two immiscible glasses: one rich in Al_2O_3 and the other in SiO_2. This microphase glass-in-glass separation and the resulting tendency for crystallization tightens the structure of the glass and therefore increases the density beyond that calculated from theory based on a perfectly random structure. A check of the literature for this system revealed only one density value of 2.359 g/cm for a 23 wt % Al_2O_3 glass;[14]

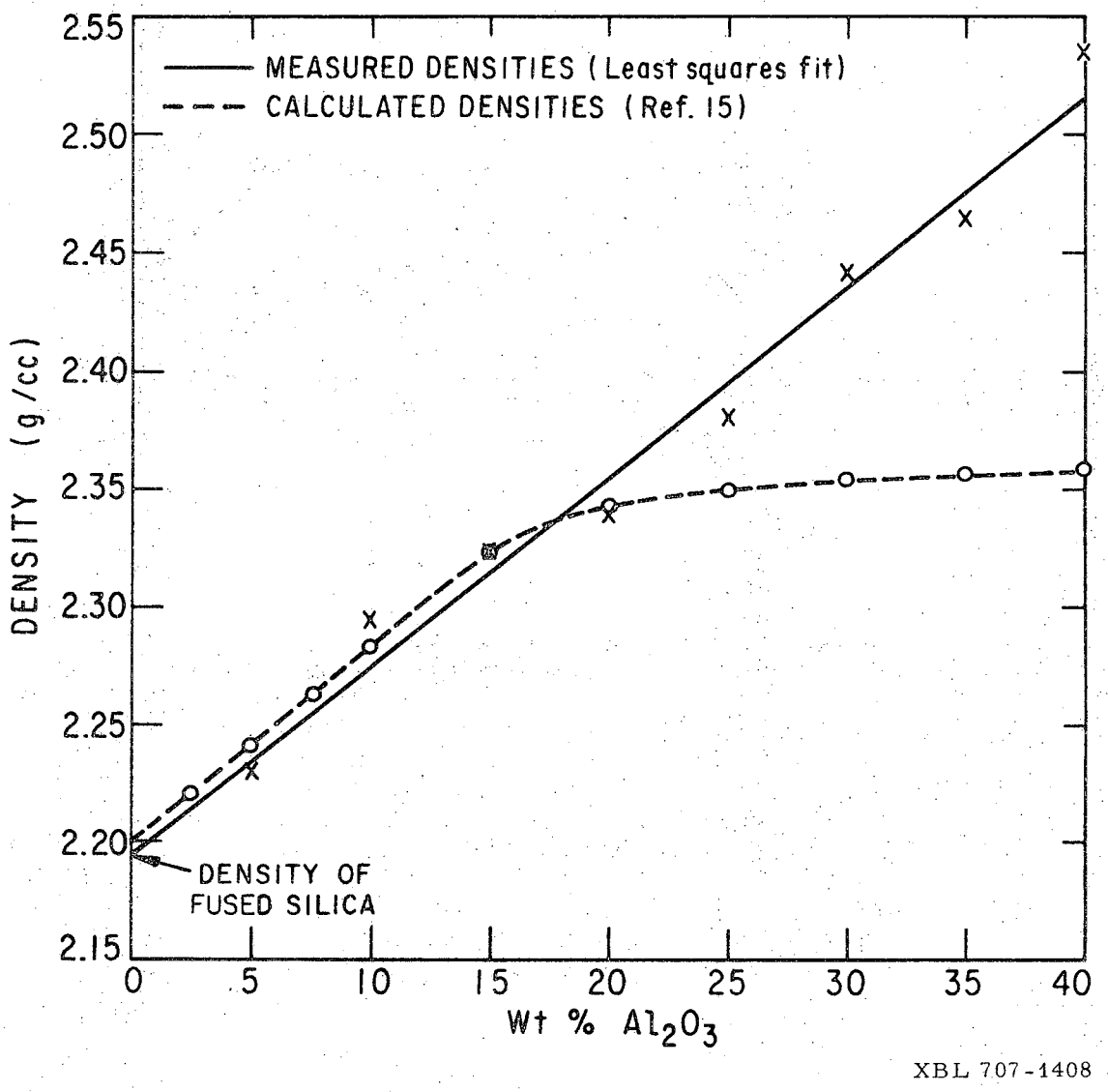

Fig. 5. Comparison of measured and theoretically calculated densities for aluminosilicate glasses.

a value between the two curves.

The equation for the data of Fig. 5 is quite adequate for the determination of the concentration of Al_2O_3 in the glass in these studies since the maximum composition at the highest temperature of 1800°C is 42.2 wt%. At the interface, however, the diffusion profiles go quickly through a range of wt % Al_2O_3 values until they reach the value for mullite or sapphire depending on the type of diffusion couple examined.

In order for the computer to determine the concentration of Al_2O_3 throughout the complete range of wt % Al_2O_3 values and to produce a continuous curve of concentration versus distance, "IF" statements are used to guide the computer to the correct density equation for the Al_2O_3 content for that data point. The calculated density is then multiplied by the corresponding wt % Al_2O_3 to obtain a value of Al_2O_3 concentration (grams/cm^3). Since above 40 wt % Al_2O_3, only the densities of the mullite solid solution and sapphire are known, hypothetical density curves must be drawn from the measured curve to mullite and from mullite to Al_2O_3(Fig. 6). The short horizontal curve represents the solid solution range of mullite. This is not to imply that these curves are the actual densities of the glasses at these Al_2O_3 compositions since the density of a mullite or alumina glass would obviously be lower than its crystalline modification. This inaccuracy, is, however, not critical since these compositions are not actually found in the diffusion profile. The equations for these curves serve only to smooth the portion of the concentration versus distance profiles from the interfacial composition to that of the oxide component of the diffusion couple.

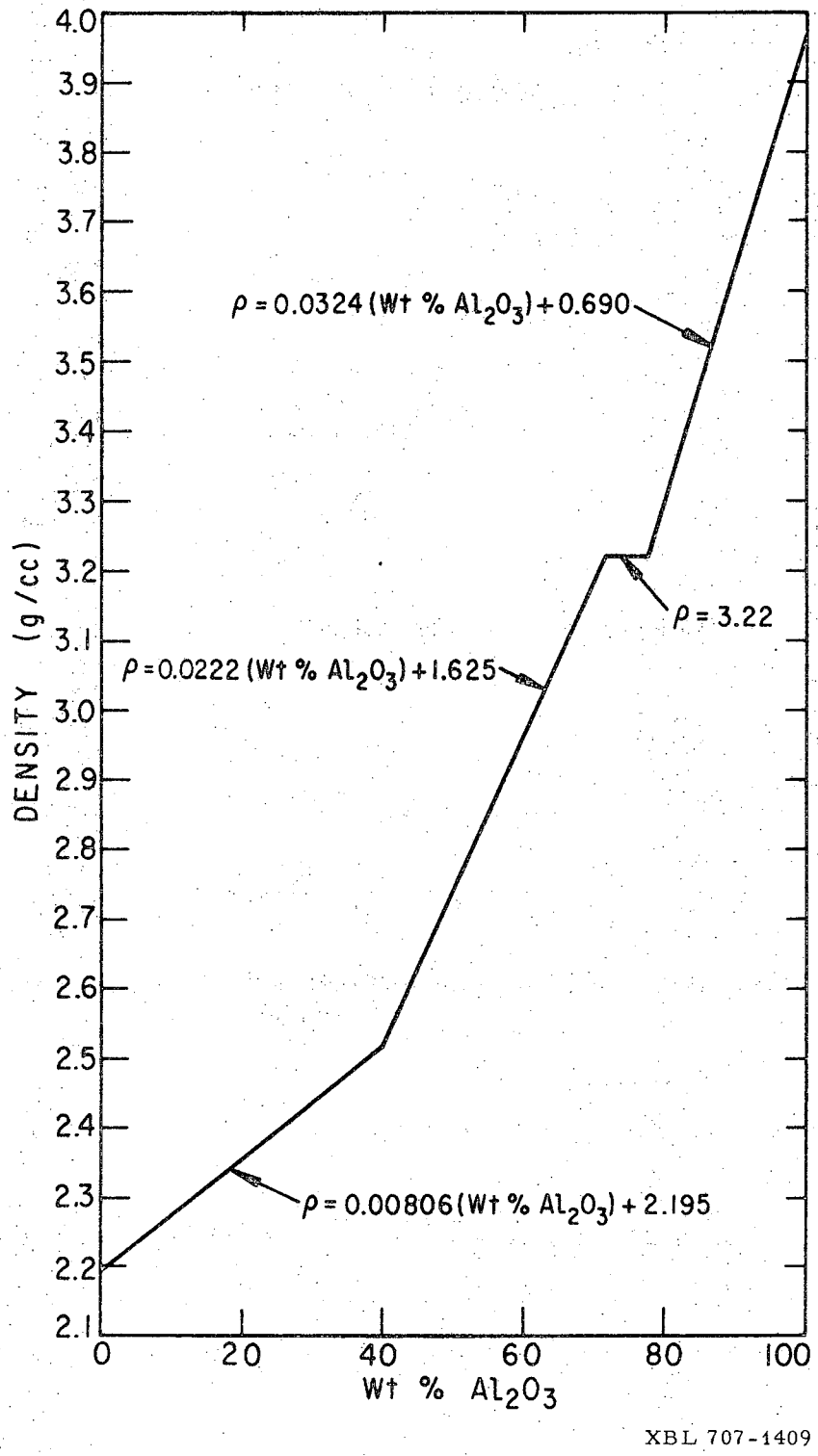

Fig. 6. Measured and hypothetical density curves from fused silica to sapphire.

Additional programs were written and incorporated into those of Frazier, et al.[12] which carried out the above calculations, determined the Al atom concentration from that of Al_2O_3, and plotted the concentration of Al versus distance profiles on graph paper.

E. Coordination Number of Al in Glass

The wavelength of the characteristic X-radiation emitted by certain elements depends to an extent upon the valence state of the element.[15] For certain elements of low atomic number, the wavelength of the characteristic X-radiation is also influenced by the coordination number of the site occupied by the element. In K-emission X-ray spectroscopy of light elements in the third period, the ejection of an inner K-electron triggers a spectrum of Kα and Kβ lines (and bands) generated by L→K and M→K electronic transitions, respectively. The discovery by White, et al.[16] that the Kα emission wave length of aluminum is affected significantly when the coordination number changes from four to six, paved the way for determination of the coordination number of this ion in disordered clay minerals by Brindley and McKinstry[17] and in sodium aluminosilicate glasses by Day and Rindone[18] using X-ray fluorescence techniques.

More recently Dodd and Glen[19] have adapted an electron microprobe into a versatile X-ray spectrometer and measured the complete Kα and Kβ emission spectra for Mg, Al, and Si as elements and as selected six-fold and four-fold coordinated crystalline oxides. This technique was adopted for the measurement of Al coordination number in the 5-40 wt % aluminosilicate glasses.

The sample preparation was similar to that for the 15 wt % Al_2O_3 glass described in section A above. As for the microprobe, a small strip-chart

recorder motor with a speed of .05 rpm was attached to the spectrometer adjustment wheel to effect a very slow (.005 Å/min) movement of the KAP crystal through a range of wavelength values which included the wavelengths for the different aluminum coordinations. The beam diameter was 1μ and the spectrometer slit .005 in. The counter was connected to a Honeywell Electronik 17 strip chart recorder, having a speed of 5 small divisions per minute, which reproduced the change in X-ray intensity monitored by the detectors as the crystal moved through the wavelength range for that particular coordination. Sample current was adjusted so as to produce similar peak heights for all Al_2O_3 compositions. The electron beam potential was 15 KV and 20 KV for Kα and Kβ studies, respectfully.

The procedure for measuring the peak position of the Al Kα and Al Kβ radiation was similar to that of Day and Rindone.[18] This method consists of measuring the peak positions at half the total height for aluminum metal and the relative displacement of this position for the aluminosilicate glasses. The displacement of the Kα and Kβ peaks from the aluminum metal position for aluminum ions in four fold and six fold coordination was determined by using $AlPO_4$ and Al_2O_3, respectively, as standards.

Since the changes in Kα and Kβ wavelengths with coordination number of aluminum are small, certain precautions must be observed. The room temperature was held to within ± 1°F during all measurements. The microprobe was allowed to stabilize for twelve hours before measurements were made. All peaks were scanned three times for each sample and the average of these values was taken to be the position of the peak. Using this technique, the peak position could be determined to within ± 0.0004 Å.

The results and conclusions drawn from these experiments are given in Section IV.

III. MATHEMATICAL ANALYSIS

A. General

Diffusion is a process by which chemical units distribute themselves in order to establish and maintain homogeneity or chemical equilibrium in a system. For a single phase at constant temperature and pressure, diffusion occurs in a direction that decreases the activity gradient. The quantity of material that diffuses past a unit area normal to the diffusion direction in unit time is proportional to the activity gradient. Because it is difficult to determine the activity gradient accurately in various diffusion experiments, concentration gradients are usually used in the diffusion equations. Fick's first law for a binary one-dimensional case states that the driving force for the diffusion process is the chemical concentration gradient.

$$J_i = -\left(D \frac{\partial C_i}{\partial X}\right) \tag{1}$$

The change of concentration of the diffusing substance with time is given by Fick's second law:

$$\frac{\partial C_i}{\partial t} = D \frac{\partial^2 C_i}{\partial X^2} \tag{2}$$

where J = flux of species i passing a plane of unit area in unit time, C_i = concentration of species i per unit volume, X = distance in the diffusion direction, t = time, and D = the diffusion coefficient or diffusivity.

If there is no net mass transfer, $D = D_i^*$, which is the self-diffusion coefficient of i; when mass transfer is involved, $D = \tilde{D}$, a chemical interdiffusion coefficient. Numerous texts are available which discuss diffusion theory in detail and give solutions to the differential equations for specific initial and boundary conditions.[20,21,22]

Fick's equations as written require that D be independent of concentration. This assumption greatly simplifies the solution of the differential equation; it is, however, rarely found in actual practice over more than a limited composition range.

The data of this study are treated in two ways. For the profiles of the aluminum ion diffusion in silica glass, the concentration dependence of the interdiffusivities is determined by the Boltzmann-Matano method. For the diffusion of the aluminum ion through the mullite layer formed in the 15% Al_2O_3 glass-sapphire couples, the diffusivity is assumed constant and determined from an analysis derived by Wagner[23] and presented in Jost.[20]

B. Concentration Dependent Diffusion in the Liquid Phase

The extent of the growth of the mullite solid solution in the sapphire-silica couples is very small and does not exist in the mullite-silica samples. Dissolution of Al_2O_3 or mullite occurs in the silica-rich liquid phase. Chemical diffusivity of Al in SiO_2 is analyzed by the following method.

In the more general case where D (subsequently referred to as $\tilde{D}$) is a function of the concentration of the diffusing species, Fick's second law becomes

$$\frac{\partial C_i}{\partial t} = \frac{\partial}{\partial X}\left(\tilde{D}\ \frac{\partial C_i}{\partial X}\right) \tag{3}$$

for the one-dimensional case. Rigorous solutions of this equation are not usually available; therefore, graphical solutions are used to obtain numerical values of $\tilde{D}$. Boltzman[24] has shown that if the initial conditions can be described in terms of one variable $\eta = X/t^{1/2}$, C_i is a function of η only, and Eq. (3) can be transformed into an ordinary homogeneous differential equation

$$-\frac{\eta}{2}\ \frac{dC}{d\eta} = \frac{d}{d\eta}\left(\tilde{D}\ \frac{dC}{d\eta}\right). \tag{4}$$

This transformation coupled with the procedures outlined below was first used to determine $\tilde{D}$ (c) experimentally by Matano.[25]

If two infinite media are brought together at t = o, the diffusion coefficient and its concentration dependence may be deduced from the concentration vs penetration curves observed at some known time. This type of diffusion couple can be described by the following initial conditions:

$$C = C_A \text{ for } X < 0, \text{ at } t = 0$$

$$C = 0 \text{ for } X > 0, \text{ at } t = 0$$

where C is the concentration of the component of interest, and X = 0 is the position of the original interface of the two components at t = 0. Integration of Eq. (4) with respect to η results in

$$-\frac{1}{2}\int_{c=0}^{C=C_i} \eta dC = \left[\tilde{D}\frac{dC}{d\eta}\right]_{C=0}^{C=C_i} \qquad (5)$$

where C_i = any concentration along the profile. The known data for C(X) are obtained at some fixed time so that substituting for η and realizing that at C=0, dC/dX=0, one obtains

$$-\frac{1}{2}\int_{C=0}^{C=C_i} XdC = dt\left[\frac{dC}{d\eta}\right]_{C=0}^{C=C_i} = \tilde{D}t\left(\frac{dC}{dX}\right)_{C=C_i} \qquad (6)$$

Rearranging Eq. (6), $\tilde{D}(C_i)$ can be found from the graphical integration and differentiation of C(X) using the equation

$$\tilde{D}_{C=C_i} = -\frac{1}{2t}\left(\frac{dX}{dC}\right)_{C_i}\int_0^{C_i} XdC \; . \qquad (7)$$

Figure 7 shows the quantities needed and the slopes and areas involved in the solution Eq. (7).

C. Concentration Independent Diffusion in the Mullite Phase

$\tilde{D}$ in mullite that is growing in a system in which no dissolution in the reacting phases occurs, can be determined in the following manner. The Al_2O_3 concentration range in the mullite solid solution layer is very small (2.5 wt %) and, thus, the diffusivity can be assumed to be constant across this phase. Figure 8 is a schematic representation for the difusion profile in the compound. The concentration designations C_A, C_S, $C_{II,I}$, and Co are the concentrations of the diffusing species in (1) phase III (Al_2O_3), (2) the upper and lower limits of the solid solution phase

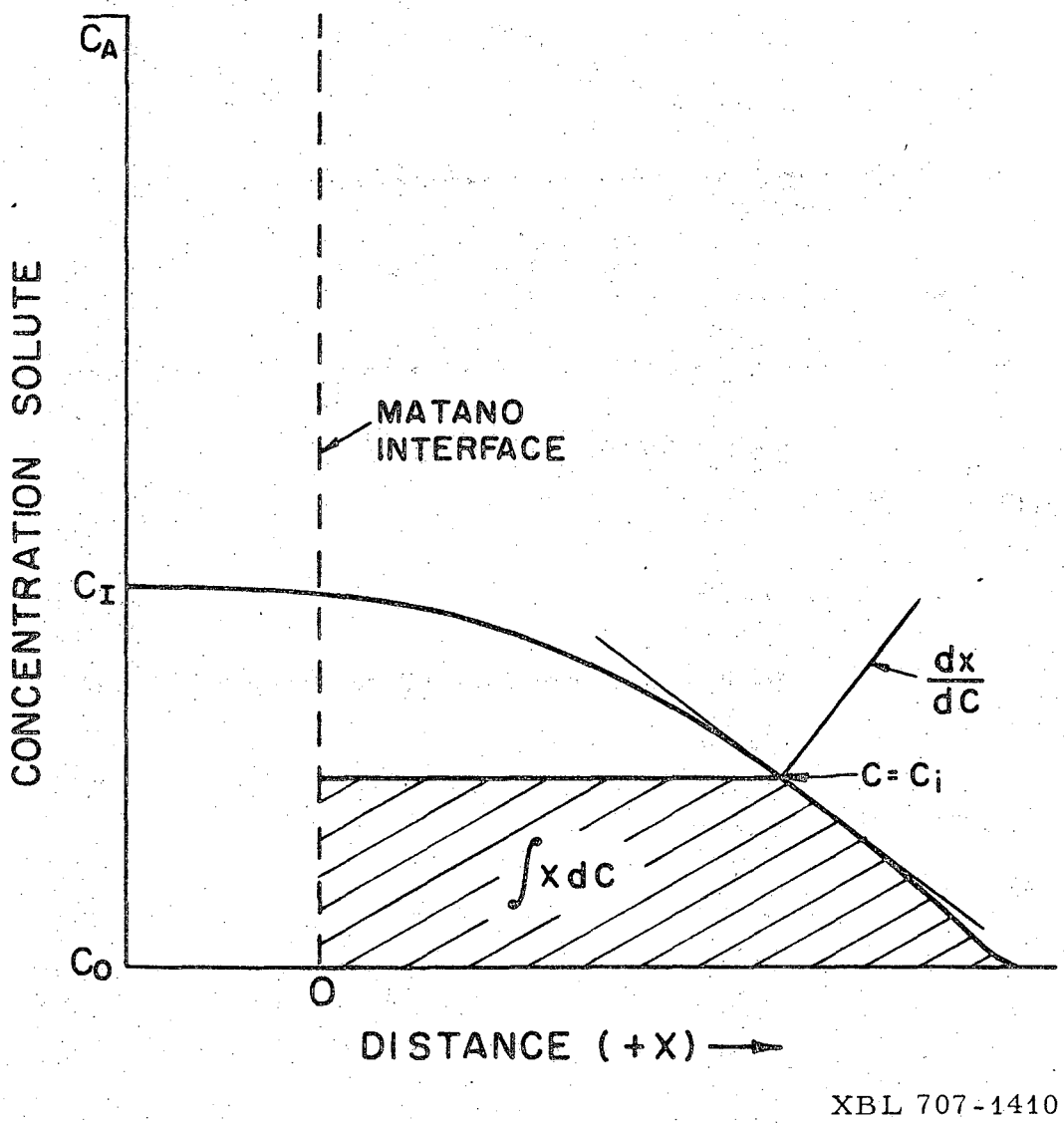

Fig. 7. Diagram for Boltzmann-Matano solution.

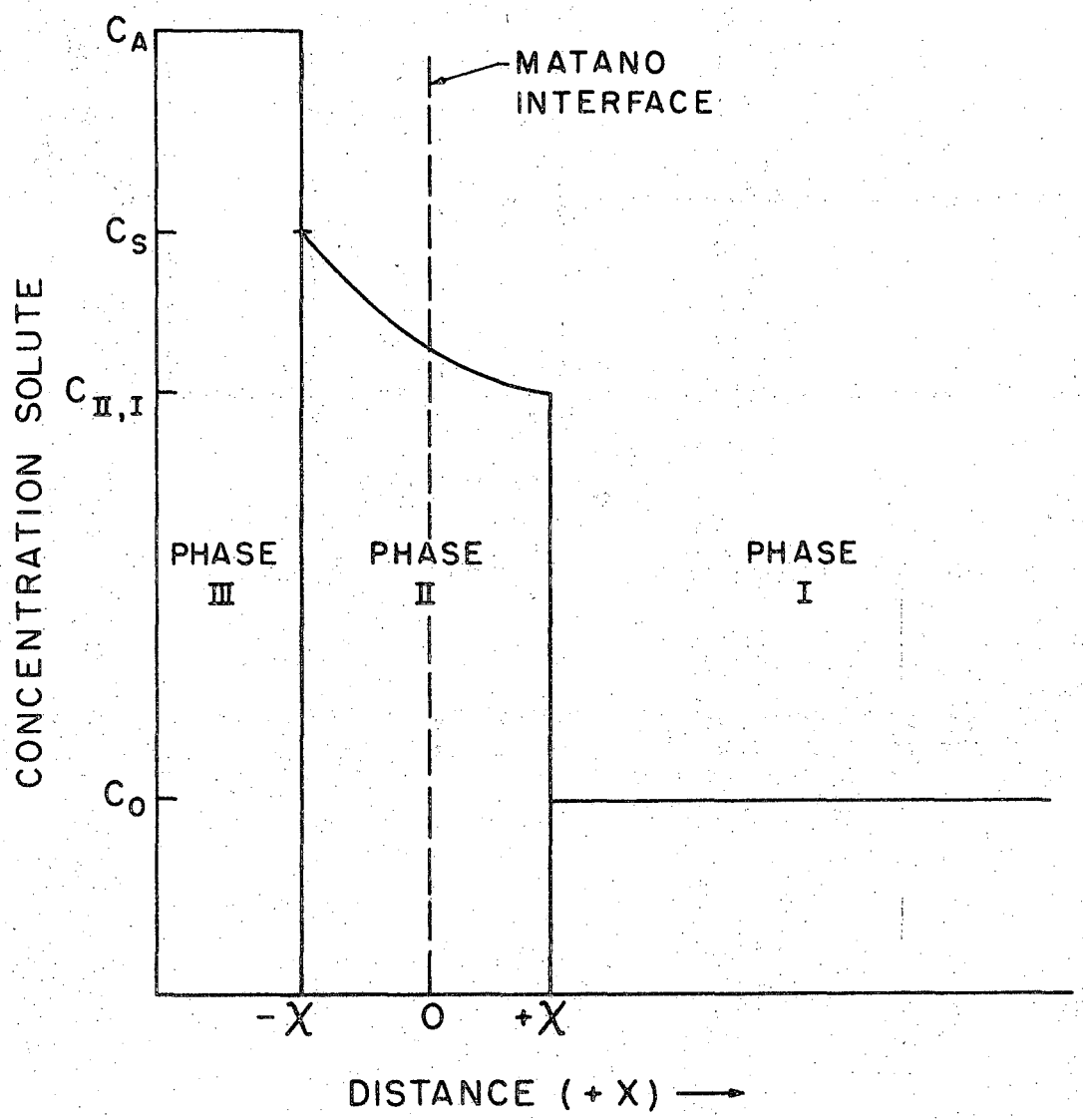

XBL 707-1568

Fig. 8. Schematic diagram of concentration vs. distance profile for the growth of a new phase (II) in a phase saturated with solute (I).

(mullite), and (3) Phase I (the saturated glass), respectively. As diffusion proceeds in phase II, reactions will continue to occur at each interface in order to maintain equilibrium compositions and thus growth of the phase. At time t, the region of this phase will extend from $x = -\chi$ to $x = +\chi$. The system, as shown, is considered to be one of constant volume; and, therefore, the position of the original interface (X=0) does not move with respect to a fixed point in either phase.

The diffusion process will be governed by Eq. (2) where a concentration independent diffusion coefficient has been assumed. The concentrations at the interfaces are assumed constant and equal to the equilibrium values.

While the interface between phase I and phase II is displaced by $d\chi$ in time dt, the amount $[C_{II,I} - Co]\, d\chi$ of diffusing substance must be supplied per unit area from the region $X < +\chi$, thus

$$[C_{II,I} - Co]\, d\chi = - \tilde{D} \left(\frac{\partial C}{\partial X}\right) dt \qquad (8)$$

A particular integral of Eq. (2) is

$$C = C_s - B \operatorname{erf} \left[\left(\frac{X}{2\sqrt{\tilde{D}t}}\right)\right] \text{ , for } -\chi < X < +\chi. \qquad (9)$$

Wagner[23] has assumed that the planes of discontinuity at $+\chi$ and $-\chi$ are shifted proportionally with $\sqrt{t}$; therefore

$$\chi - (-\chi) = 2\gamma\sqrt{\tilde{D}t} \qquad (10)$$

where γ is a dimensionless parameter. Knowing that at $X = +\chi$, $C=C_{II,I}$, and substituting Eqs. (9) and (1) into Eq. (8), one obtains

$$C_s - C_{II,I} = B \text{ erf } (\gamma) \tag{11a}$$

and

$$C_{II,I} - Co = \frac{B}{\sqrt{\pi\gamma}} \exp (-\gamma^2). \tag{11b}$$

By eliminating B, one obtains

$$\frac{C_s - C_{II,I}}{C_{II,I} - Co} = \sqrt{\pi}\, \gamma e^{\gamma^2} \text{ erf } (\gamma) \equiv F(\gamma). \tag{12}$$

The constant, γ, may be determined for a given system from a plot of $F(\gamma)$ versus γ as shown in Fig. 9. $\tilde{D}$ may now be determined from the observed displacement of $\chi - (-\chi)$ by means of Eq. (10) which gives

$$\tilde{D} = \frac{[\chi - (-\chi)]^2}{4\gamma^2 t} . \tag{13}$$

D. Temperature Dependence of Diffusivity

The diffusivity is a function of temperature as well as concentration. The nature of this temperature dependence is given by the equation

$$D = D_o \exp (- Q/RT) \tag{14}$$

where D_o is a constant incorporating the mean free path of atomic movement, the lattice vibration frequency and the entropy of activation exp $(\Delta S/R)$. The energy of activation, Q, and the pre-exponential term, Do,

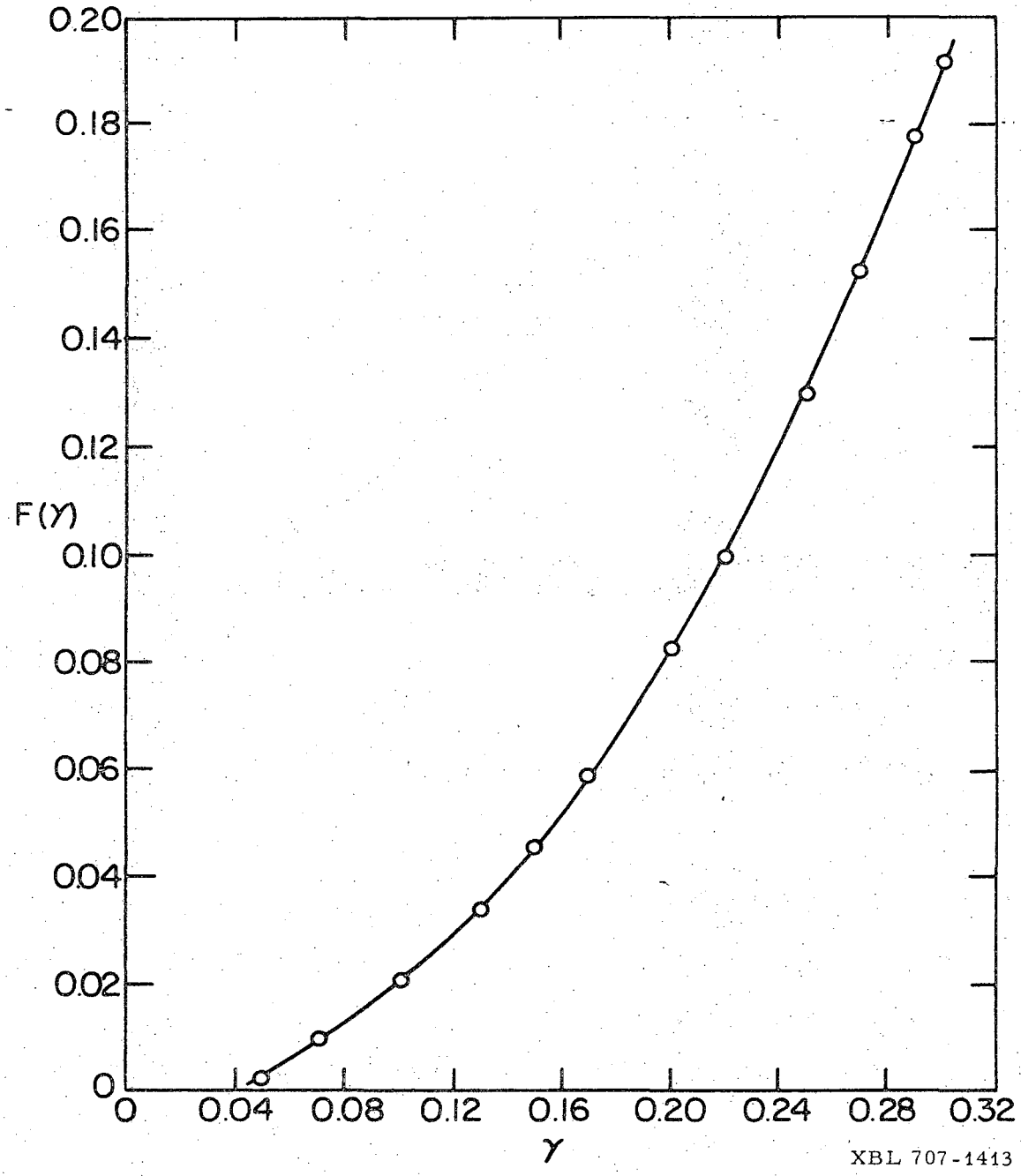

Fig. 9. Curve of F (γ) vs. γ where F (γ) = $\sqrt{\pi}\gamma e^{\gamma^2}$ erf (γ).

may be found by rearranging (11) to

$$\ln D = \ln Do - \frac{Q}{R}\left(\frac{1}{T}\right) \tag{15}$$

or

$$\log_{10} D = \log_{10} D_o - \frac{Q}{2.303R}\left(\frac{1}{T}\right) \tag{16}$$

and subsequently plotting $\log_{10}$ (or ln) D versus 1/T. From the slope and intercept of the curve, these quantities may be determined.

IV. RESULTS AND DISCUSSION

A. Diffusion Profiles and Phase Equilibria

The experimental conditions and data obtained from these experiments necessary for calculations of diffusivities in the liquid phase are presented in Table II. The silica was found to be insoluble in the sapphire at the temperatures employed. The diffusion profiles for each of the couples were plotted by the computer as concentration of aluminum ion versus distance. The choice of this parameter was made in lieu of the concentration of Al_2O_3 or other Al-O species due to a lack of knowledge of the actual diffusing species. A discussion of the possible species and mechanisms involved in the diffusion process will be presented later in this section. Figure 10 has been included as a reference graph for the conversion of aluminum ion concentration into the concentration of Al_2O_3 in terms of grams per cubic centimeter, weight percent, or mole percent.

Typical plots of concentration versus distance profiles are exemplified by those for sapphire-silica couples shown in Figs. 11 and 12 which were obtained at 1800° and 1650°C in an He atmosphere. These two curves are for the extremes of temperature for which diffusion coefficients were calculated and demonstrate the progressive flattening of the profiles with a decrease in temperature. Mullite was found by means of optical microscopy to develop at the alumina-silica interface in measurable amounts at test temperatures of 1650° to 1750°C. It was not possible to determine the amount of mullite at 1800°C because of the relatively short annealing time and the considerable crystallization on cooling. Its detection was also hindered at the interface by the

Table II. Experimental conditions and data for diffusion runs

Sample Designation	Temp. (°C)	Time (Sec. X10^{-3})	Interface Conc. C_I - (g/cc Al)	Interface Conc. C_I - (wt% Al_2O_3)
900 H	1400	1209.6	.1071	9.2
206†	1550	1209.6	.0863	7.2
210†	1550	1382.4		
205†	1580	691.2	.0891	7.4
209†	1580	1209.6		
026 H	1650	604.8	.112	9.3
126 H*	1650	604.8		
526 A	1650	604.8		
626 A*	1650	604.8		
027 H	1650	777.6		
127 H*	1650	777.6		
527 A	1650	777.6		
627 A*	1650	777.6		
028 H	1650	950.4		
128 H*	1650	950.4		
528 H	1650	950.4		
628 H*	1650	950.4		
029 H	1700	345.6	.155	12.9
030 H	1700	604.8		
031 H	1700	777.6		
032 H	1700	950.4		
033 H	1750	172.8	.285	22.8
034 H	1750	259.2		
035 H	1750	345.6		
039 H	1800	14.4	.572	42.2
040 H	1800	21.6		
041 H	1800	28.8		

* - Mullite-fused SiO_2 couples
† - Cristobalite-sapphire couples
All others - sapphire-fused silica couples

H - Helium
A - Argon

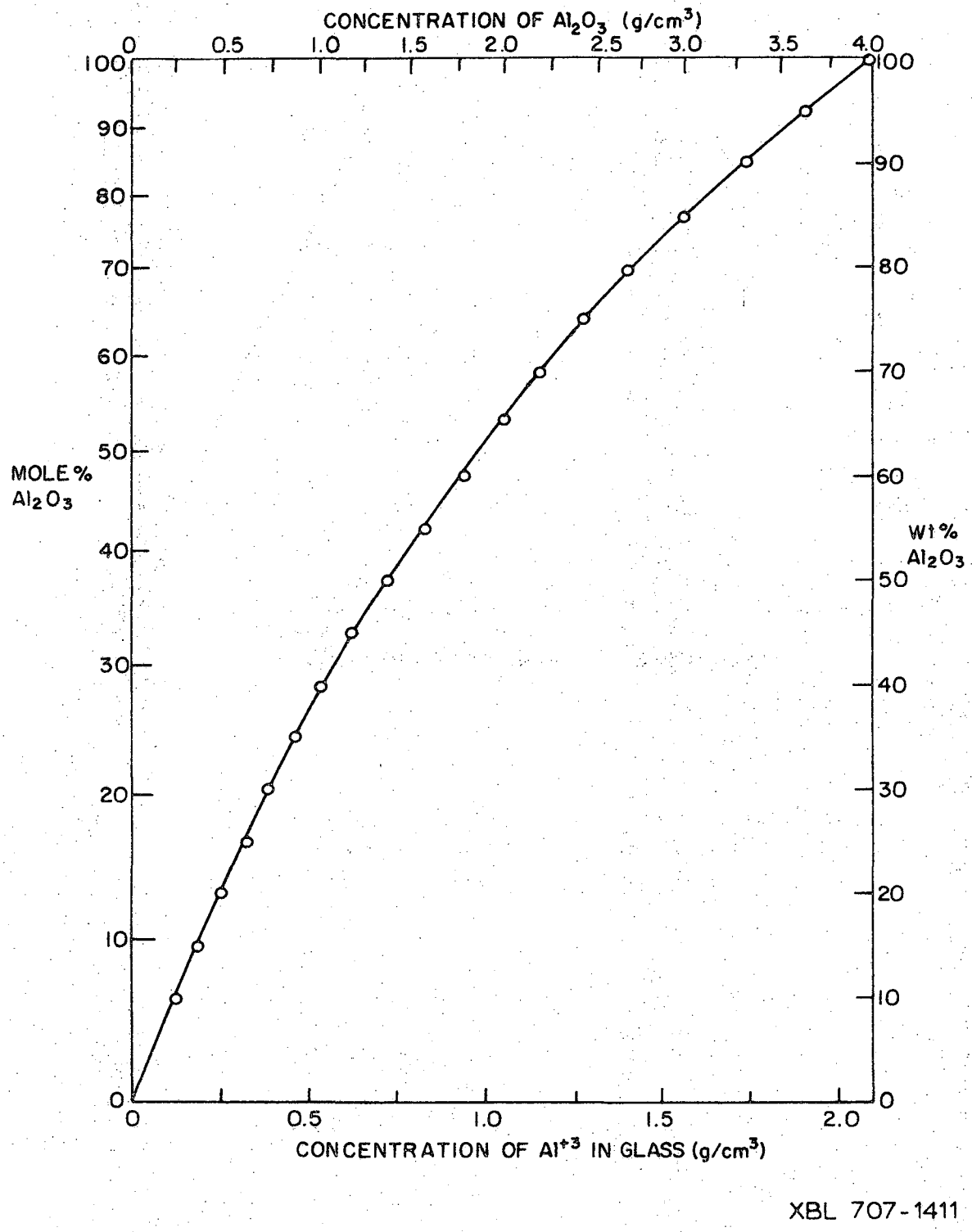

Fig. 10. Reference graph relating concentration of aluminum ion to concentration of Al_2O_3 in terms of grams/cc, weight, and mole percent.

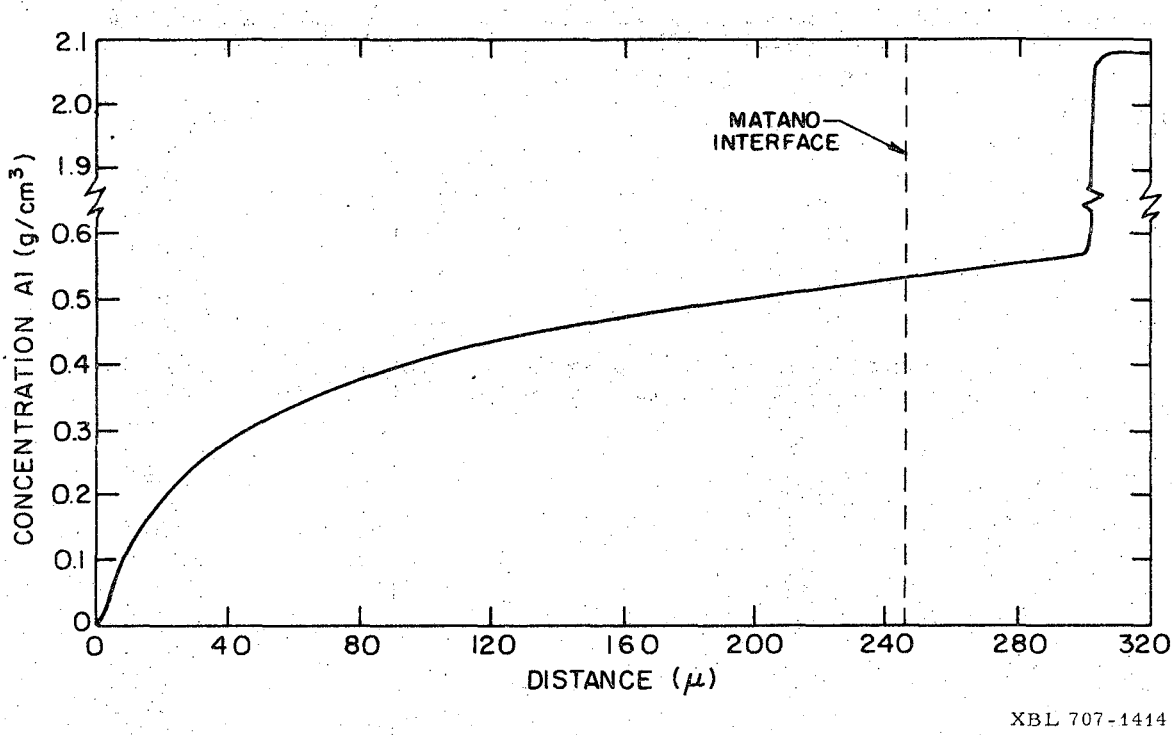

Fig. 11. Concentration of aluminum ion vs. distance determined at 1800°C for Al_2O_3-SiO_2 couple fired in He for 4 hours.

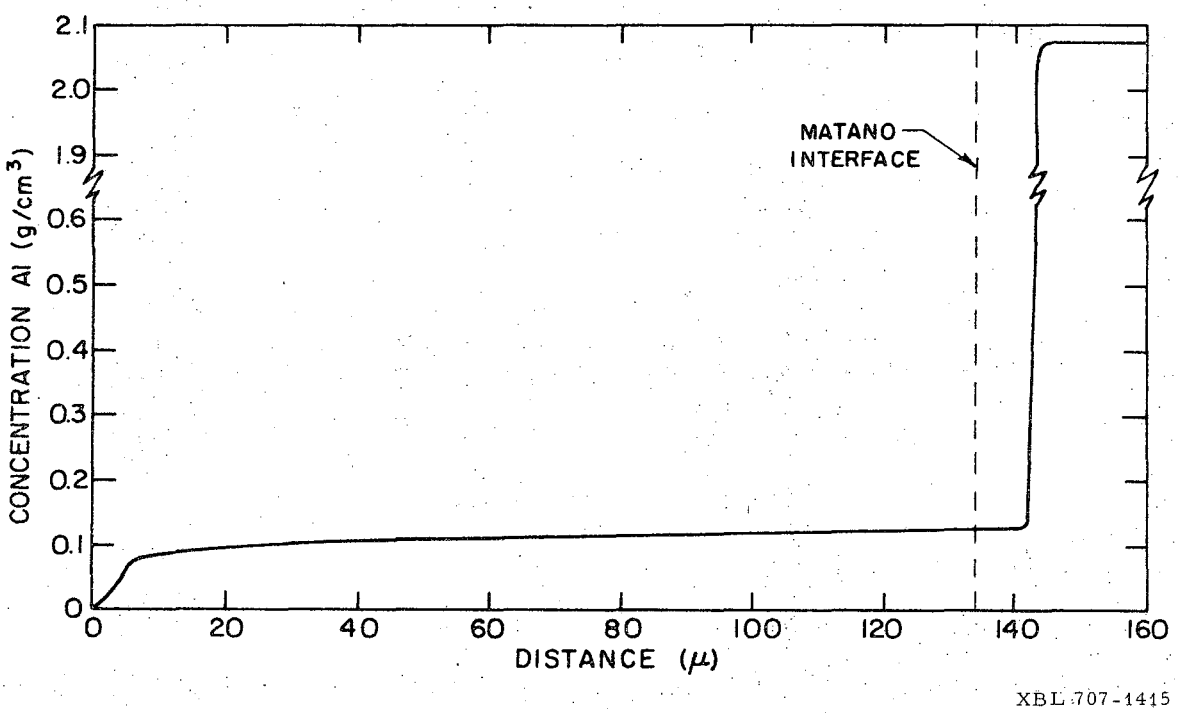

Fig. 12. Concentration of aluminum ion vs. distance determined at 1650°C for Al_2O_3-SiO_2 couple fired in He for 11 days.

aforementioned low resolution of the microprobe for light elements. The concentration of aluminum at the final interface and the general shape of the diffusion profile of the alumina-silica couples remained constant with increasing heating times for each temperature indicating that diffusion in the liquid and not the entry of the Al_2O_3 (i.e., the dissolution of mullite) into the liquid was the rate controlling step.

The profiles for the sapphire-fused silica couples annealed at 1650°C for different lengths of time matched those obtained under equivalent conditions for mullite-fused silica and sapphire-cristobalite couples, suggesting that the interfacial and diffusion conditions were similar. Heating similar couples in air at 1650°C produced essentially identical curves and interfacial compositions as those obtained in He, implying no effect from atmosphere on diffusion.

Mullite-silica couples fired in He at temperatures higher than 1650°C could not be successfully analyzed due to a mullite decomposition reaction at low oxygen pressures which resulted in the formation of Al_2O_3 on the surface of the mullite and the entrapment of the vapor species in the form of bubbles in the fused silica. These bubbles created convection currents which resulted in profiles varying in composition and length within the same couple. This decomposition was found to occur to a very small degree in air, however, even when the mullite was fired for eleven days at 1650°C. Further details of this reaction are presented in Appendix II.

Short and Roy[26] and Swindells[27] have demonstrated how diffusion data can be used to yield information on equilibrium phase diagrams. Much of the binary interdiffusion data in ceramic materials has been obtained for

systems in which both components were completely soluble in each other. In the Al_2O_3-SiO_2 system, however, the diffusion couples have compositions which fall in two-phase regions. If the compositions of the two phases are constant, no composition gradients exist, and diffusion and growth cannot occur. Consequently, only one-phase regions will be observed, for here composition gradients do occur, and the composition will vary between the limits of solubility. It must be noted, however, that the thermodynamic requirements are not an infallible criterion for determining which phases actually will be formed in a reacting system. Since the atomic motion in solids is strongly resisted and requires large energies of activation, unstable phases may form at lower temperatures and coexist with other phases for extremely long times. Such a case will be discussed later in connection with the visible absence of mullite at subsolidus temperatures.

If the concentrations in the respective phases at the phase boundary remain constant with an increase in time at a given temperature, as is the case for the diffusion couples prepared in this study, they represent the equilibrium concentrations for that temperature and, as such, can be used to verify and improve the accuracy of the curves determined by other methods.

The Al_2O_3 concentration at the interface for a given temperature was determined by averaging the concentrations for different times at points 3-6μ preceding the point of discontinuity in order to avoid interference from the mullite or sapphire during microprobe measurements. These data constitute points on the liquidus curve between mullite and the mullite-silica eutectic. The results are presented in Table II and in Fig. 13 as

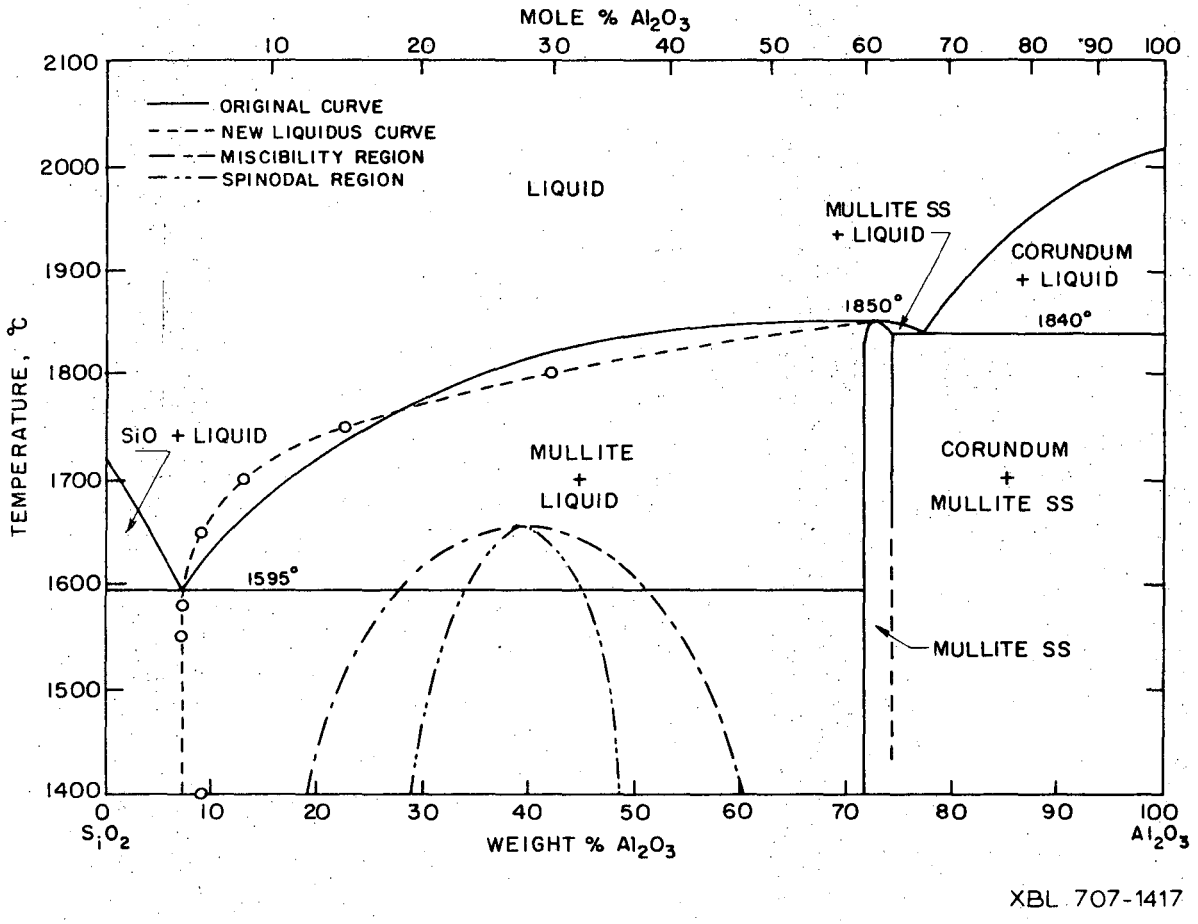

Fig. 13. New mullite liquidus curve shown with region of liquid immiscibility superimposed on the Al_2O_3-SiO_2 diagram determined by Aramaki and Roy.[28]

the dotted curve superimposed on the Al_2O_3-SiO_2 phase diagram after Aramaki and Roy.[28] It can be seen that the new liquidus curve has a small change in slope from mullite to approximately 20 wt % Al_2O_3. At this composition it begins to drop more sharply to the eutectic temperature. This shape is indicative of a rather high rate of evaporation of the silica from the melt[28-30] as well as the existence of a liquid immiscibility gap.

Such a region of metastable liquid immiscibility has been found by MacDowell and Beall[14] (Fig. 13 shows the portion above 1400°C) and was shown to be the essential cause of the formation of mullite on heating the glasses above 1000°C. The classical mechanism of nucleation and growth was discovered to be operative during two-liquid phase separation in the composition regions of 11-30 wt % and 48-67 wt % Al_2O_3, while a spinodal mechanism appeared to be functioning in the region from 30 to 48 wt % Al_2O_3. The temperature of the upper consolute point of the immiscibility gap is thought to be approximately 100°C below the liquidus as no phase separation was observed by these authors on cooling melts just below the liquidus. This liquid immiscibility is to be expected in this system because of the high field strengths of the cations, as well as the limited ability for Al^{+3} ions to remain in four-fold coordination, especially at subsolidus temperatures where the available thermal energy is low.

The points on the liquidus curve below the eutectic temperature were obtained due to the formation of amorphous diffusion zones. The inability to detect mullite at the interface does not, however, rule out its occurrence. A discussion of the formation of mullite and its subsequent

growth to an observable thickness at higher temperatures is given in the following section on microstructure.

B. Microstructure

The microstructure of the diffusion zones reveals important clues concerning the formation or absence of mullite and the accompanying liquid phase.

The microstructures of the 1400°, 1550° and 1580°C cristobalite-sapphire specimens are shown in Fig. 14. For the 1550° and 1580°C temperatures the diffusion zone is denoted by an amorphous phase bounded by sapphire (below) and cristobalite (above). The diffusion profiles extend approximately 5-10μ past the beginning of the grain boundary structure in cristobalite. The 1400°C photographs do not reveal an obvious glassy layer as such, but what appear to be grains of cristobalite which extend to the alumina interface. Microprobe analysis reveals a definite diffusion profile having an average interfacial concentration of 9.2 wt % Al_2O_3. Staley[7] also found a similar microstructure in pellets of corundum and cristobalite heated together at 1500°C. An optical examination by Staley of a thin section of the reaction zone revealed a glass region adjoining the corundum; this region corresponded to the diffusion zone revealed by the microprobe analysis in this study. Mullite was not observed at the glass-sapphire interface for any of these temperatures.

The subject of concern is, thus, the occurrence of an amorphous phase at subsolidus temperatures instead of the intermediate mullite solid solution zone as indicated by the phase diagram.

This anomaly has been reported at temperatures as low as 1200°C by Wahl, et al.[31] for reactions in cristobalite-corundum powder mixtures

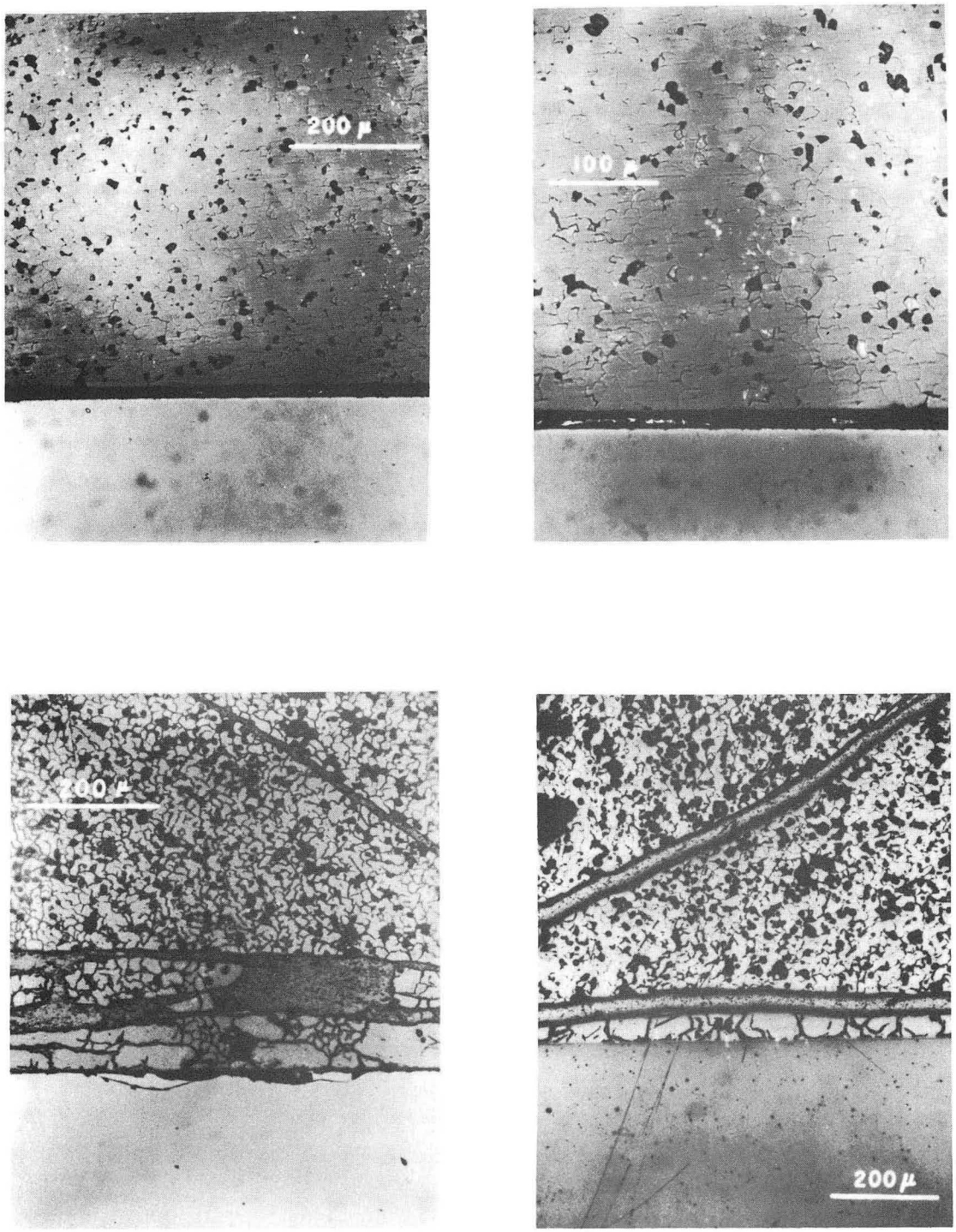

XBB707-3035

Fig. 14. Microstructure of the diffusion zones formed between cristobalite (top) and sapphire (bottom) annealed under the conditions of (a), (b) 1400°C, 14 days; (c) 1550°C, 16 days; (d) 1580°C, 8 days. The amorphous phase is clearly revealed at the interface only in (c) and (d). The worm-like structure in (c) and (d) is the mounting resin.

analyzed by high-temperature X-ray diffraction. In this case, mullite did not develop until 1450° unless the starting materials were very finely ground.

In studies of the reactions at the interface between compacts of alumina and cristobalite at 1600°C, DeKeyser[6] found a glassy phase having a composition of about 8.4 wt % of Al_2O_3 at the interface which penetrated both pellets. Mullite formation was confined, however, to the alumina side of the interface. By increasing the compaction and density of the alumina pellet, the depth of the silica penetration was decreased, thus implying that the glassy phase moved along the grain boundaries of the alumina compact. The Al_2O_3 content of the liquid and the 1600°C temperature employed in DeKeyser's experiments indicate equilibrium conditions in terms of a eutectic temperature of 1590° ± 10°C and composition of 8.2 wt % Al_2O_3.[34]

Staley[7] has conducted similar reaction experiments at 1500 and 1550°C using couples of pressed pellets of corundum and cristobalite, and cristobalite pellets and sapphire, as well as mixed powders of these phases. He also noted the formation of an amorphous phase and concluded that it was an essential feature of the subsolidus reactions in the system and not the result of liquid formation (i.e., the eutectic would actually be below 1500°C) or the vitrification of cristobalite. A summary of his results is as follows.

(1) The rate and degree of formation of mullite in powder mixtures increased at about the same rate as corundum decreased, and thus was inversely dependent on the particle size of the alumina phase. On the other hand, the amount of noncrystalline material increased at about the

same rate as the cristobalite decreased and was found to be extensive regardless of the silica particle size. A kinetic analysis of the coarse-grained powders reacted at 1500°C indicated that the initial amount of corundum decreased primarily by the mechanism of ionic diffusion through a solid oxide medium, while that of cristobalite decreased by a mechanism based on phase boundary motion. If the polycrystalline alumina pellets were replaced by sapphire in the diffusion couples, the penetration of silica into the alumina ceased and the amount of the non-crystalline phase notable increased.

(2) It was inferred that the poor development of mullite was not caused by a nucleation problem, as an appreciable amount of this phase developed in the first few hours of reaction. It appeared that a requirement for mullite growth was rapid enough dissolution of corundum to cause sufficient alumina saturation of the glassy phase. Consequently, with the dissolution of cristobalite being more rapid than that of corundum, a silica rich glassy phase would be favored for a longer period of time as the sizes of the cristobalite and corundum crystals increased.

The absence of the thermodynamically stable phase of mullite at the subsolidus temperatures is not unique. In the Al-Ni system, for example, four phases are indicated in the equilibrium diagram. The β phase has a zero solubility range, the γ and ε phases moderate ranges, and the δ phase a relatively wide range. However, in diffusion experiments at annealing temperatures below the eutectic, only the β and γ phases were observed and the high melting δ and ε phases were not detected.[33]

From a theoretical viewpoint, Kidson[34] has shown that the application of Fick's first law to polyphase diffusion in binary systems leads

to expressions for the interface positions as functions of time and temperature. Figure 15 shows a concentration versus distance curve for a binary system in which a single intermediate phase occurs.

It is assumed that the concentrations at the interfaces are constant and equal to the equilibrium values. If we consider first the flux of material from right to left, the rate of advance of the interface at $\chi_{\beta\gamma}$ is given by

$$[C_{\beta\gamma} - C_{\gamma\beta}] \frac{d\chi_{\beta\gamma}}{dt} = J_{\beta\gamma} - J_{\gamma\beta}. \tag{17}$$

That is to say, $J_{\beta\gamma}$, the flux from the β phase at the interface, must supply the surplus quantity $(C_{\beta\gamma} - C_{\gamma\beta})\, d\chi_{\beta\gamma}$ per unit time in order to advance the β phase into the γ phase region. Substituting for J from Fick's first law Eq. (1), one obtains

$$\frac{d\chi_{\beta\gamma}}{dt} = \frac{1}{C_{\beta\gamma}-C_{\gamma\beta}} \left[\left(- \frac{D\partial C}{\partial X} \right)_{\beta\gamma} - \left(- \frac{D\partial C}{\partial X} \right)_{\gamma\beta} \right]. \tag{18}$$

This portion of the system fulfills the conditions required for the application of the Boltzmann theorem,[28] and the concentration C (X,t) may be expressed as a function of a single parameter $\lambda = X/\sqrt{t}$. Using the definition of λ, one has

$$\frac{\partial C}{\partial X} = \frac{dC}{d\lambda} \frac{\partial \lambda}{\partial X} = \frac{1}{\sqrt{t}} \frac{dC}{d\gamma}. \tag{19}$$

Since the concentrations at the interface have been assumed as constant, the value of λ must be constant. But $dC/d\lambda$ is again a function of λ

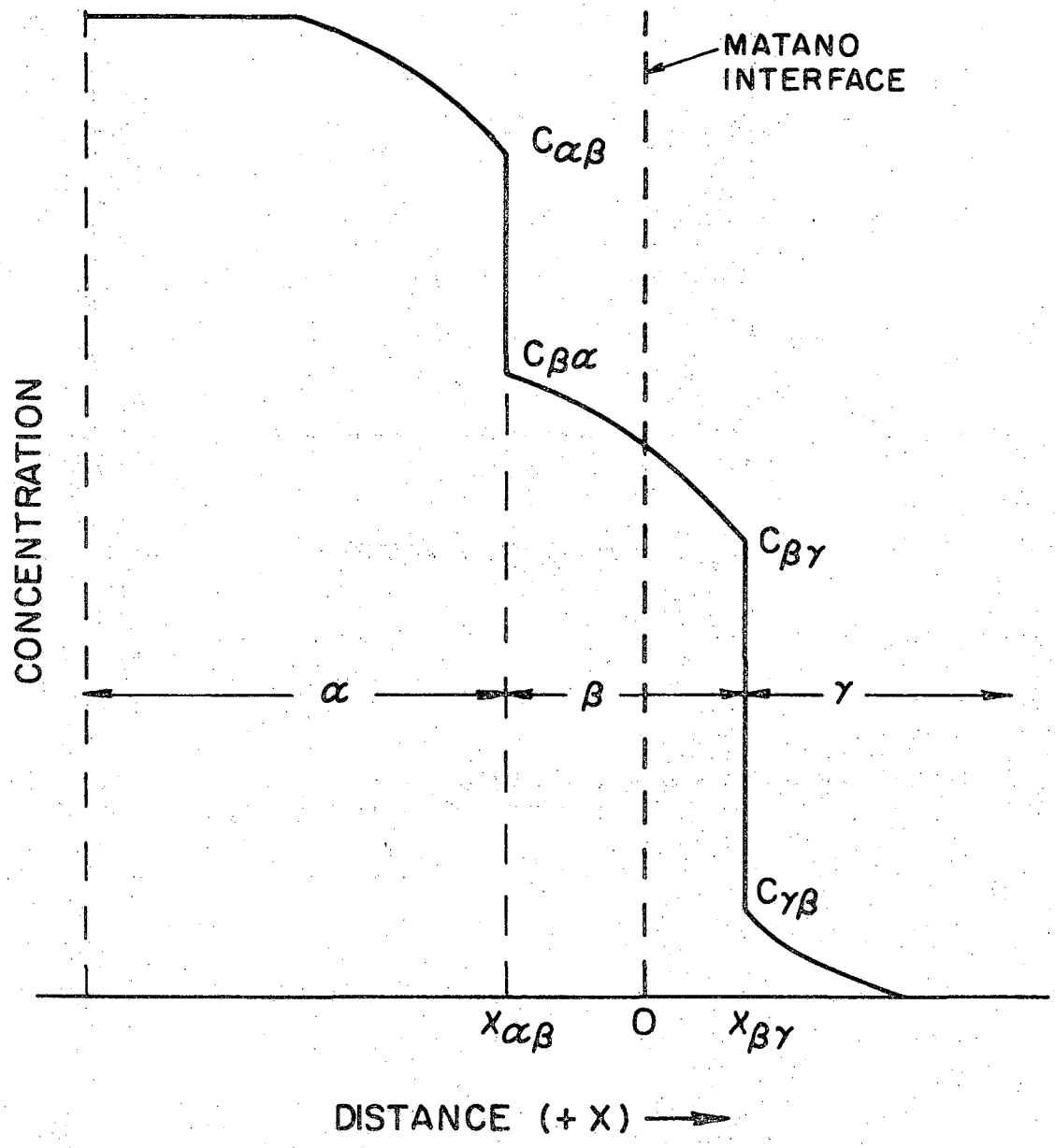

XBL 707-1416

Fig. 15. Concentration vs. distance curve for a system in which a single intermediate phase occurs.

alone, and hence it is also constant at the interface. Thus (14) may be rewritten as

$$\frac{d\chi_{\beta\gamma}}{dt} = \left[\frac{(DK)_{\gamma\beta} - (DK)_{\beta\gamma}}{C_{\beta\gamma}-C_{\gamma\beta}}\right] \frac{1}{\sqrt{t}} \tag{20}$$

where

$$K_{ij} = \left(\frac{dC}{d\lambda}\right)_{ij} - \sqrt{t}\left(\frac{\partial C}{\partial X}\right)_{ij} .$$

Integrating (16) one gets

$$\chi_{\beta\gamma} = 2\left[\frac{(DK)_{\gamma\beta} - (DK)_{\beta\gamma}}{C_{\beta\gamma}-C_{\gamma\beta}}\right]\sqrt{t} \tag{21}$$

and similarly for the $\chi_{\alpha\beta}$ interface

$$\chi_{\alpha\beta} = 2\left[\frac{(DK)_{\beta\alpha} - (DK)_{\alpha\beta}}{C_{\alpha\beta}-C_{\beta\alpha}}\right]\sqrt{t} . \tag{22}$$

The width of the β phase layer as a function of time is simply

$$W_\beta = \chi_{\beta\gamma} - \chi_{\alpha\beta}$$

$$= 2\left[\frac{(DK)_{\gamma\beta} - (DK)_{\beta\gamma}}{C_{\beta\gamma}-C_{\gamma\beta}}\right] - \left[\frac{(DK)_{\beta\alpha} - (DK)_{\alpha\beta}}{C_{\alpha\beta}-C_{\beta\alpha}}\right]\sqrt{t} = B_\beta t. \tag{23}$$

Equation (19) exhibits the experimentally observed parabolic time dependence of the interface movement with a temperature dependent growth rate constant (B_β) which involves the diffusion coefficients in its two

bordering primary phases, as well as those in the β phase itself.

Equation (19) indicates that from an algebraic point of view, B_β may be positive, zero, or negative depending upon the relative values of the solid solution range of the phases of the equilibrium diagram and the DK terms involved. The two interfaces can both move left or right with different rates or in opposite directions relative to the Matano interface ($\chi = 0$).

For $B_\beta > 0$, the rate of formation of the new β phase from the γ phase is greater than the transition of the β to the α phase; and, consequently, the width of the β phase increases with time. $B_\beta \leq 0$ implies either a dynamic balance or that the rate of supply of material from the α phase to the β phase be so fast compared to the diffusion rate in the β phase that there would be no time for the β phase to form from the γ phase. The absence of the β phase must, however, be rejected on thermodynamic grounds as it implies an infinite chemical potential at the α-γ interface. This is a contradiction to the requirement that the chemical potential be continuous and monotonic throughout the specimen. Castleman[35] has shown that $B_\beta \leq 0$ implies $D_\beta \leq 0$; thus one must conclude that while the growth rate constants can vary over a wide range, they must be positive and finite however small. The apparent absence of intermediate phases, as reported in the literature, including mullite at subsolidus temperatures, suggests that the rate constants are too small to permit detection of the phase layers by ordinary microscopic techniques.

The magnitude of the diffusion coefficient in the β phase is also an important factor in its growth. If D_β is small compared to those of its neighboring phases, the rate of supply of material at the β-γ

interface required to advance the β phase into γ will be low. This effect will tend to make the growth rate of the β phase small in the direction of γ. Conversely, if D_β is relatively large, the β phase will tend to grow rapidly both into α and γ. Thus the occurrence or non-occurrence of a phase is governed by conditions peculiar to a particular annealing temperature and does not depend solely upon sufficiently high temperatures or long times.

The experimental and theoretical observations of the above authors, as well as those of this author, demonstrate that mullite (i.e., the β phase) does not have to occur to a visible magnitude even though it is the thermodynamically stable phase at low temperatures. However, mechanistic explanations should accompany these observations for a complete understanding of this phenomenon.

Staley[7] has shown that at 1500° and 1550°C, mullite does begin to grow in the amorphous phase once the latter is saturated with Al_2O_3. This fact, reinforced by Kidson's[34] arguments, demonstrates that nucleation of the mullite must occur at the Al_2O_3-SiO_2 interface as a rapid step in the overall diffusion process. However, the presence of an extensive amorphous phase at these low temperatures leads this author to believe that in order for nucleation to occur, it must be preceded by the formation of a metastable glassy phase, particularly in the case of cristobalite-sapphire couples. Such a phase would form more easily due to the greater ease of rearrangement in the glass phase relative to that of cristobalite and sapphire.

The phenomenon of the metastable glass phase formation necessitates a single eutectic type of phase diagram shown in Fig. 16 where the liquidus

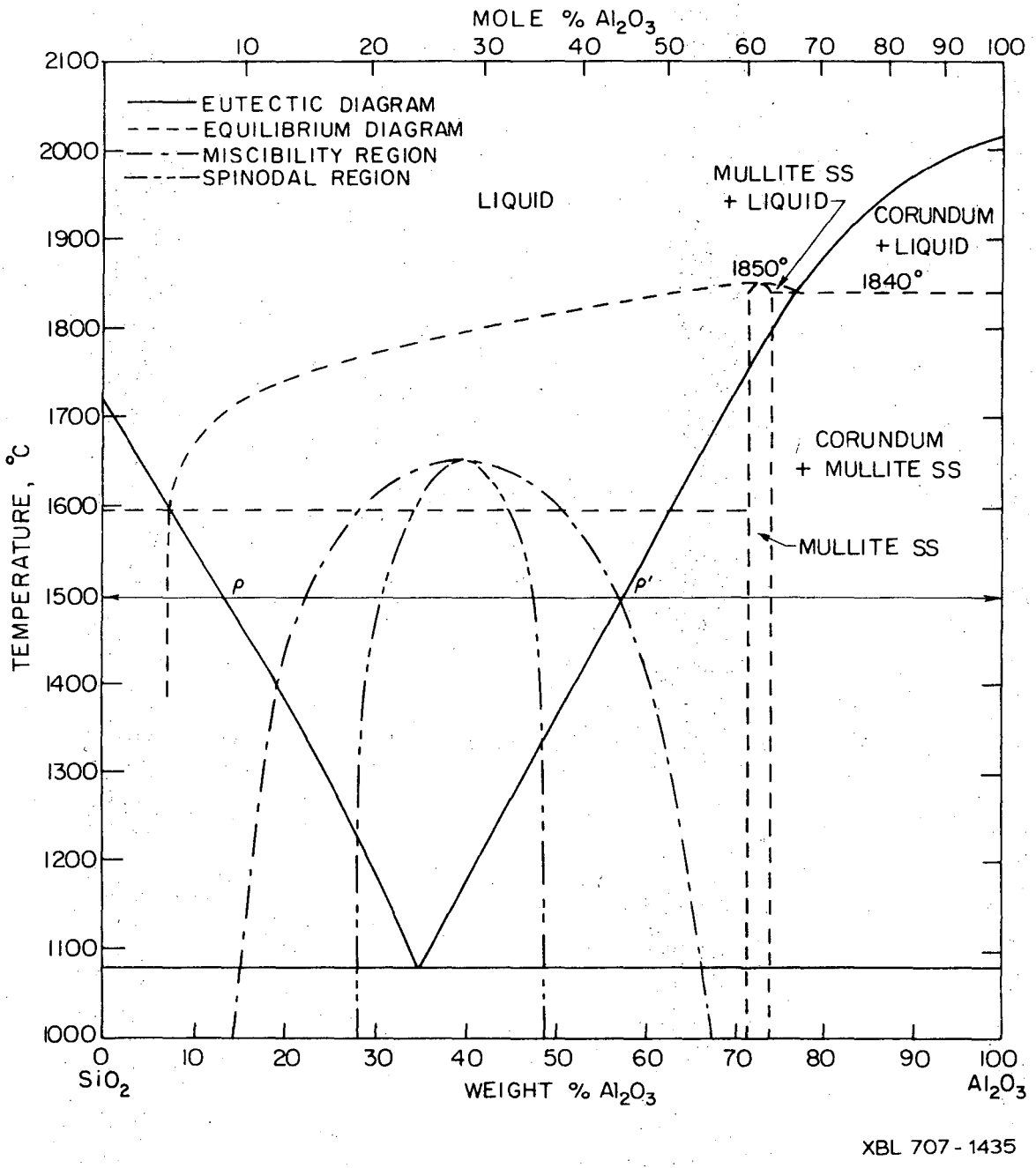

Fig. 16. Single eutectic metastable phase diagram proposed to explain glass formation at subsolidus temperatures in the Al_2O_3-SiO_2 system.

curves originating at the extremities of the system are extended to a point of intersection.

The first step in the diffusion process (e.g. at 1500°C) would be the formation of a liquid phase having a composition range from p at the silica interface to p' at the sapphire interface. On the basis of the work of MacDowell and Beall,[14] it is believed that the alumina-rich glass would then readily react with the sapphire surface to nucleate mullite since p' is within the metastable immiscibility region. This reasoning is especially true if the consolute point should be nearer the liquidus curve than is shown in Fig. 16. Once mullite is formed, the system reverts to the equilibrium diagram (shown dotted in Fig. 16), and the remaining liquid attempts to reach its equilibrium composition indicated by the extended liquidus through dissolution of cristobalite. This mechanism would account for the liquidus points below the eutectic temperature indicated in Fig. 13. The higher Al_2O_3 content for the liquid at 1400°C is an indication of the lack of equilibrium within the time of the anneal. The formation of the amorphous phase may appear to be controlled by a mechanism based on phase boundary motion of cristobalite,[7] but, in actuality, is governed by the rate of diffusion of Al_2O_3 towards the silica-rich zone. This is true since cristobalite is dissolved as the Al_2O_3 content exceeds the SiO_2 liquidus amount at a given temperature. This mechanism of the formation of a liquid phase at subsolidus temperatures may not be necessary, however, for those systems that contain a glassy phase such as vitreous silica as a starting material.

Once nucleated, the mullite phase fails to grow to an observable magnitude at the lower temperatures. This can be explained on the basis that the growth rates of mullite are slower than its dissolution rates in unsaturated silica glass. If all the mullite dissolves, (a possibility in this case since the presence of a metastable liquid phase prevents the chemical potential from becoming infinite) the phase relationships return to that of the single eutectic system to repeat continuously the sequence of entrance of alumina, phase separation of glass, and the formation and subsequent dissolution of mullite. This and all succeeding series of events would occur regardless of the initial form of silica.

When the silica phase becomes saturated with alumina, the mullite grows to an observable size. This analysis may be applied to the experimental evidence of Staley[7] who showed that mullite began to grow when the initially formed interface liquid moved to occupy the grain boundaries and pores of the corundum and became saturated with Al_2O_3.

As the temperature of the diffusion experiments is increased above the eutectic temperature, the formation of a stable liquid occurs, which readily leads to nucleation of mullite at the sapphire interface. Figures 17 and 18 show the microstructure of the diffusion zones and their relationship to the fused silica and sapphire or mullite boundary phases for 1650°, 1700°, 1750°, and 1800°C.

At 1650°C, as at the subsolidus temperatures, the diffusion zone is primarily an amorphous phase. As before, the aluminum profile extends 5-10μ beyond the boundary of cristobalite. In this case, the cristobalite is formed at temperature by crystallization in the fused silica. As the Al-containing species diffuse toward the cristobalite, the

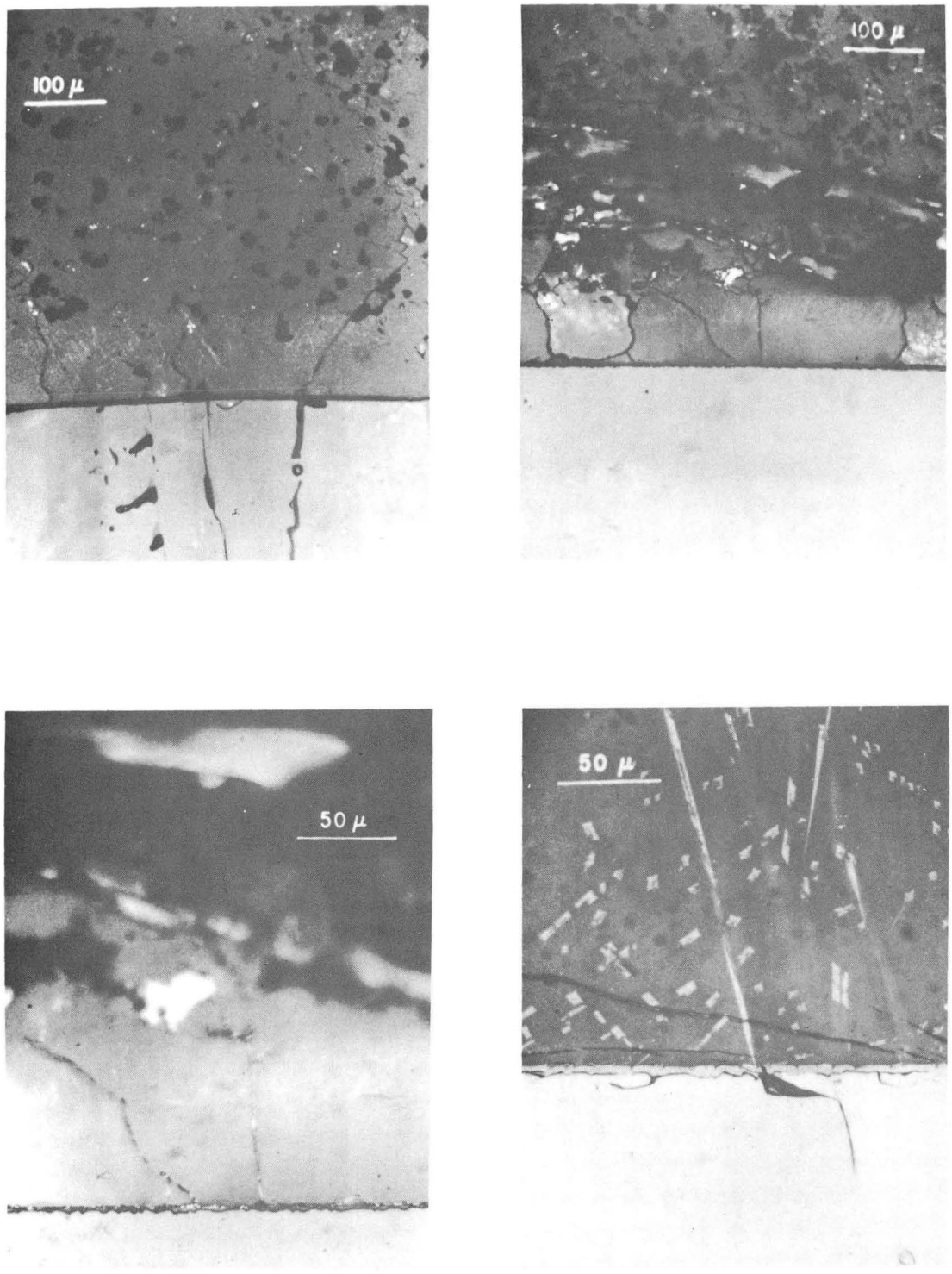

XBB 707-3036

Fig. 17. Microstructure of the diffusion zones formed between (a) mullite-silica, 1650°C, 7 days; (b), (c) alumina-silica, 1650°C, 7 days; (d) alumina-silica, 1700°C, 4 days. Position of phases is the same as Fig. 14 with the addition of a thin layer of interfacial mullite in (c) and (d) and crystallization of mullite on cooling in (d).

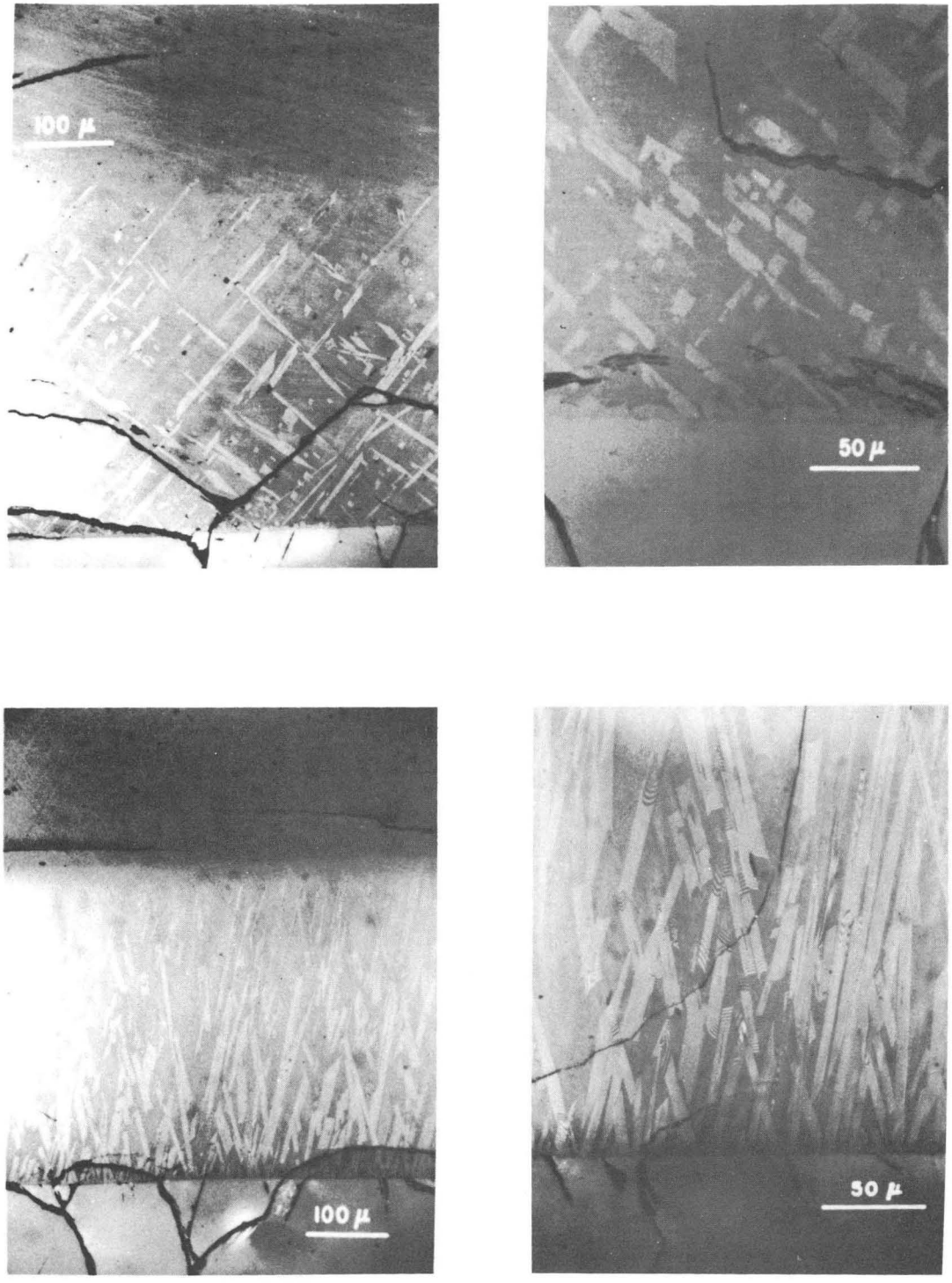

XBB707-3033

Fig. 18. Microstructure of the diffusion zones formed between (a), (b) alumina-silica, 1750°C, 2 and 4 days; (c), (d) alumina-silica, 1800°C, 6 hours. Position of phases is the same as in Figs. 14 and 17 with the addition of increased crystallization on cooling.

cristobalite is gradually redissolved. One of the most important features is the small but discernable growth of mullite at the interface (Fig. 17c). This indicates that the rate of overall growth of the mullite has surpassed its solution rate in the liquid phase. The growth can occur at either or both the mullite-liquid and mullite-sapphire interfaces. The assumption is made that growth at both interfaces is dependent on counterdiffusion in mullite of $4Al^{+3}$ and $3Si^{+4}$ in essentially a fixed oxygen lattice. Because of extreme experimental difficulties, it should be noted that mullite could not be detected in every specimen annealed at 1650°C due to the disruption of the mullite-sapphire phase boundary on cooling.

As the temperature is increased to 1700°C and above, the rate of growth of mullite at the interface increases, and the fused silica retains its amorphous structure. Mullite, however, also crystallizes in the glass diffusion zone on cooling. This mullite can be discerned from that which grows at the interface except in the specimens held at 1800°C. In this case, a large number of long mullite needles extending throughout the diffusion zone are heterogeneously nucleated by the mullite previously grown at the alumina surface. Their composition was determined by microprobe analysis to be 74 wt % Al_2O_3. The classical mullite composition ($3Al_2O_3 \cdot 2SiO_2$) has 71.8 wt % Al_2O_3; while mullite formed by crystallization on cooling from a melt of mullite composition has 77.4 wt % Al_2O_3 ($2Al_2O_3 \cdot SiO_2$).[28,36] It is suggested by this author that the lower Al_2O_3 compositions of the diffusion zones relative to that of a 3:2 mullite melt is responsible for the Al_2O_3 content lower than the 2:1 composition.

In order to determine the composition range of the interfacial mullite grown at temperature, and thus establish the boundaries of the mullite solid solution, a 15 wt % Al_2O_3-85 wt % SiO_2 glass was prepared as described in Section II and heated in contact with sapphire at 1700°C for 11 days. At this temperature, the glass is essentially saturated with alumina. Mullite nucleated at the interface can grow to a greater extent (Fig. 19) since there is no competitive dissolution process. The solid solution range determined by point beam microprobe analysis is about 70.5 wt % Al_2O_3 near the glass boundary to 73.5 wt % Al_2O_3 near the sapphire boundary. These values are averages of a number of profiles extrapolated to the boundary interfaces. Caution was taken to avoid concentrations measured exactly at the mullite boundaries as these values would be affected by the adjacent phases because of the measuring method. The composition of the mullite prepared from the crystallization of a melt on cooling and used as an end member in the 1650° diffusion couples was determined to be almost invariably 76.3 wt % Al_2O_3.

Mullite has been shown to be incapable of a higher concentration of silica than $3Al_2O_3 \cdot 2SiO_2$(71.8 wt % Al_2O_3).[28] As discussed above, mullite crystallized on cooling from a melt of its composition has been found to consistently have a concentration of $2Al_2O_3 \cdot SiO_2$ (77.4 wt % Al_2O_3). Within experimental errors, the values related to mullite compositions obtained in this study can be considered to agree with the values determined by Aramaki and Roy.[28]

Calculations were made to determine the temperature at which mullite would cease to be recognized by optical methods in the SiO_2-Al_2O_3 diffusion couples. Mullite thickness versus the square root of

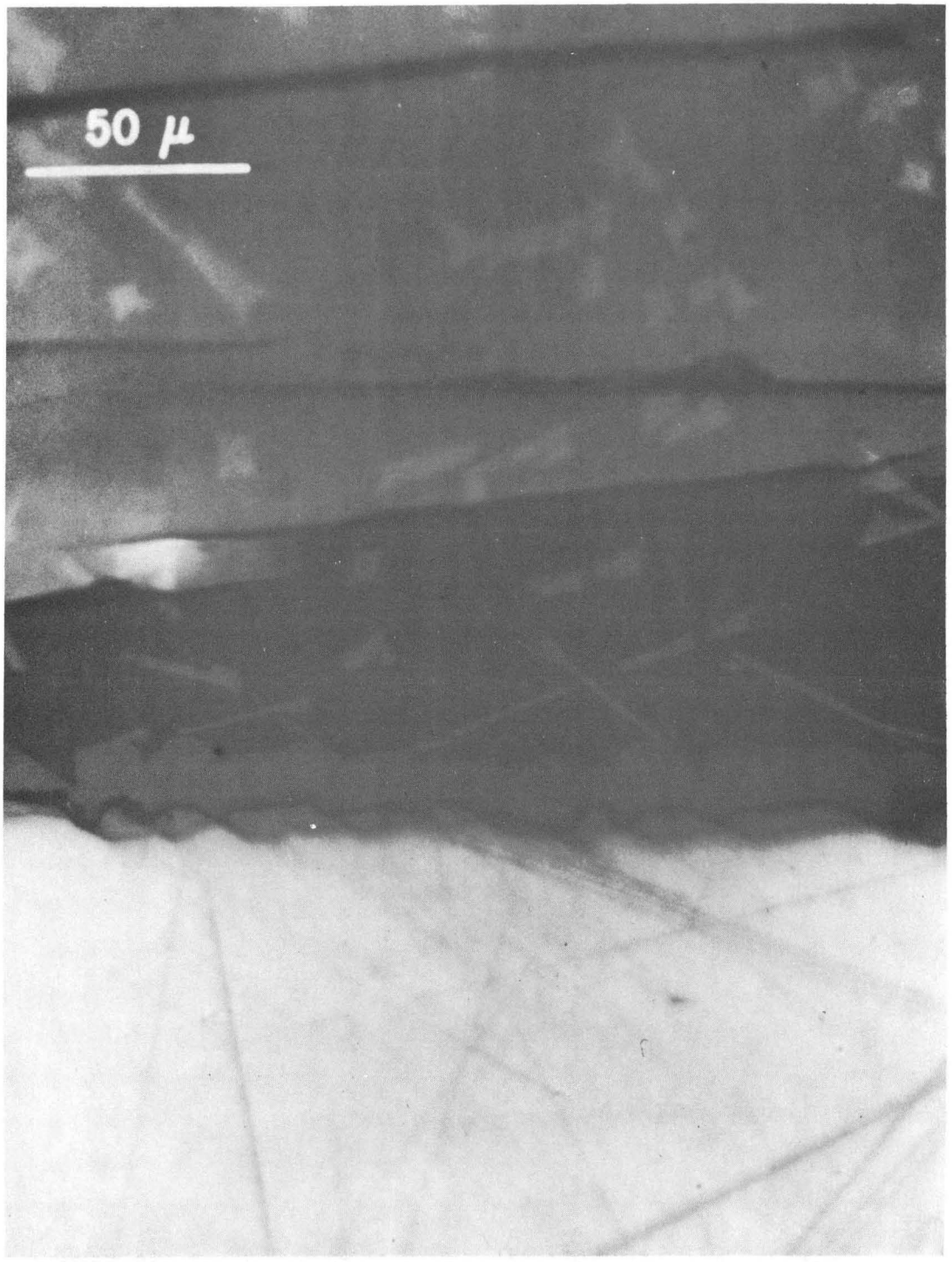

XBB707-3034

Fig. 19. Microstructure of the 15% Al_2O_3-sapphire couple annealed at 1700°C for 11 days. Mullite is shown as a solid layer at the interface as well as random crystals throughout the glass.

time was first plotted for 1650°, 1700°, 1750°C (Fig. 20) from the data of Table III. The thickness values for a number of constant times were then plotted versus temperature (Fig. 21) and extrapolated to zero thickness. This procedure showed that mullite would not be observed below 1634°C. This does not imply that mullite does not form or nucleate at these temperatures, but that the dissolution rate is so fast that it cannot be observed to grow. This is in agreement with Kidson's argument[34] that the growth rate constant of the intermediate phase must be positive and finite however small.

Lastly, thickness values for 4, 6, and 8 hours (the times used in the 1800°C runs) from Fig. 20 were plotted versus temperature in Fig. 21 as before. The resulting lines were extended to 1800°C, indicating that the thickness of the interfacial mullite that should appear after 4, 6, and 8 hours would be 1.9, 2.3, and 2.6μ, respectively. These small amounts of growth, coupled with the extensive crystallization on cooling, demonstrate why one is unable to discern a distinct interfacial layer of mullite at 1800°C for these short times.

C. Diffusion Data and the Coordination Number of the Aluminum Ion

To ascertain if the diffusion coefficient of Al^{+3} is functionally dependent on the concentration along the profile, one may use the Boltzmann-Matano equation (Eq. 7) to solve for $\tilde{D}$. As discussed in Section III, the fundamental assumption made by Boltzmann in obtaining his solution to Fick's second law was that the process is diffusion controlled. This means that the distance from the Matano interface (i.e. X=0, Fig. 7) for a given concentration of the diffusing species

Table III. Thickness of mullite formed at different times at the interface of the alumina-silica and 15% alumina glass-sapphire couples

A. Alumina-Silica Couples

Temperature (°C)	Time (Days)	(Time$^{1/2}$) (sec$^{1/2}$)	Thickness (Microns)
1650	7	777.5	1.24
1650	9	882.0	1.41
1650	11	975.0	1.56
1700	4	587.9	3.60
1700	7	777.5	4.91
1700	9	882.0	5.60
1700	11	975.0	6.05
1750	2	415.7	4.71
1750	3	509.2	5.51
1750	4	587.9	6.40

B. 15% Alumina Glass-Sapphire Couples

1650	7	777.5	7.65
1650	9	882.0	8.83
1650	11	975.0	10.00
1700	4	587.9	8.53
1700	7	777.5	11.30
1700	9	882.0	13.35
1700	11	975.0	15.10
1750	2	415.7	6.62
1750	3	509.2	8.42
1750	4	487.9	9.43

must be directly proportional to the square root of time. That such a criterion holds for this system is shown by Figs. 22-26.

The interdiffusivities ($\tilde{D}$) of the aluminum ion as a function of composition were determined by computer analysis of the concentration

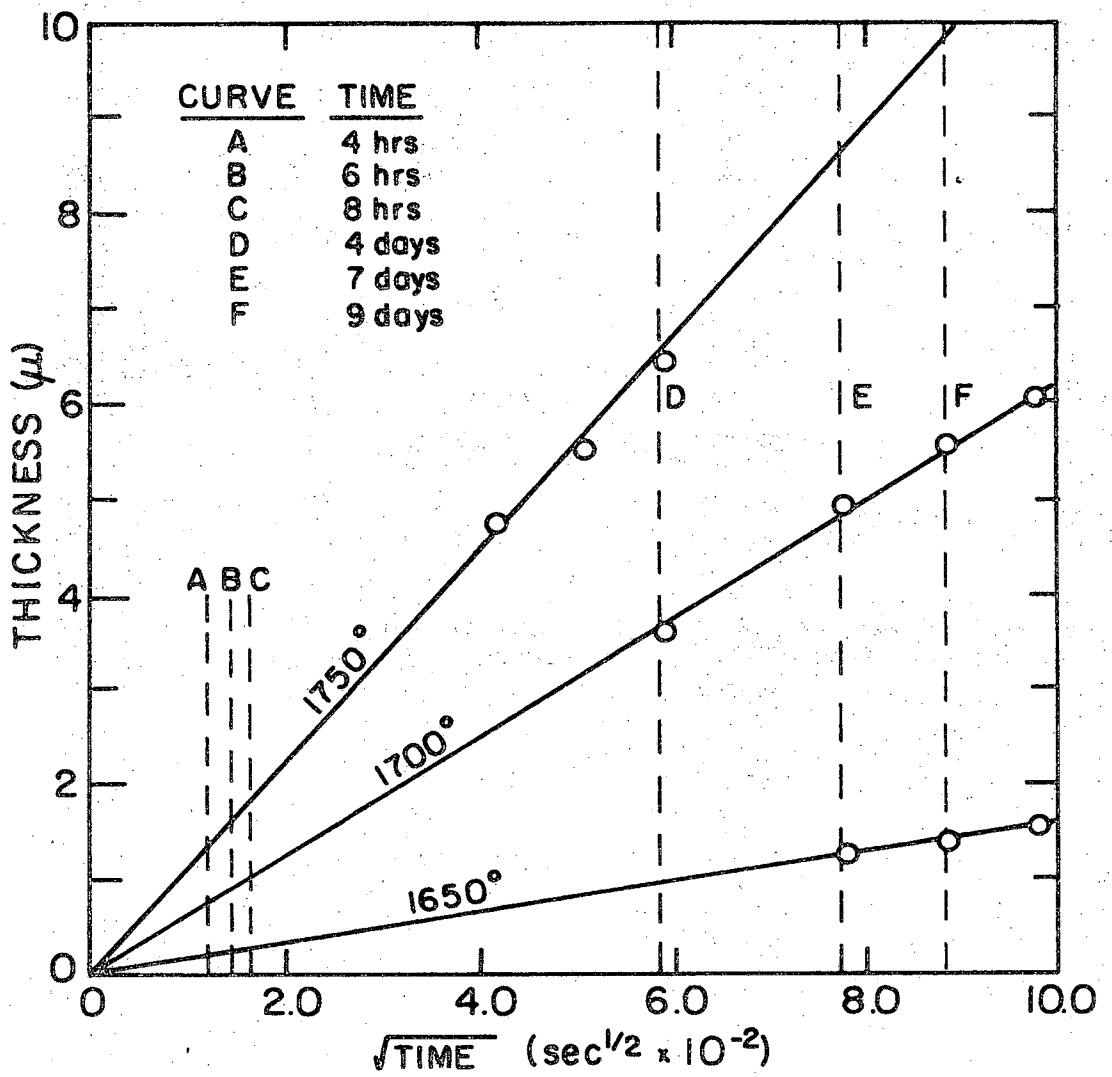

XBL 707-1418

Fig. 20. Plots of thickness of mullite growth in Al_2O_3-SiO_2 diffusion couples vs. square root of time for 1650, 1700 and 1750°C. Broken lines represent constant times.

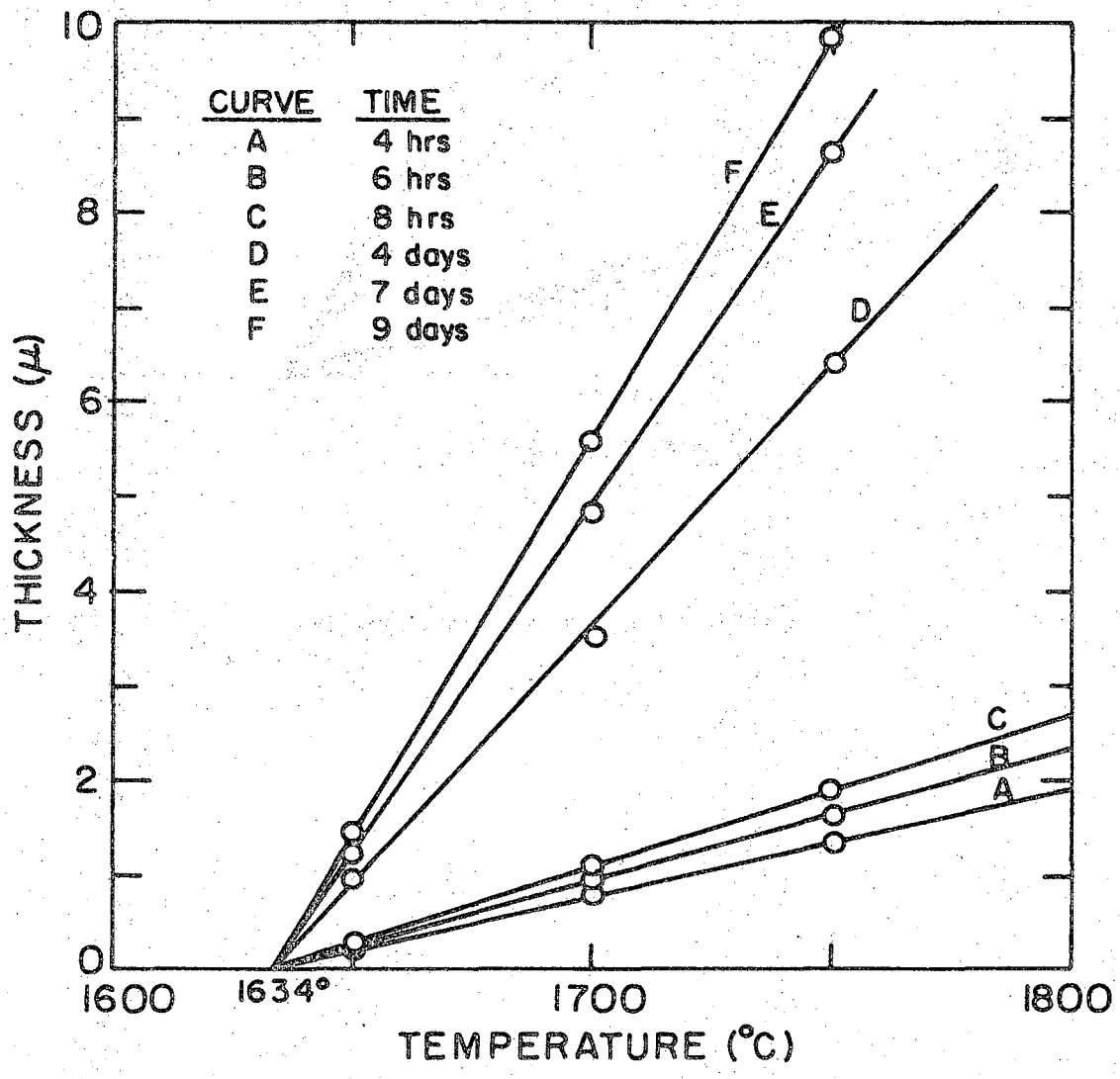

XBL 707-1419

Fig. 21. Graph of thickness of mullite for various times vs. temperature.

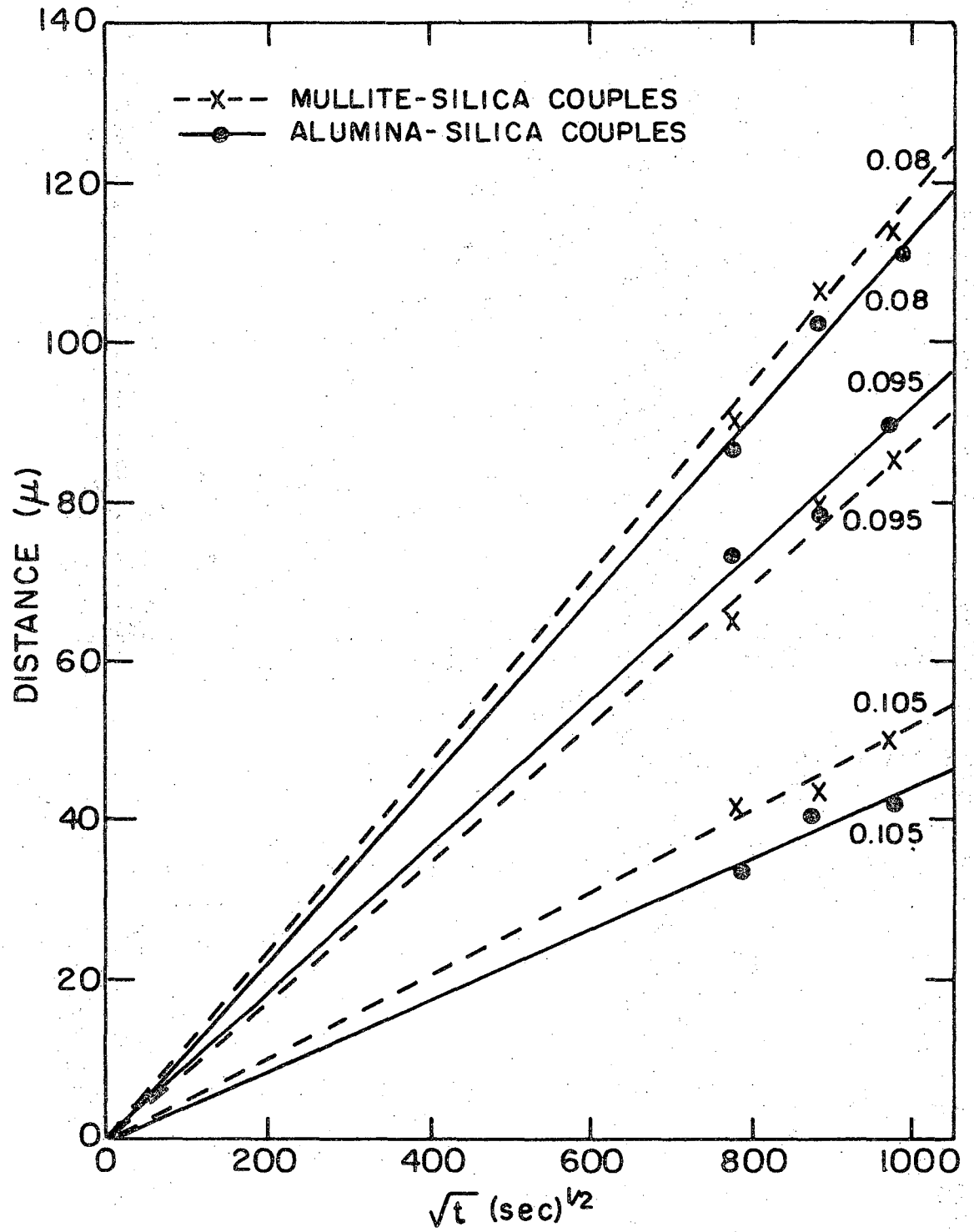

Fig. 22. Graph of distance vs. square root of time at 1650°C in helium for three concentrations of Al^{+3}.

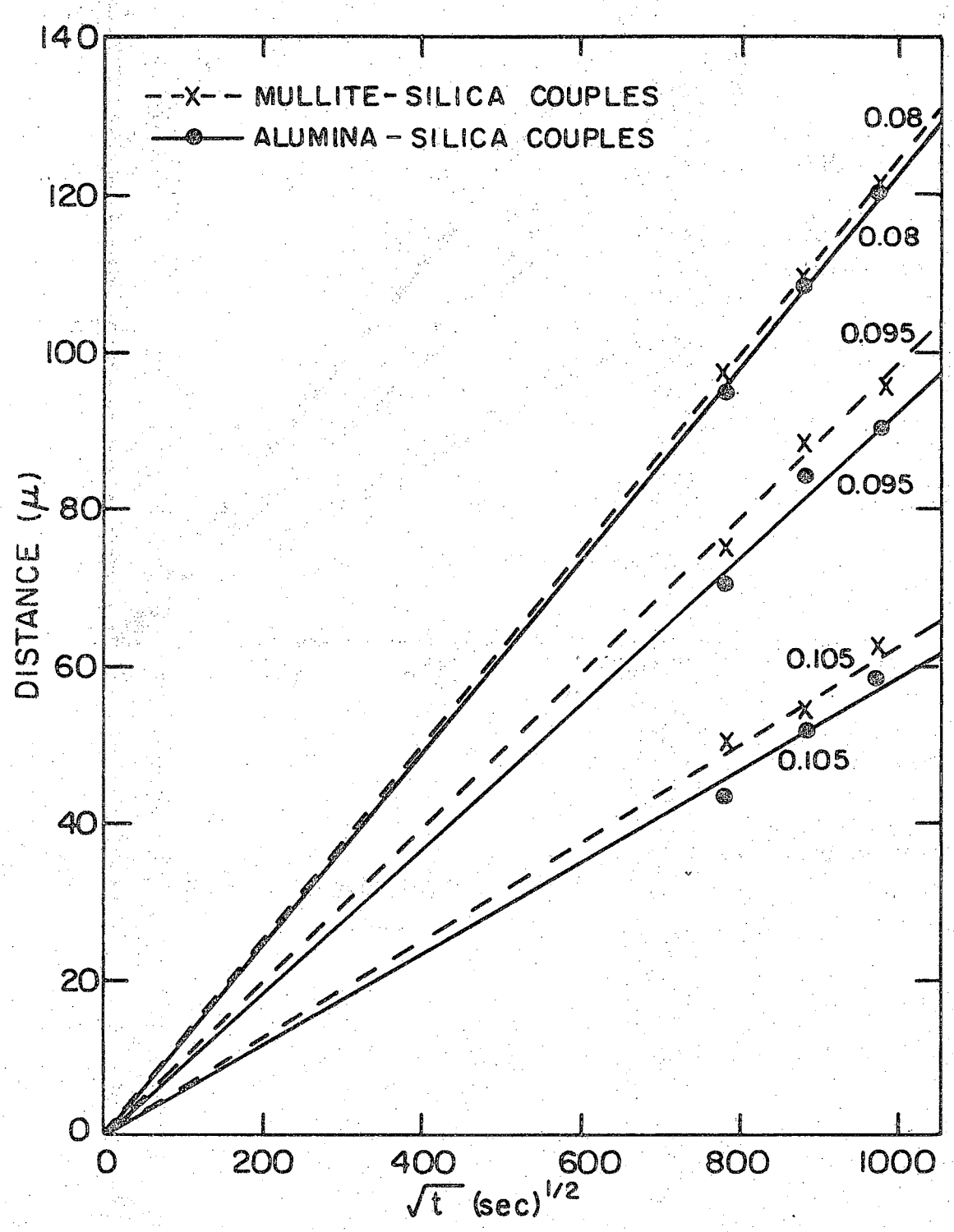

Fig. 23. Graph of distance vs. square root of time at 1650°C in air for three concentrations of Al^{+3}.

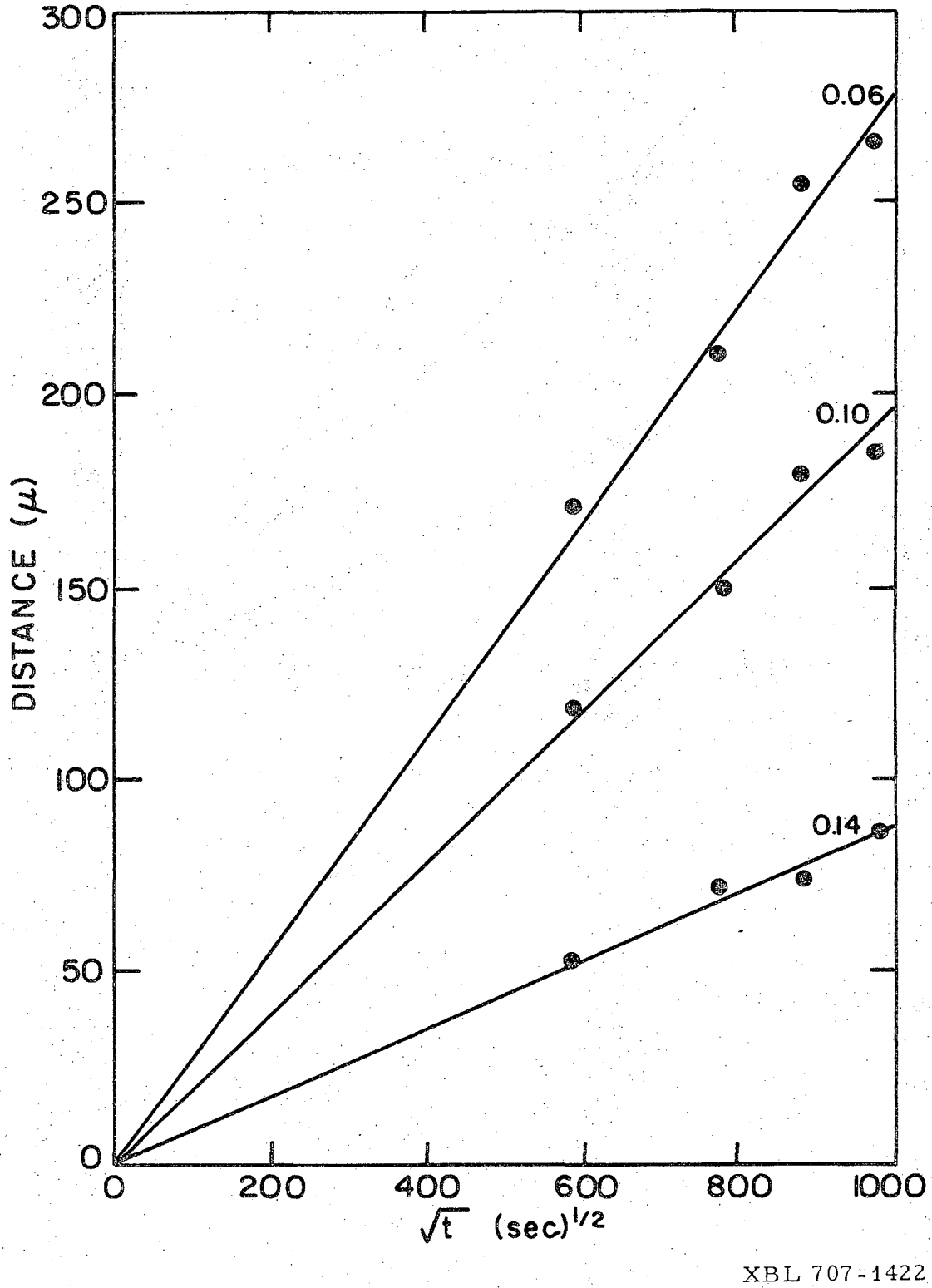

Fig. 24. Graph of distance vs. square root of time at 1700°C for three concentrations of Al^{+3}.

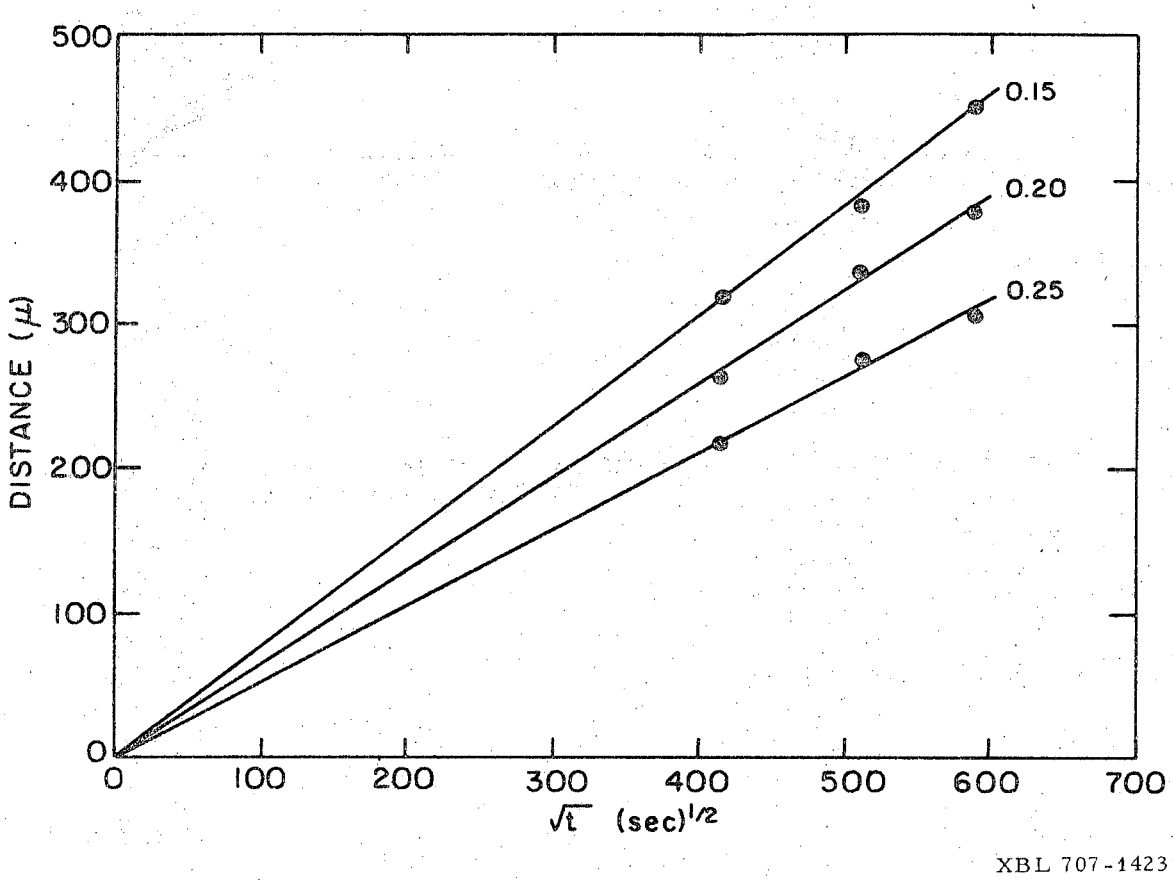

Fig. 25. Graph of distance vs. square root of time at 1750°C for three concentrations of Al^{+3}.

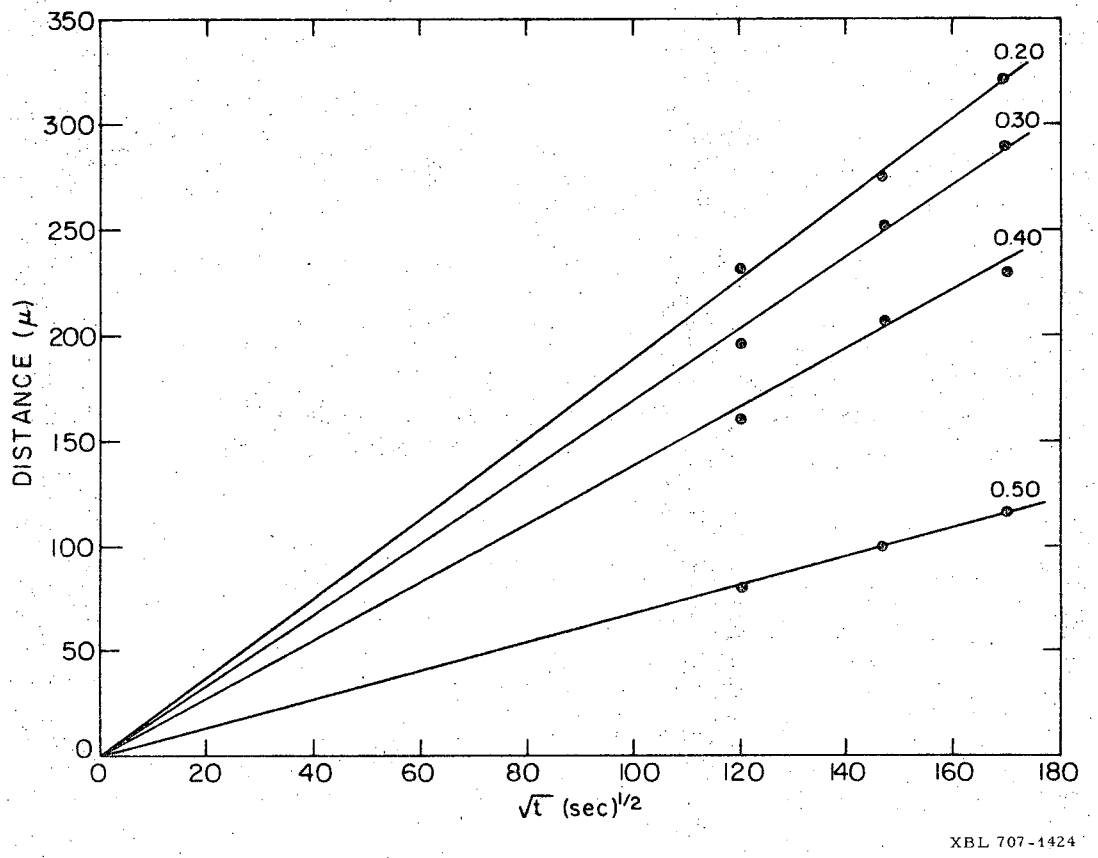

Fig. 26. Graph of distance vs. square root of time at 1800°C for three concentrations of Al^{+3}.

versus distance profiles (e.g., Figs. 11 and 12). These values were found to vary exponentially with the aluminum ion concentration over a range of approximately three orders of magnitude for each temperature, as shown by the sample curves in Figs. 27-30. These graphs and the equations which describe them are typical of those determined for all times at a particular temperature. From the equations determined for these graphs, $\tilde{D}$ values were determined for several values of concentration for each temperature and plotted against the reciprocal of absolute temperature (Fig. 31). A least squares analysis of each Arrhenius plot resulted in an equation for the temperature dependence of D which gives the values of D_o and the activation energy, Q, for each concentration, as presented in Table IV.

Table IV. Diffusivity data for the $Al_2O_3 \cdot SiO_2$ system

C Al^{+3} (gm/cm^3)	C Al_2O_3 (wt %)	D_o (cm^2/sec)	Q (Kcal/mole)
.05	4.30	3.47×10^{23}	307.5 ± 1.0
.07	5.96	2.43×10^{21}	286.2 ± 1.0
.09	7.60	1.64×10^{19}	264.8 ± 0.4
.11	9.24	1.66×10^{17}	245.0 ± 0.3
.15	12.40	9.93×10^{12}	203.3 ± 0.4
.20	16.40	6.29×10^{7}	151.9 ± 0.5
.25	20.10	3.38×10^{2}	99.9 ± 0.6
.30	23.75	2.06×10^{-3}	48.4 ± 0.9

It should be noted that at the higher concentration values, the interdiffusivities are calculated from $\tilde{D}$ versus concentration curves extrapolated to concentrations which do not exist in the actual profile.

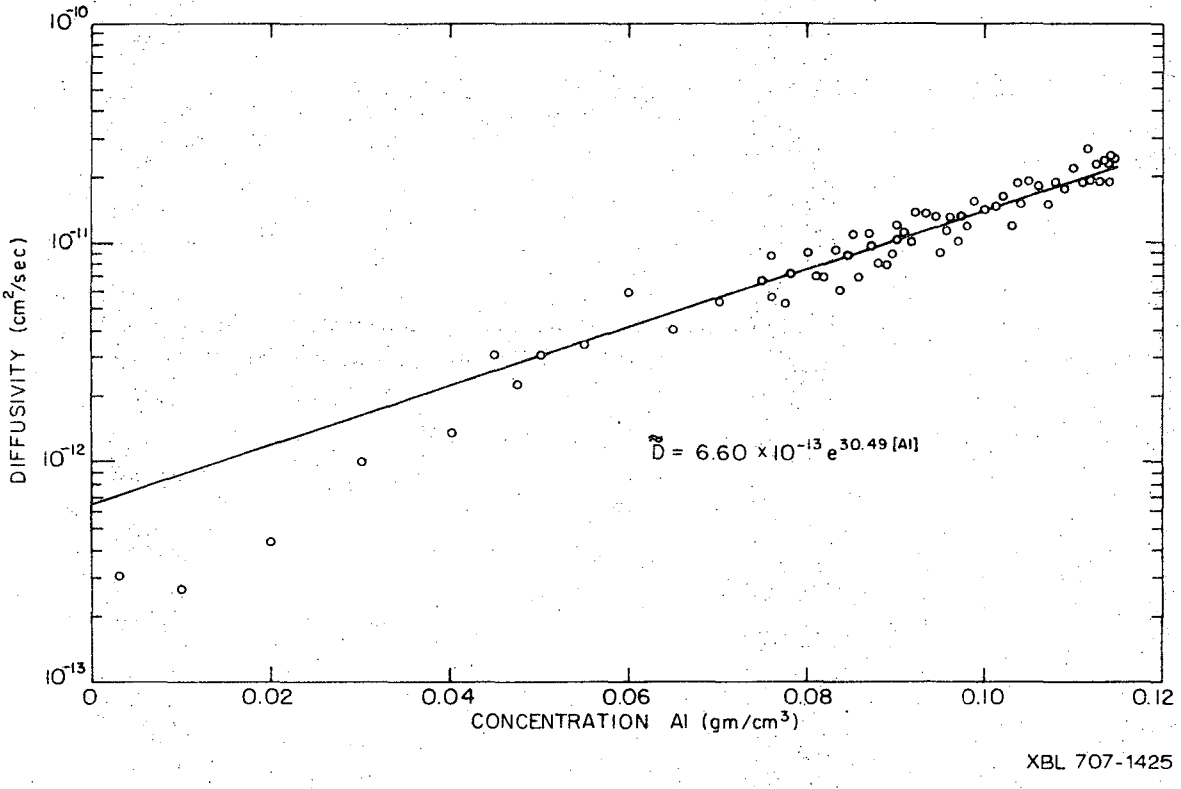

Fig. 27. Plot of computer determined diffusivities vs. concentration for Al_2O_3-SiO_2, 1650°C, 9 days, He

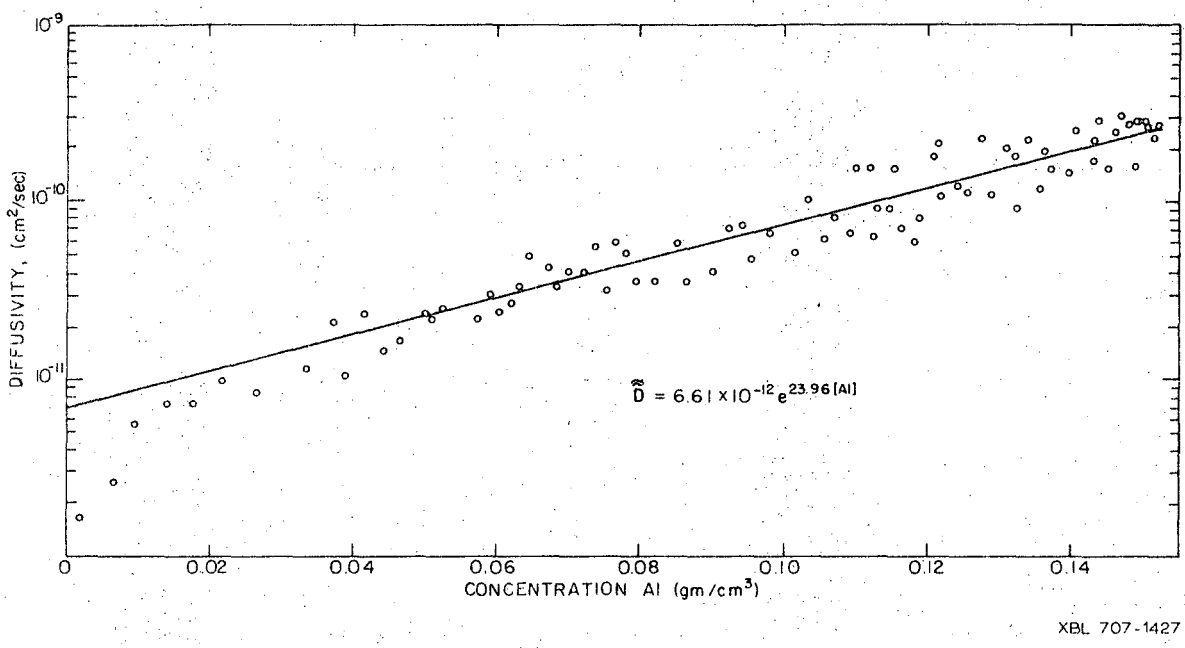

Fig. 28. Plot of computer determined diffusivities vs. concentration for Al_2O_3-SiO_2, 1700°C, 4 days, He.

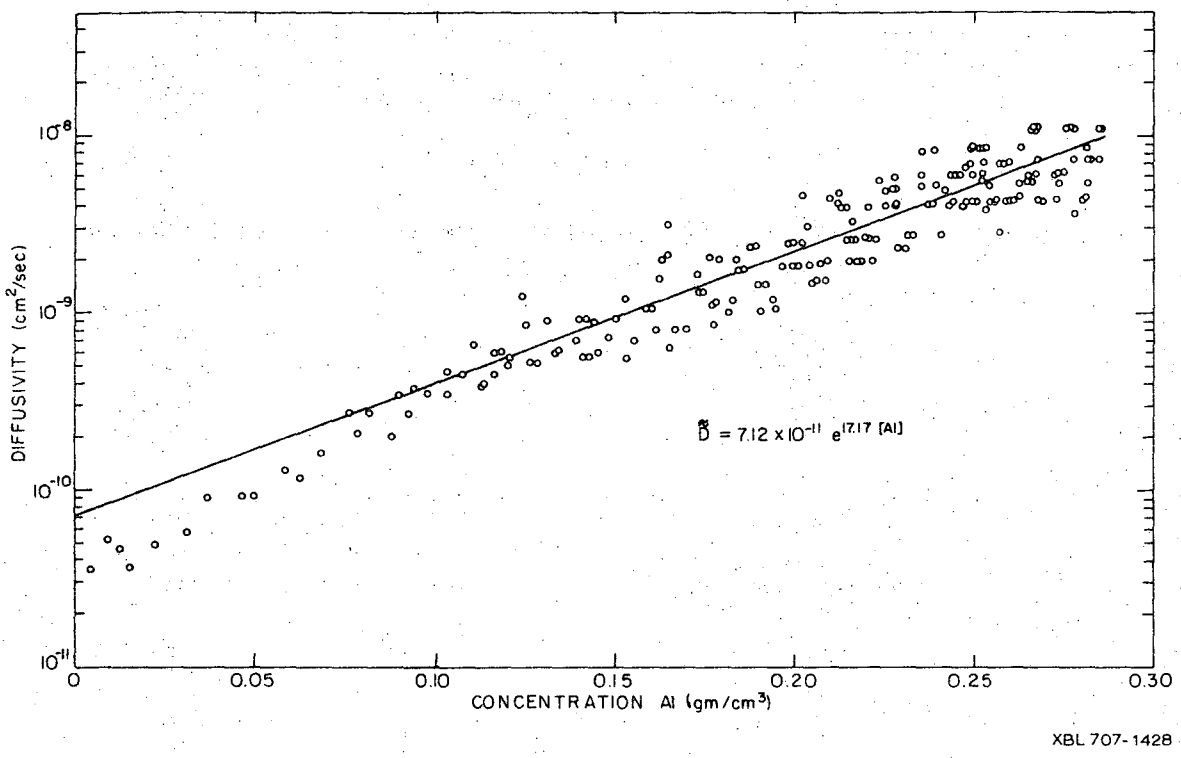

Fig. 29. Plot of computer determined diffusivities vs. concentration for Al_2O_3-SiO_2, 1750°C, 3 days, He.

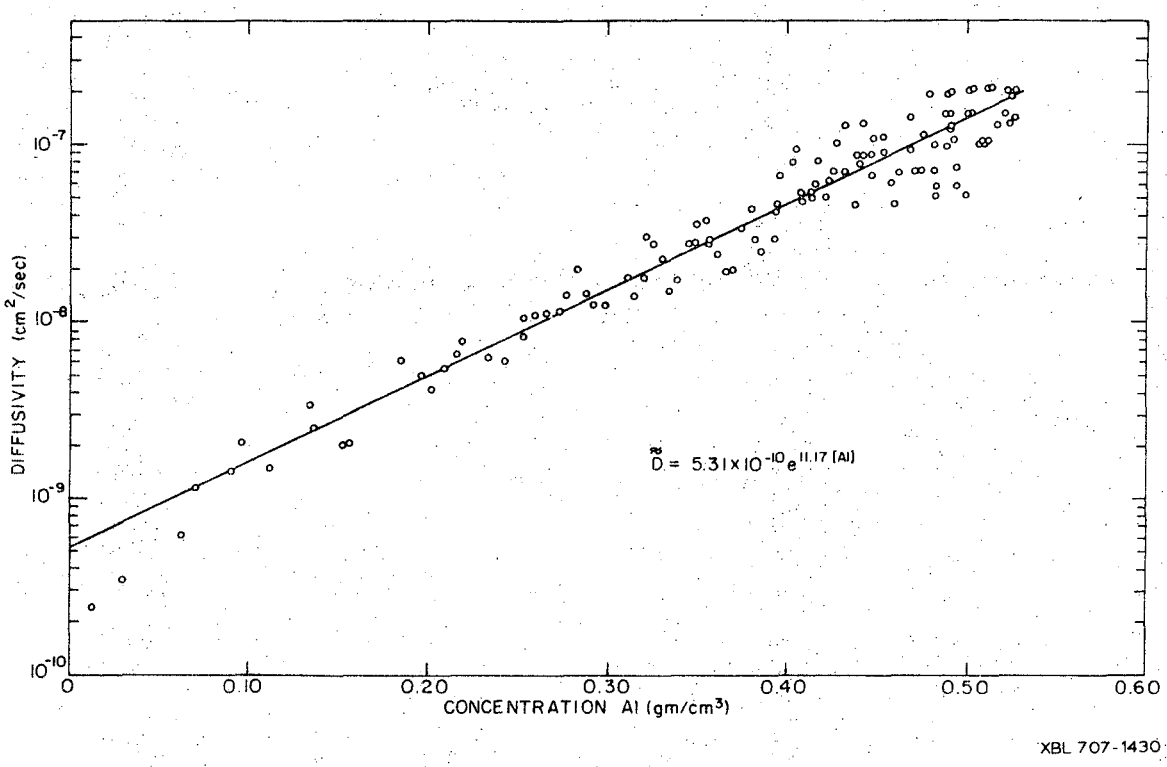

Fig. 30. Plot of computer determined diffusivities vs. concentration for Al_2O_3-SiO_2, 1800°C, 4 hours, He.

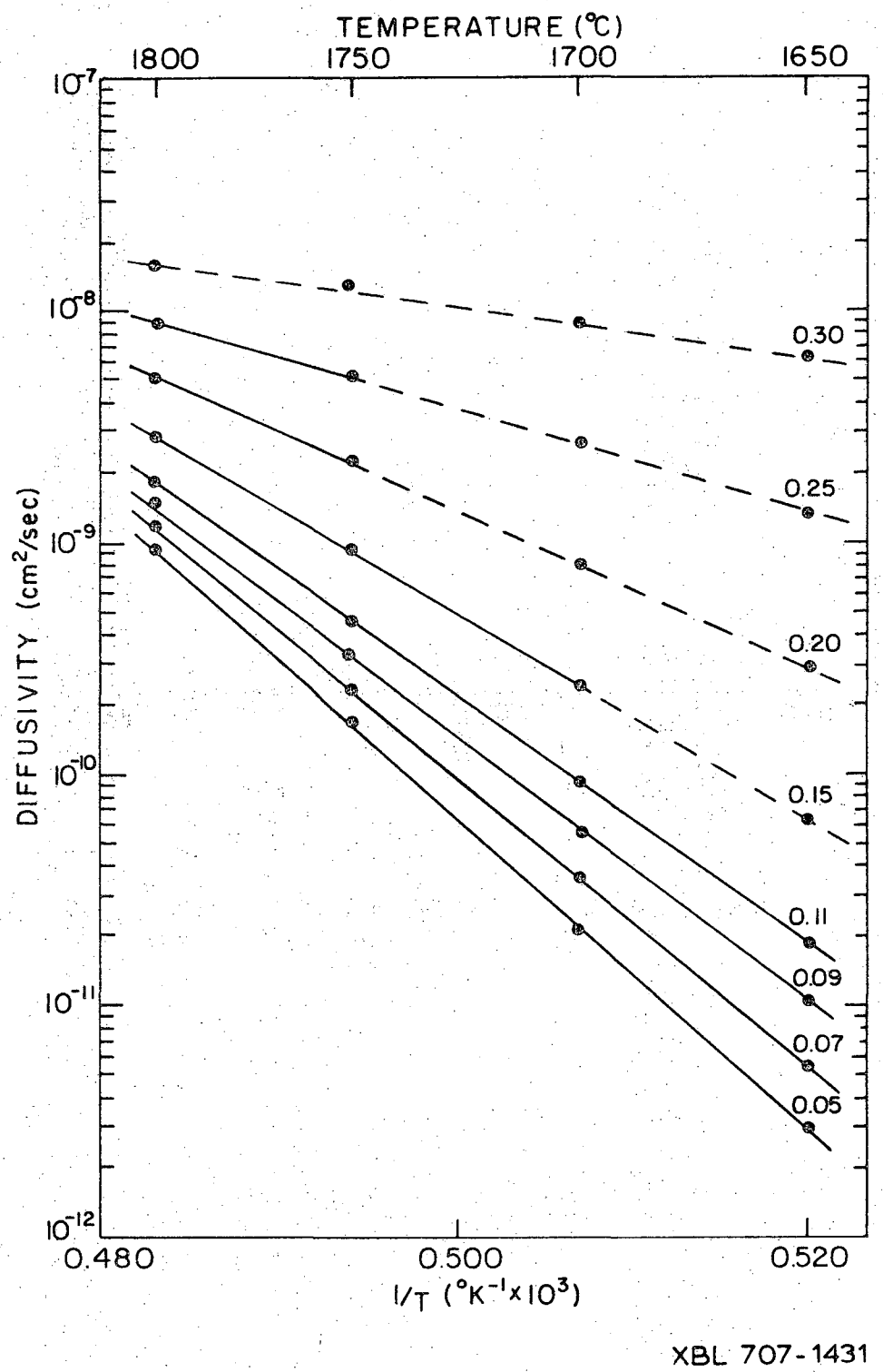

Fig. 31. Diffusivity vs. reciprocal of absolute temperature for eight Al^{+3} concentrations.

These values were found to fall on the extended portions of the straight lines (shown broken in Fig. 31) drawn through the experimental points and were used to calculate D_o and Q.

The results of the Boltzmann-Matano analysis reveal that both the diffusivity and the activation energy vary greatly with the aluminum concentration and temperature. As a result, it was found that the activation energy and the pre-exponential (D_o) values are extremely high at the low aluminum concentrations and decreased with an increase of Al so that at approximately 20 wt % Al_2O_3, the values are similar to those normally associated with interdiffusion in oxides.

To attempt to understand why the diffusion parameters of $\tilde{D}$ and Q are so large at low concentrations of aluminum and steadily decrease with an increase in aluminum composition, one must consider the structure of fused silica, the effect on this structure of increasing amounts of Al_2O_3, and the ionic or molecular species which are likely to be in motion through the glass.

The structural unit of vitreous silica consists of a silicon coordinated by four oxygen atoms at the corners of a tetrahedron. Two tetrahedra are joined at a corner by sharing an oxygen. The orientation of the tetrahedra in space is, however, completely random with the result that the Si-O-Si bond angle is not necessarily 180° as in some crystalline forms of silica, but may range from 180 to 150 degrees or less.

When Al_2O_3 is introduced into this structure, the question of structural position immediately arises. The answer must be primarily inferred from data and conclusions gathered by authors using ternary

glasses, as very little information is available concerning the properties of the glasses in the Al_2O_3-SiO_2 binary system. The interpretation of these studies is, however, subject to conjecture. For example, recent studies have not agreed as to coordination of the aluminum ions in sodium aluminosilicate glasses with Al/Na > 1.0. Isard[37] found that the activation energy for electrical conduction in these glasses shows a pronounced minimum at compositions having this 1:1 aluminum-sodium ratio but increases again as more aluminum is added. He concluded that the size of the oxygen shells around Na increases as AlO_4 tetrahedra are introduced into the network up to the limit Al/Na = 1.0. Beyond this point, aluminum is assumed to go into six-fold coordination as a network modifier allowing the coordination shell of the sodium ion to decrease again. Day and Rindone[18,38] have similarly proposed that all excess Al^{+3} ions in this system go into octahedral coordination. They based their argument on measurements of refractive index, density, infrared absorption, and internal friction, as well as X-ray fluorescence shifts of the aluminum K_α peaks for the glasses in question.

Lacy[39] has subsequently argued from a standpoint of geometry and energetics that AlO_6 octahedra would be unstable in these glasses above the 1:1 ratio and proposed that a proportion of individual oxygen atoms are shared between an AlO_4 group and two SiO_4 tetrahedra. In other words, one oxygen atom tribridges three such tetrahedra for every aluminum-for-silicon replacement to maintain charge balance. This implies that this oxygen is not chemically bonded to the aluminum. Figure 32 is a two-dimensional representation of this "triclustering" of tetrahedra for alumina substitution in fused silica.

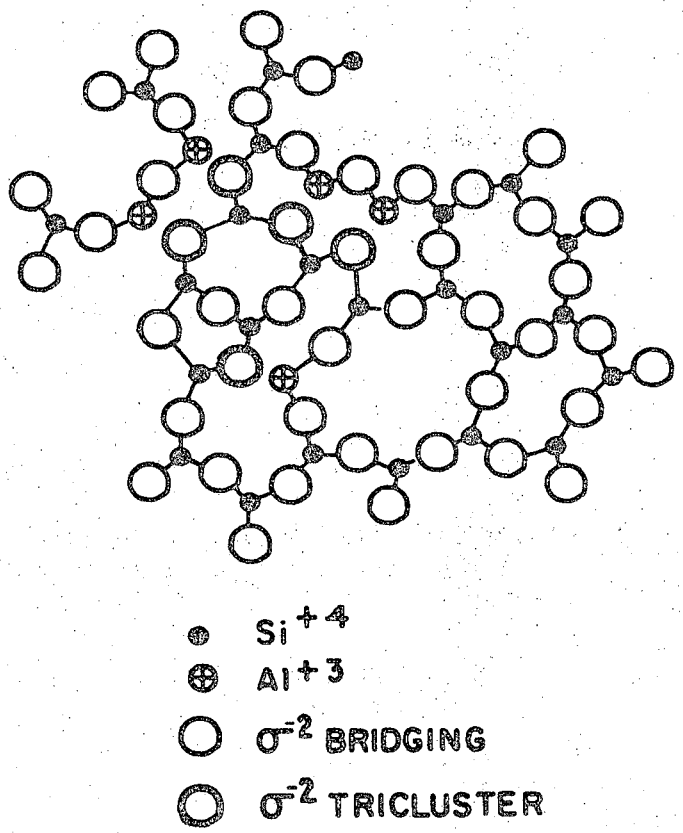

XBL 707-1426

Fig. 32. Two-dimensional structural model showing the triclustering of AlO_4 and SiO_4 tetrahedra.

Heckman, et al.[40] and Terai[41] have incorporated Lacy's arguments into their explanations of the self-diffusion and electrical conductivity in the sodium-aluminosilicate glasses. Terai suggests that the increase in microhardness of these glasses in the composition range Al/Na = 1.0-2.0 is indicative of the disappearance of non-bridging oxygen ions, i.e., the formation of triclusters.

Lastly, Riebling has considered molar volume models as well as viscosity and expansion data and concluded that the best structural model for glasses having Al/Na > 1.0 involves only some of the excess aluminum ions in octahedral environment. He noted that only 50% of the Al^{+3} ions are in six-fold coordination in sillimanite ($Al_2O_3 \cdot SiO_2$) and that a pressure of 22 kilobars was required to force all the aluminum ions into octahedral coordination at 1500°C to form kyanite.

Extending these thoughts to the binary Al_2O_3-SiO_2 system and coupling them with experimental evidence, it is possible to postulate the change in fused SiO_2 structure as Al_2O_3 is added. A portion of this research has involved electron microprobe measurements of the AlK_α and AlK_β wavelength shifts of the 5-40 wt % Al_2O_3 glasses described in Section II. The results of the AlK_α measurements compared to aluminum metal, $AlPO_4$, and Al_2O_3 as standards are given in Table V. They show that at 5 wt % Al_2O_3, the aluminum ions are in tetrahedral coordination. At compositions of 10 wt % and higher, the measurements indicate a definite shift to octahedral coordination. The AlK_β studies gave analogous results for concentrations above 15% Al_2O_3. Below this composition, the very weak X-ray intensity and the large scatter prevented any meaningful analysis. These results give a direct indication of the

Table V. Aluminum coordination data determined from AlK_α X-ray emission spectra. $AlPO_4$ and Al_2O_3 were the 4-fold and 6-fold coordinated standards.

Material	Peak Position Half Height (Å)	Displacement λ from Al Metal
Al	8.3390	0.0000
$AlPO_4$	8.3357	0.0033
Al_2O_3	8.3339	0.0051
5% Al_2O_3	8.3353	0.0037
10% "	8.3340	0.0050
15% "	8.3339	0.0051
20% "	8.3337	0.0053
25% "	8.3339	0.0051
30% "	8.3337	0.0053
35% "	8.3336	0.0054
40% "	8.3336	0.0054

environment of the initial concentrations of the aluminum ion; however, they should be substantiated by other types of research.

Rossin, et al.[42] have measured the high temperature viscosities and activation energies for viscous flow at several compositions in the Al_2O_3·SiO_2 binary system. These viscosity values were extrapolated to the temperatures of the diffusion runs (Table VI) and plotted as a function of the concentration of Al_2O_3 and also the reciprocal of absolute temperature (Figs. 33 and 34). A large and continuous decrease in the viscosity is noted as the amount of alumina is increased. This trend suggests that while the low concentrations of the aluminum ion may

Table VI. Viscosity data of Rossin et al.[42] extrapolated to temperatures of the diffusion anneals.

Composition Wt % Al_2O_3	Log η			
	1650°	1700°	1750°	1800°
0.0	7.14	6.81	6.47	6.16
9.6	5.44	5.11	4.79	4.55
20.0	4.04	3.81	3.60	3.43
31.0	2.78	2.56	2.34	2.16
62.6	11.11	0.97	0.84	0.65

be in AlO_4 tetrahedra, the change in coordination to octahedral is gradual rather than discontinuous as would be inferred from the X-ray emission studies. Lacy[39] has noted that triclusters have a smaller oxygen requirement than a fully connected network (O/Si ratio = 2.0) while AlO_6 groups have a greater one. It is therefore possible that at a certain low Al^{+3} concentration, enough oxygen is made available to initiate the formation of octahedral groups. These deductions are also supported by the continuous increase in density (Fig. 5) and decrease in activation energy for diffusion with higher concentrations of Al_2O_3 (Fig. 35).

In addition, MacDowell and Beall[14] have found that Al_2O_3-SiO_2 glasses having 5 mole % (8.2 wt %) Al_2O_3 or less did not phase separate or crystallize even when cooled very slowly. On the other hand, the 10 mole % (15.9 wt %) glasses showed phase separation even when rapidly quenched. The explanation can be most easily visualized by considering that the structure of sillimanite or mullite consists of an ordered

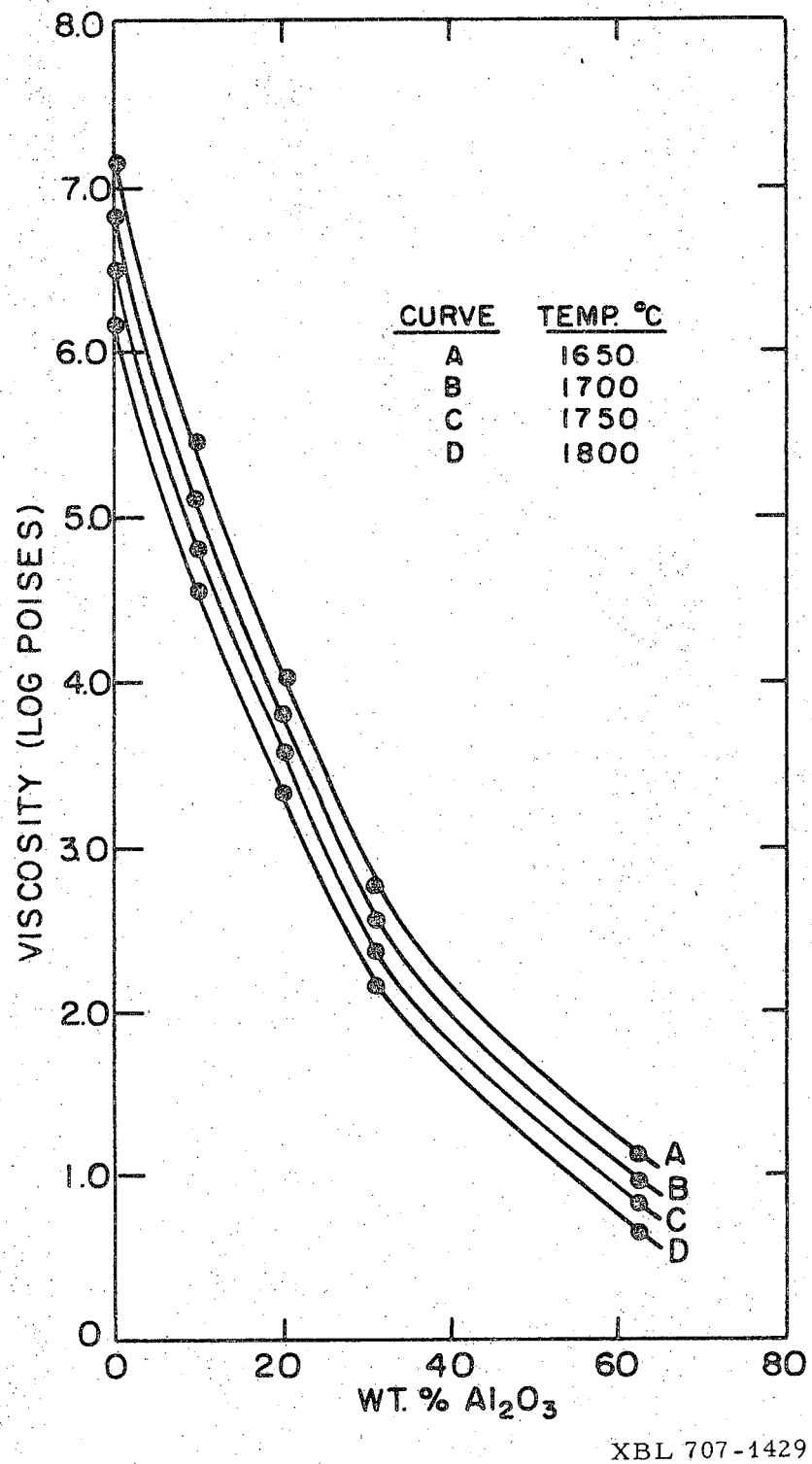

Fig. 33. Curves of viscosity vs. Al_2O_3 concentration for the temperaures of the diffusion anneals.

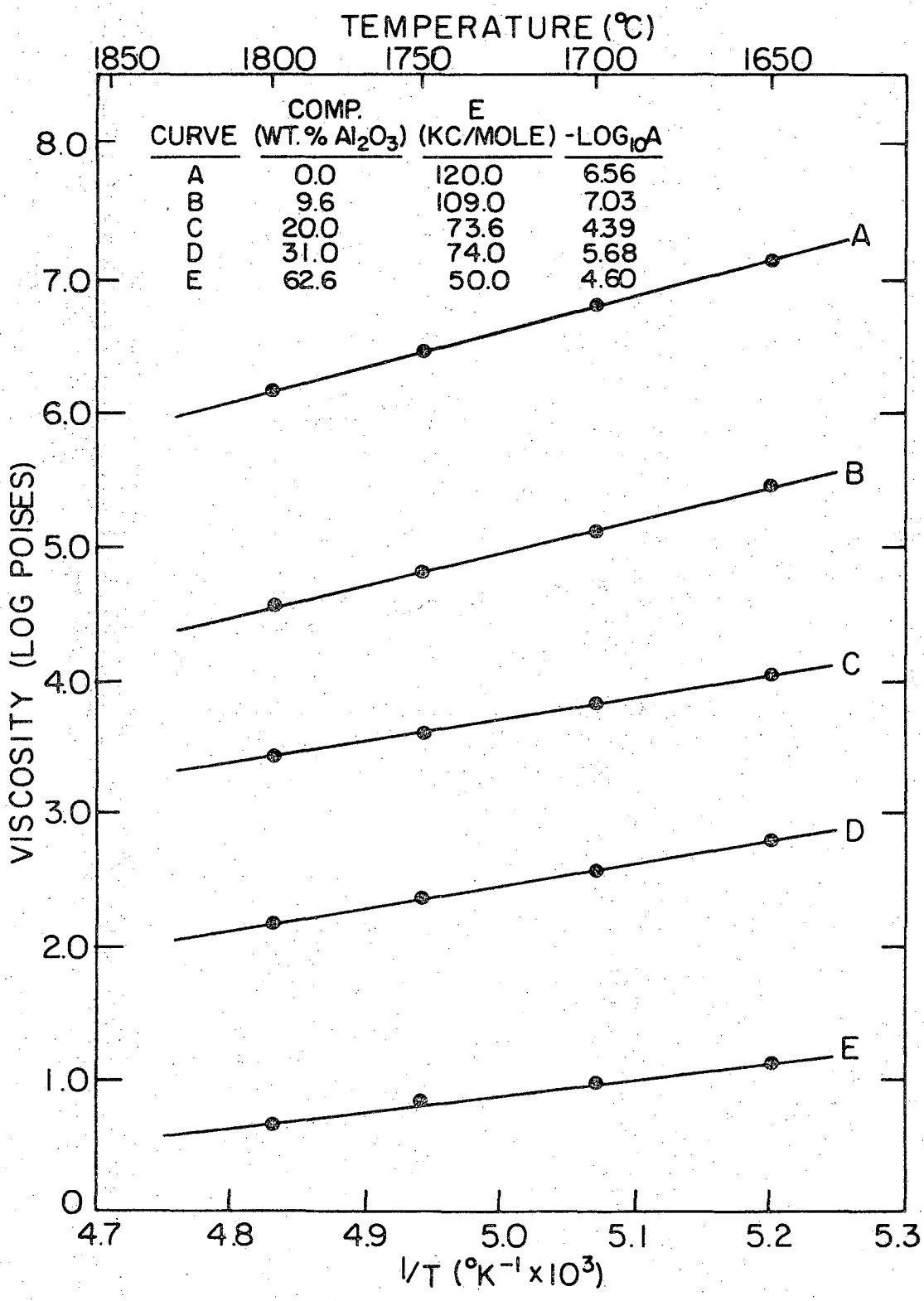

Fig. 34. Plots of viscosity vs. 1/T for five concentrations of Al_2O_3 in SiO_2.

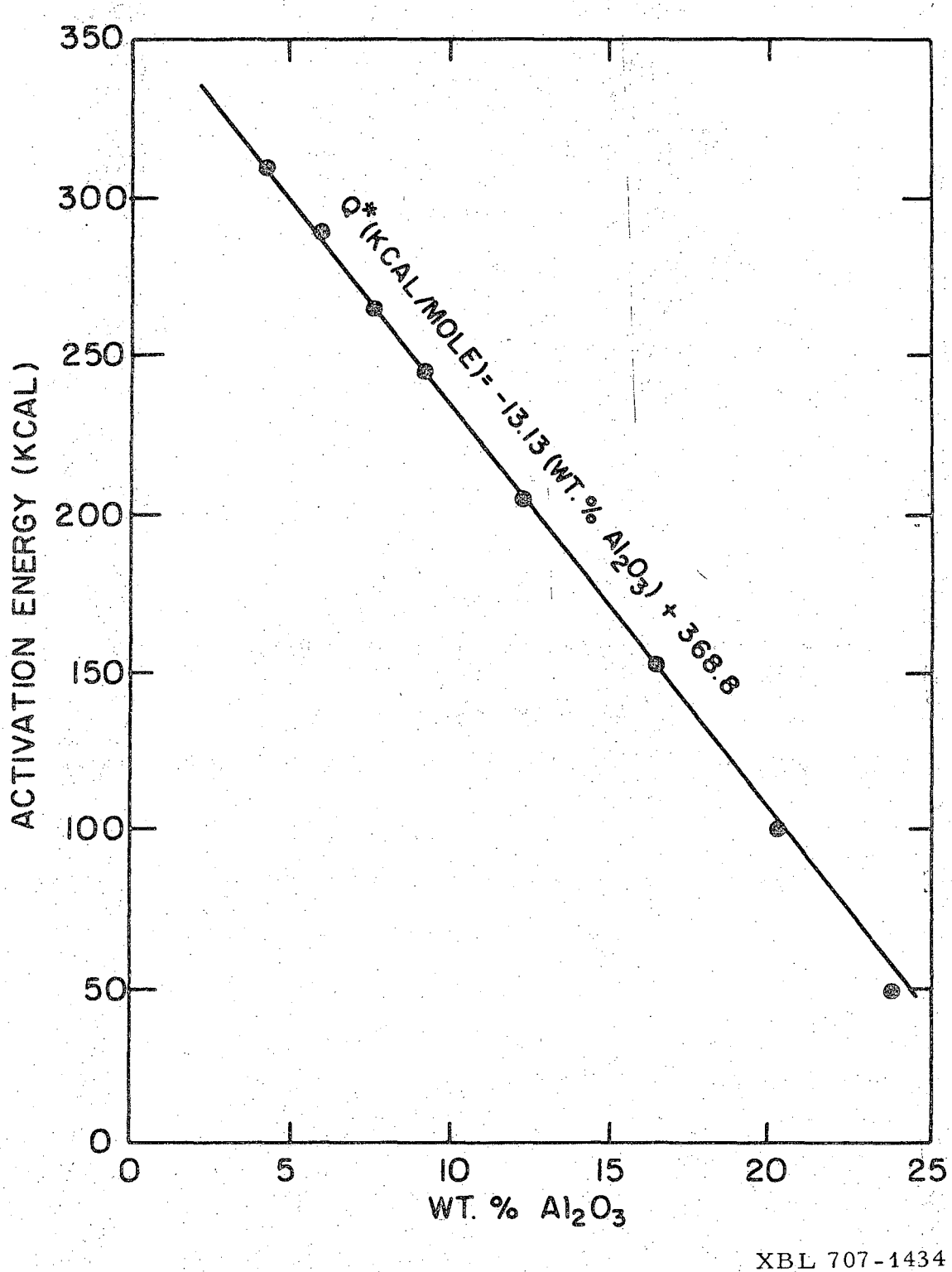

Fig. 35. Curve of activation energy for diffusion vs. Al_2O_3 concentrations.

distribution of four-and six-coordinated aluminum and four-coordinated silicon atoms. The structural backbone can be considered to be composed of infinite chains of edge-shared AlO_6 octahedra. This mixed oxygen coordination can be assumed to exist in the aluminosilicate glasses, particularly those with higher Al_2O_3 content. When phase separation occurs, one can thus speculate that the octahedral portion of the aluminum ions plays the major role in forming the dispersed glass phases.

This reasoning is supported by the knowledge that an analogous coordination change occurs in titanium dioxide when it is added to a glass composition. Weyl[43] has shown that at high temperatures, the Ti^{+4} ion may assume a coordination of four compatible with the SiO_2 network and miscible in the melt. During cooling of the melt, the tendency will be for the titanium ions to assume the equilibrium coordination number of six, be displaced from the silicate network, and appear as a separate phase or in combination with other modifying oxides. This phase separation created by TiO_2 is the basis of almost all glass-ceramic reactions. By comparison, Al_2O_3 with its lower radius ratio is even more likely to assume tetrahedral coordination, especially at high temperatures. However, its +3 valence and high field strength ($\frac{Z}{r^2} = 12.0$) also encourages octahedral coordination and subsequent competition with SiO_2 to form a second phase.

From the above results and theories, the following hypotheses can be made concerning the structure of the aluminosilicate glasses.

(1) Al_2O_3 is incorporated into the fused SiO_2 structure at low temperatures with Al essentially in four-fold coordination up to a concentration of approximately 9 wt % Al_2O_3. This configuration occurs

through the formation of triclusters composed of one AlO_4 and two SiO_4 groups tribridged by an oxygen ion. A continuation of this structure produces a tightening of the tetrahedral rings (two-dimensional) or cages (three-dimensional) of the SiO_2 glass and results in a high energy configuration.

(2) As the Al_2O_3 concentration is increased, this high energy condition is alleviated by the formation of AlO_6 octahedral groups. This, in turn, permits the formation of normal AlO_4 tetrahedral groups, if necessary. It is the author's thinking that the continued addition of Al_2O_3 and formation of the AlO_6 groups loosens the structure permitting more AlO_4-SiO_4 triclusters to form silumtaneously as well. Nazarenko[44] has shown that the formation of Al-O-Al bonds is favored over the Si-O-Al structure by increasing temperature, particularly above 1600°C. The shape of the diffusion profiles in Figs. 11 and 12 suggests nonideality which is probably positive in nature due to the formation of Al-O-Al bonds. This also indicates that the AlO_4 and AlO_6 groups occur in close proximity to one another rather than randomly throughout the glass. The structural arrangement would thus be analogous to that of mullite or sillimanite with short range order. The reason that the K_α studies revealed a sharp change from tetrahedral to octahedral coordination at 10 wt % Al_2O_3 rather than a gradual shift in the peaks, is probably due to the limitations of the instruments and analysis.

(3) As mentioned above, the glass structure which forms at the higher Al_2O_3 concentrations is probably a randomized version of mullite. The fact that mullite crystallizes on cooling to form the "2:1" composition points directly to the initial formation and continued existence

of aluminum in four-fold coordination.

In conclusion, it is interesting to note that Aramaki and Roy[28] found that heat treatment of both $3Al_2O_3 \cdot 2SiO_2$ and $2Al_2O_3 \cdot SiO_2$ mullite compositions increased the a and c cell parameters. This is again a reflection of the Al-Si disorder which can occur at high temperatures.

D. Mechanisms of Diffusion

With this background on the coordination of the aluminum ion, it is of interest to postulate some mechanisms of diffusion and the nature of the diffusing species.

In a search of the literature on related studies, it is revealed that Sucov[5] has employed the stable isotope ^{18}O and mass spectrometer analysis to determine the diffusivity of oxygen in fused silica over the temperature range 925-1225°C. He concluded from the 71 Kcal/mole activation energy that the oxygens participating in the diffusion must be singly bonded to silicon and move through the interstitial voids of the glass. Sucov noted that these oxygens would, by necessity, be those which coordinate the various impurities and contribute to the creation of defects, just as in the case of multicomponent glasses, rather than bridging oxygens which furnish continuity to the fused silica network. Extrapolation of his diffusivity values to the temperature range of interest in this research gives values which are close to those measured for aluminum (Fig. 36). Thus, it is possible to hypothesize the movement of an Al_xO_y complex.

Kingery and Lecron[45] using a 20 $Al_2O_3 \cdot 40$ $CaO \cdot 40$ SiO_2 glass have supported Sucov's argument that the oxygen ion can move independently of silicate groups. This opinion was deduced from the fact that Q for

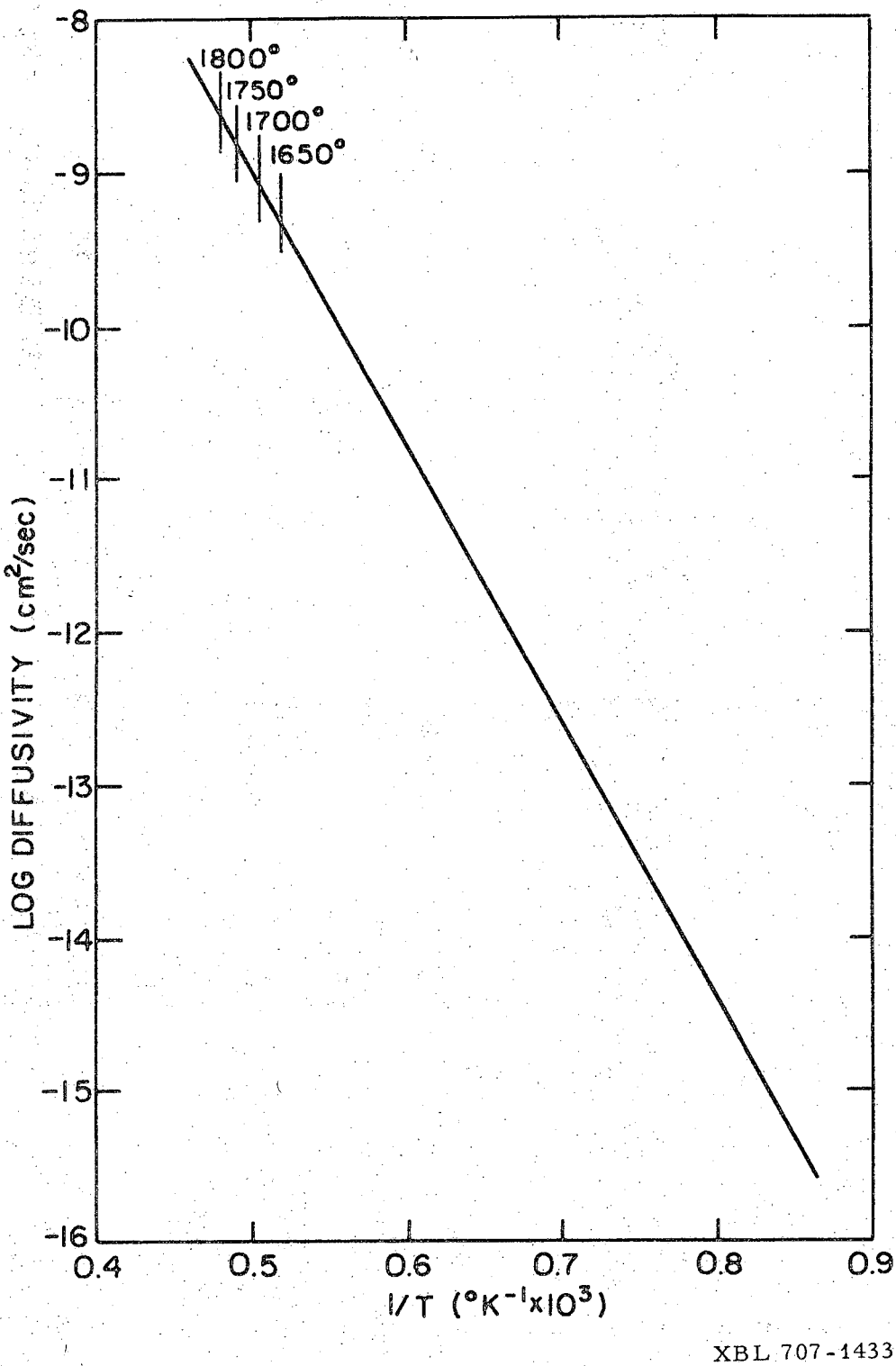

Fig. 36. Extrapolation of low temperature data for the diffusivity of oxygen in fused SiO to the temperature range of this research.

oxygen diffusion was 1/2 Q for viscous flow. These authors' views are not, however, without their opponents.

King and Koros,[46] using the same calcium aluminosilicate glass, have found higher diffusivity and activation energy values for oxygen than for the cations, as shown in Table VII below. They ruled out the movement of single oxygen ions since they would be primary contributors to electrical conduction.

Table VII. Values of Diffusivity and Activation Energy for Ca, Si and O from King and Koros[46]

Atom Type	D (cm^2/sec)	Q (Kcal/mole)
Ca	10^{-6}	70
Si	10^{-7}	80
O	4×10^{-6}	95

Towers and Chipman,[47] in earlier research on this glass, have shown that the activation energy for diffusion of the calcium ion is much higher than that for conduction and agree with King and Koros that the movement of calcium also involves the oxygen ion as well.

Doremus[2] has countered this reasoning with the argument that King and Koros measured the diffusivity of "dissolved oxygen," (i.e., oxygen which is introduced from a gas phase and diffuses as a molecule), while Kingery and Lecron measured the diffusivity of lattice oxygen. This author feels that Doremus is incorrect, since the actual experimental setup of Kingery and Lecron involved the incorporation of ^{18}O from an oxygen gas phase while that of King and Koros was the capillary effusion

method in which the ^{18}O is incorporated directly into a silicate.

Reed and Barrett[48] have also refuted Doremus' conjecture by showing that in a real Ca, Si, and O concentration gradient, the diffusion rate of oxygen must be controlled by the calcium migration rate. Also, the oxygen must be partially covalently bonded to Al^{+3} and Si^{+4} ions at all times or it will again contribute to electrical conductivity.

In reference to this last statement, Towers and Chipman[47] and King and Koros[46] also found $D_{Si} = 1/10\ D_{Ca}$. Furthermore, the work of Bockris, et al.[49] seems to indicate that the diffusing species is not an ion of charge +2 or +4 because of transport numbers. The diffusion of silicon would, therefore, appear to be something other than simple cationic movement. A mechanism involving the rupture of two of the bonds by which a SiO_4 tetrahedra is held to the silicate network or to a large ion would permit movement of two oxygens along with the silicon resulting in no net transfer of charge. The addition of oxygen ions to Si would make the diffusion coefficient of oxygen only two or three times that of the cations instead of more than an order of magnitude. Other considerations are the large energies required to move silicon and aluminum from their lattice positions (105 and 80 Kcal/mole, respectively) and the low conductivity of these ions in glasses.[49] Thus it suggests that neither Si^{+4} nor Al^{+3} exists in a free state in glasses.

This background information, although differing in results and conclusions, is useful in a discussion of the nature of diffusion in the Al_2O_3-SiO_2 system. As discussed above, the fact that the extrapolation of the oxygen diffusivity data reported by Sucov[5] coincides with the diffusivity of aluminum at the higher concentrations is a direct

indication of the concurrent movement of both aluminum and oxygen in this system. Considering that the oxygen data is obtained from the singly bonded oxygens surrounding the impurities in fused SiO_2, it is quite likely that the value of the diffusivity of a doubly bonded or bridging oxygen is close to that measured for the low alumina concentrations.

Coupling these ideas with the facts of high bond strength and viscosity, one is drawn to the conclusion that the diffusion in the binary glass is a cooperative movement of large oxygen-containing aluminum and silicon complexes. As Al_2O_3 (or mullite) enters the fused silica structure, the oxygens must adjust to form the glass configuration--an entity which is also in a state of constant change. With the movement of the Al complex along the concentration gradient, there must be a corresponding flux of the Si complex toward the interface. These complementary movements may be viewed on the molecular scale as viscous masses progressing through the fused silica structure in a type of ring mechanism of diffusion in which several bonds must be broken and the structure (particularly that of oxygen) rearranged to allow the movement of each species.

This species which effects the diffusion through the glass becomes progressively smaller with the onset of AlO_6 octahedra formation and the corresponding formation of non-bridging oxygen. This is noted in the decreased activation energies for diffusion and viscosity with increasing Al_2O_3 content. No attempt was made to directly relate viscosity and diffusivity values to the size of the mobile species by the use of the Stokes-Einstein equation. Doremus[2] and others have observed that while phenomenological comparisons are valid to an extent, particularly in

liquids, no exact correlation exists between the diffusion coefficients or their temperature dependence and the viscosities of noncrystalline silicates. A detailed interpretation of the diffusion process in terms of the activation energy was not attempted, for as Samaddar, et al.[50] have pointed out, the liquidus composition and consequently the driving force for the diffusion process changes with temperature. With this change, there will be corresponding changes in the effective diffusion coefficient with temperature which are more complex than any activated process alone. The diffusion coefficients in silicate systems depend greatly on the composition and liquid structure. All these factors combine to make interpretation of dissolution behavior on the basis of activation energy rather ineffective.

Finally, an attempt has been made to indirectly measure the diffusion coefficients of Al^{+3} in the interfacial mullite formed at the higher temperatures utilizing the mathematical scheme described in Section III. The averages of these results are reported in Table VIII and plotted on a partial graph of the diffusivities of Al^{+3} in glass versus 1/T in Fig. 37.

Table VIII. Experimental data for the calculations of diffusivity of Al^{+3} in mullite

Temperature (°C)	$\frac{C_c - C_{II,I}}{C_{II,I} - C_o} = F(\gamma)$	γ	γ^2	$D = \frac{\chi^2}{4\gamma^2 t}$ $\frac{cm^2}{sec}$
1650	7.46×10^{-2}	.191	.03648	6.90×10^{-12}
1700	7.46×10^{-2}	.191	.03648	1.52×10^{-11}
1750	7.46×10^{-2}	.191	.03648	1.79×10^{-11}

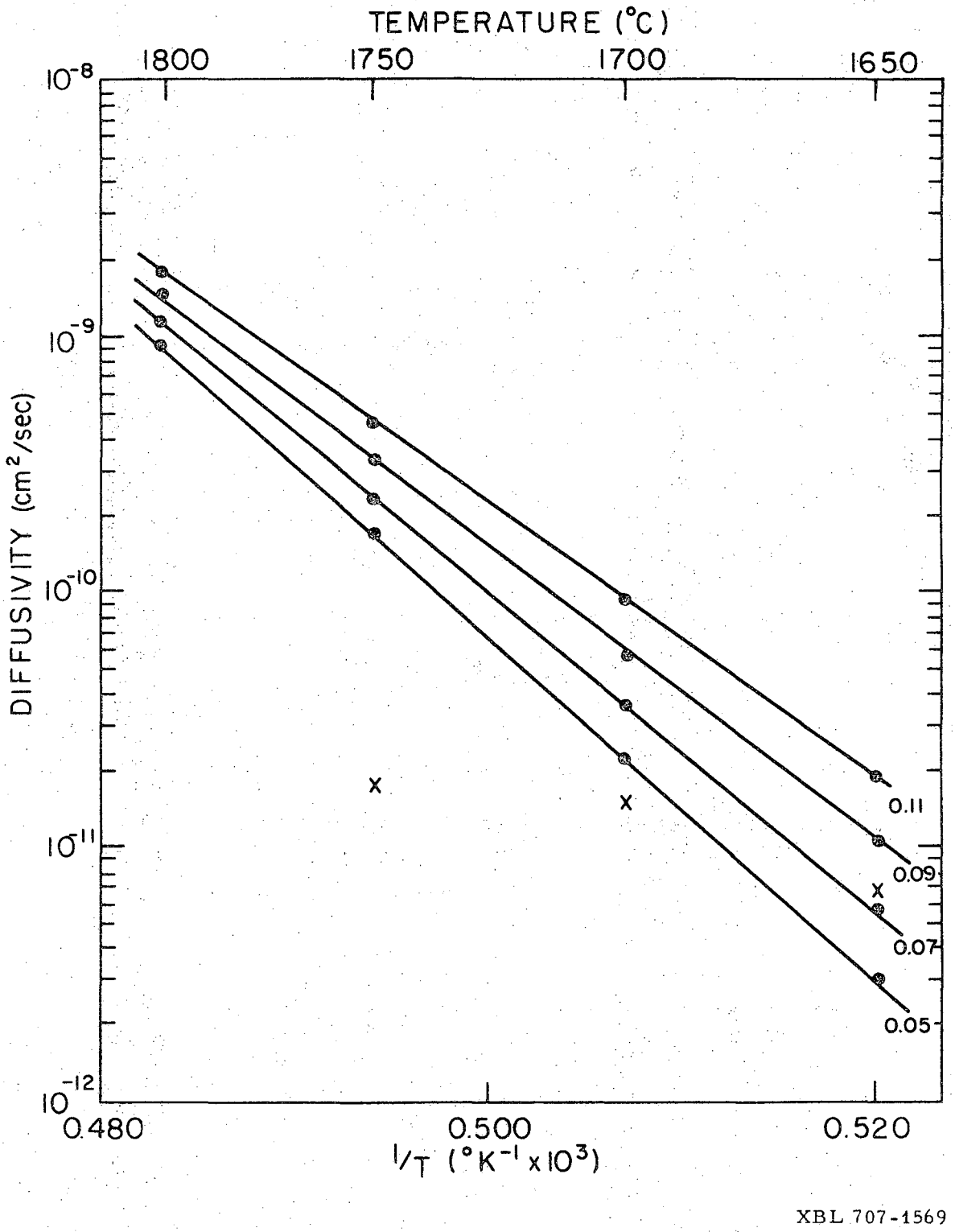

Fig. 37. Points of hypothetical mullite diffusivity (X) superimposed on diffusivity curves of Al^{+3} for four concentrations in the glass.

Also, the flux density values of Al^{+3} in the interfacial liquid composition are greater than in mullite. Furthermore, the difference in these values, as well as those of aluminum diffusivities in mullite and the interfacial liquid increases with temperature. Kidson[34] has shown, however, that the growth of mullite to an observable thickness is dependent on a higher flux density in the mullite than in the liquid at the interface.

This discrepancy can be explained on the basis of the nature of the diffusing species. In the mullite there is an interdiffusion of Al^{+3} and Si^{+4} cations, while in the liquid, the species must be some aggregate complex which includes oxygen ions as well as cations acting as a unit. The concentration gradient of such species would be less than that for Al^{+3} based on the Al-concentration profile, and would also be dependent on the size of the diffusing species. Therefore, the flux densities of the diffusing complex would also be less and actually less than that in the mullite above about 1634°C. The increasing thickness of mullite with temperature for a given time also suggests that the size of these polyionic species changes with temperature. This behavior may be due to a lesser tendency for the formation of AlO_6 octahedra and, thus, nonbridging oxygens because of the lesser tendency for liquid immiscibility as shown by MacDowell and Beall.[14]

Of interest also, is the possibility of determining the activation energy for growth of mullite and thus the activation energy for chemical interdiffusion in mullite. The value of about 220 Kcal/mole determined from measurements made on sapphire-fused silica couples is an apparent activation energy since there is a competitive process of dissolution of

mullite by the liquid. Therefore, it is necessary to set up diffusion couples in which only the growth of mullite occurs. This condition is achieved by using liquids saturated with Al_2O_3 for corresponding temperatures. In this study only one liquid was prepared which contained 15 wt % Al_2O_3. This glass was used with sapphire in diffusion couples at 1650°, 1700°, 1750°C. The liquidus curve determined in this study shows that this liquid is saturated with Al_2O_3 at about 1680°C. This situation creates a condition of some dissolution of mullite into the liquid at 1700° and 1750°C and of some additional growth at 1650°C. A lower limit of activation energy of 125 Kcal/mole can be possibly established by assuming that the mullite thickness values at 1650° and 1700°C are correct within experimental error. On the other hand, if it is assumed that the measured $\tilde{D}$ for 1650°C is high and that for 1700°C is low, then the activation energy value would be larger and may correspond to the value of about 177 Kcal/mole obtained in creep experiments on mullite.[51]

V. SUMMARY AND CONCLUSIONS

The kinetics and mechanisms of the diffusion processes which occur between silica and alumina (sapphire) or mullite have been determined and correlated with the results of supplementary experiments and the findings of previous authors. The reaction between these materials involves the formation of mullite at the interface (sapphire-silica couples only) and the dissolution of this phase by the diffusion-controlled movement of an aluminum-rich oxygen-containing species through a silica-rich liquid. The aluminum concentration versus distance profiles are similar for the sapphire-silica and mullite-silica couples annealed at 1650°C in air and helium. This behavior indicates that the diffusion process is not controlled by reaction at the interface or affected by the surrounding atmosphere. The solid solution range of the interfacial mullite extends from 70.5 to 73.5 wt % Al_2O_3. This range agrees within experimental error with the values determined by Aramaki and Roy.[28] The composition zone on cooling from 1800°C is 74 wt % Al_2O_3; whereas $2Al_2O_3 \cdot SiO_2$ has 77.3 wt % Al_2O_3. This difference indicates that the "2:1" mullite may have a solid solution range and that its composition on crystallization is a function of the total alumina concentration in the liquid.

The experimentally determined interfacial compositions describe a revised liquidus curve which is indicative of a rather high rate of silica evaporation as well as the existence of a liquid immiscibility region. This curve was extended below the eutectic temperature due to the presence of a metastable amorphous phase at the diffusion couple interface. A single eutectic nonequilibrium phase diagram is postulated for cristobalite-sapphire couples to explain the appearance of this

initial liquid phase. The formation of the liquid or its initial presence (fused silica-sapphire couples) immediately leads to the subsolidus nucleation of mullite on the sapphire surface. This nucleation process is rapid so that, as theoretical arguments show, a "mullite complex" continues to form at the interface even at subsolidus temperatures where the rate of dissolution of mullite by the liquid becomes more rapid than the growth rate. Once a liquid is formed, the dissolution of cristobalite occurs by diffusion of the Al-O species toward the silica-rich zone. Cristobalite is, thus, unstable in liquids containing Al_2O_3 contents greater than that indicated by the SiO_2-liquidus curve in the phase diagram.

Above the eutectic temperature, the formation of a stable liquid occurs, and mullite readily grows to an observable size above approximately 1634°C if the specimens are held at temperature for a sufficiently long time. In this case, the rate of overall growth of the mullite surpasses its solution rate in the liquid phase.

The apparent chemical interdiffusivities of the aluminum ion in the liquid phase vary greatly with concentration and temperature. As a result, the apparent activation energy and the pre-exponential (D_o) values are extremely high at low aluminum concentrations and decrease as more Al_2O_3 is taken into the glass.

The interpretation of these results is based on an attempt to understand both the structural changes which occur as the Al_2O_3 concentration in fused silica increases and the nature of the diffusing species. The aluminum coordination measurements were performed and the results compared with additional physical property data reported by previous

researchers. It is postulated that the Al_2O_3 is incorporated into the silica structure to approximately 9 wt % through the formation of triclusters composed of one AlO_4 and two SiO_4 groups tribridged by an oxygen ion whose charge is satisfied only by the coordinating Si ions. As the Al_2O_3 concentration increases, AlO_6 octahedra develop which simultaneously allows the formation of normal AlO_4 tetrahedra. The glass structure thus gradually becomes analogous to that of mullite or sillimanite with short range order. At higher temperatures there is some evidence that Al begins to develop a preference for a tetrahedral coordination.

It is concluded that the diffusion process in the binary glass is a cooperative movement of large oxygen-containing aluminum and silicon complexes through the fused silica structure in a type of ring mechanism. The formation of AlO_6 octahedra and corresponding non-bridging oxygens creates progressively smaller diffusion species in the glass indicated by the gradual decrease in activation energy and viscosity with an increase in Al_2O_3 concentration. Correspondingly, the size of the species also changes with an increase in temperature at a given concentration because of an increase of tetrahedrally coordinated Al.

Calculations of the diffusivities and flux densities of the aluminum ion in the mullite layer formed at high temperatures result in lower values than those found for the aluminum movement at the liquid interface. This behavior is contrary to the requirement for mullite growth but supports the hypothesis that polyionic species are diffusing in the liquid rather than single ions.

ACKNOWLEDGMENTS

I wish to express my appreciation to Professor Joseph A. Pask for his guidance and helpful criticism throughout this research. I wish also to thank Dr. John Dorn for his constructive suggestions concerning mathematical procedure, Mr. George Dahl for polishing the many samples, Mr. George Georgakopoulos for instruction and help with the electron microprobe, Miss Kelly Radmilovic for typing the thesis, and my fellow colleagues, especially Dr. Marvin Appel and Mr. Ilhan Aksay, for their valuable discussions of the problems at hand.

I especially acknowledge the patience and encouragement of my wife, Jan, which have contributed to the completion of this work.

This work was supported by the Edward Orton Jr. Ceramic Foundation and the United States Atomic Energy Commission.

APPENDIX I

Table IX. Spectrographic analysis of sapphire, amersil, and cristobalite

Spectrographic analysis of Union Carbide alumina single crystals, Englehard Co. "Amersil," and Georgia Institute of Technology Experimental Station cristobalite reported in weight percent of the oxides of the impurity elements indicated. "P.C." indicates "Principal Constituent."

Impurity	Sapphire	Amersil	Cristobalite
Al	P.C.	.045	0.230
Ba	0.001	-	0.001
Na	0.050	-	0.080
Ca	0.001	0.0005	0.020
Mg	0.0005	0.0007	0.008
Fe	0.004	0.015	0.092
Sn	0.005	-	0.001
B	0.005	-	0.010
Mn	-	-	0.001
Cu	0.0005	0.0005	0.001
Ti	0.001	-	0.028
Si	0.210	P.C.	P.C.
Total impurities	.2880	0.0617	0.472

Analysis performed by American Spectrographic Laboratories, San Francisco, California.

Table X. Chemical analysis of mullite

Carborundum Corporation fused ingot cooled from the melt. Reported in weight percent of the oxide as an average of three separated runs.

Oxide	Percent
Al_2O_3	78.34
SiO_2	23.50
CaO	0.02
Fe_2O_3	0.16
Na_2O	0.28

Analysis performed by Coors Spectro-chemical Laboratory, Golden, Colorado.

APPENDIX II. The Decomposition of Mullite

The discovery of the decomposition of mullite at low oxygen pressures has led to a separate qualitative study of this reaction on the surface of cleaned and highly polished mullite squares having a molar composition of $2Al_2O_3 \cdot SiO_2$. A search of the literature reveals that this reaction is virtually unknown among researchers working with the Al_2O_3-SiO_2 system. Skola,[52] using X-ray analysis and optical microscopy, reports that pure synthetic mullite was partially decomposed when heated between graphite plates in a carbon resistance furnace at 1700°C since approximately 5% corundum was detected in the mullite residue after four hours.

Wright and Wolff[53] discovered that mullite bricks were severely attacked by reducing agents above 1370°C in a natural gas cracking plant. In the zone of greatest attack, a covering of porous corundum was found. They concluded that SiO_2, free or combined in the mullite, was reduced to SiO by carbon deposited from the cracked methane. The free SiO then re-oxidized elsewhere or reacted with the corundum left by the first reaction to reform mullite. This reasoning suggests that the graphite plates used in Skola's experiments acted as a reducing agent and contributed to the formation of corundum.

The author's research concerning this decomposition was prompted by the formation of gas bubbles in the fused silica when heated in He with mullite to form a diffusion couple. The initial work was, therefore, conducted at low oxygen pressures for several different times at the temperatures of the diffusion runs. The heating schedule included a rapid heating and cooling cycle with a one-hour intermediate heating step at 1200°C. The mullite pieces were not covered; thus the oxygen pressure in the

furnace was determined by the tantalum heating element and shields, as discussed below.

The results, as determined by X-ray diffraction and photography were similar to those of previous investigators, i.e., an alumina powder formed on the surface in greater amounts with time at temperature and increased with temperature at constant time, as shown in Figs. 38, 39, and 40. X-ray analysis revealed only Al_2O_3 on the surface after heating for 12 hours at all the temperatures of this research. In contrast, corresponding anneals conducted in air produced almost no decomposition even after 11 days at 1650°C (Fig. 40f).

The photographs reveal that the reaction is most intense on those crystals which appear dark (actually clear) in the unheated mullite (Fig. 38a). As heating time, and therefore the formation of alumina, increases, it can be seen that the boundaries of some of these crystals have reacted more extensively than have the crystals themselves.

To explain the mechanism of this decomposition, several reactions were proposed and their equilibrium constants evaluated at 1900°K (1627°C). Only those reactions which contained Al_2O_3 as a product in solid form had equilibrium constants high enough to be considered as the principal decomposition reactions. It should be noted that the calculations for this and the following data were conducted using mullite of a $3Al_2O_3 \cdot 2SiO_2$ composition, as data for the 2:1 composition is not available. However, there is thought to be little difference in the results, since the crystal structures are similar and the differences in composition are not large. The reactions considered to be governing the decomposition process are

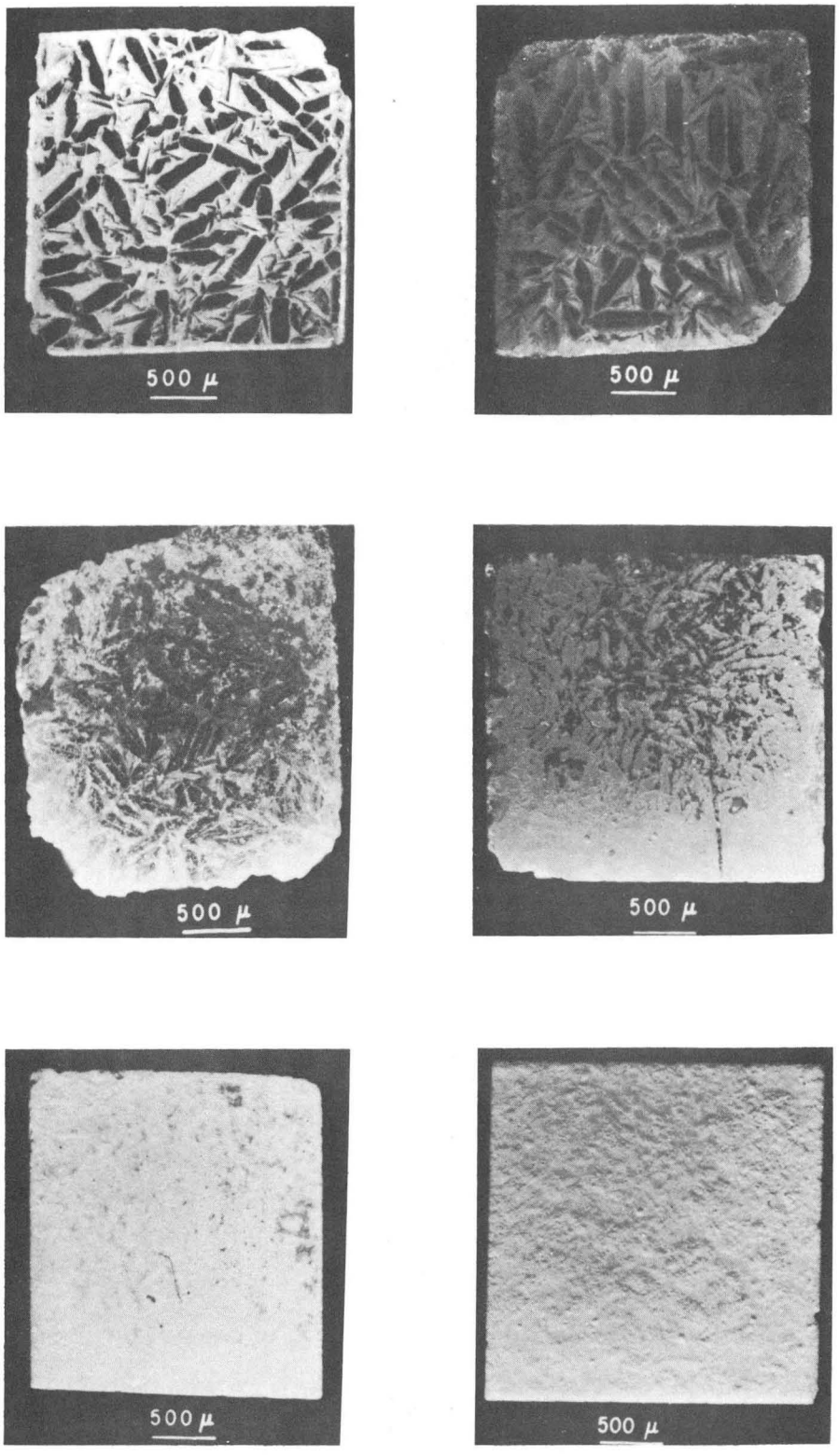

XBB707-3068

Fig. 38. Microstructure of mullite pieces fired in helium at 1700°C for (a) unfired, (b) 30 min., (c) 1 hr., (d) 3 hr., (e) 6 hr., (f) 12 hr.

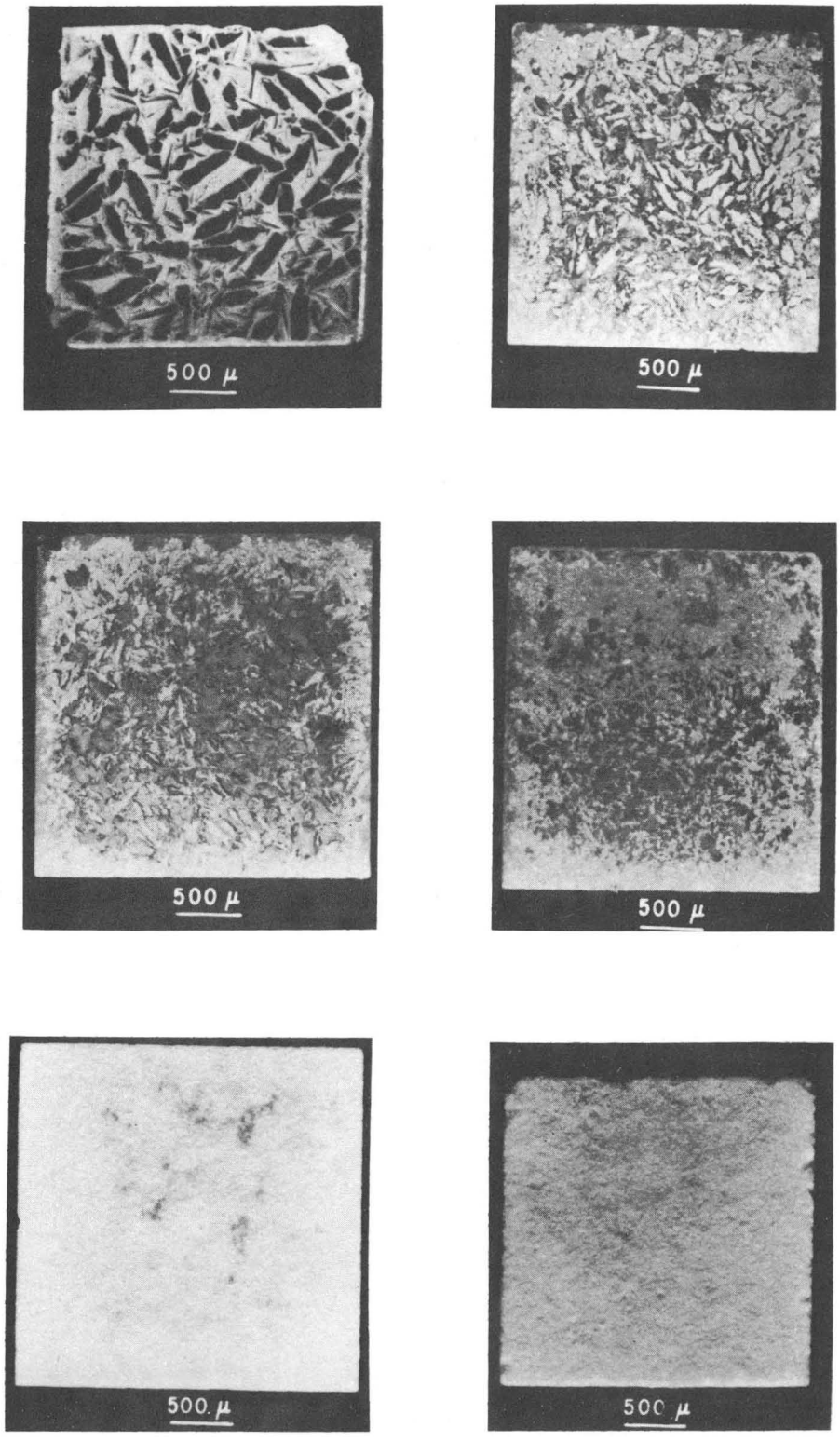

XBB707-3066

Fig. 39. Microstructure of mullite pieces fired in helium at 1700°C for (a) unfired, (b) 30 min., (c) 1 hr., (d) 3 Hr., (e) 6 hrs., (f) 12 hr.

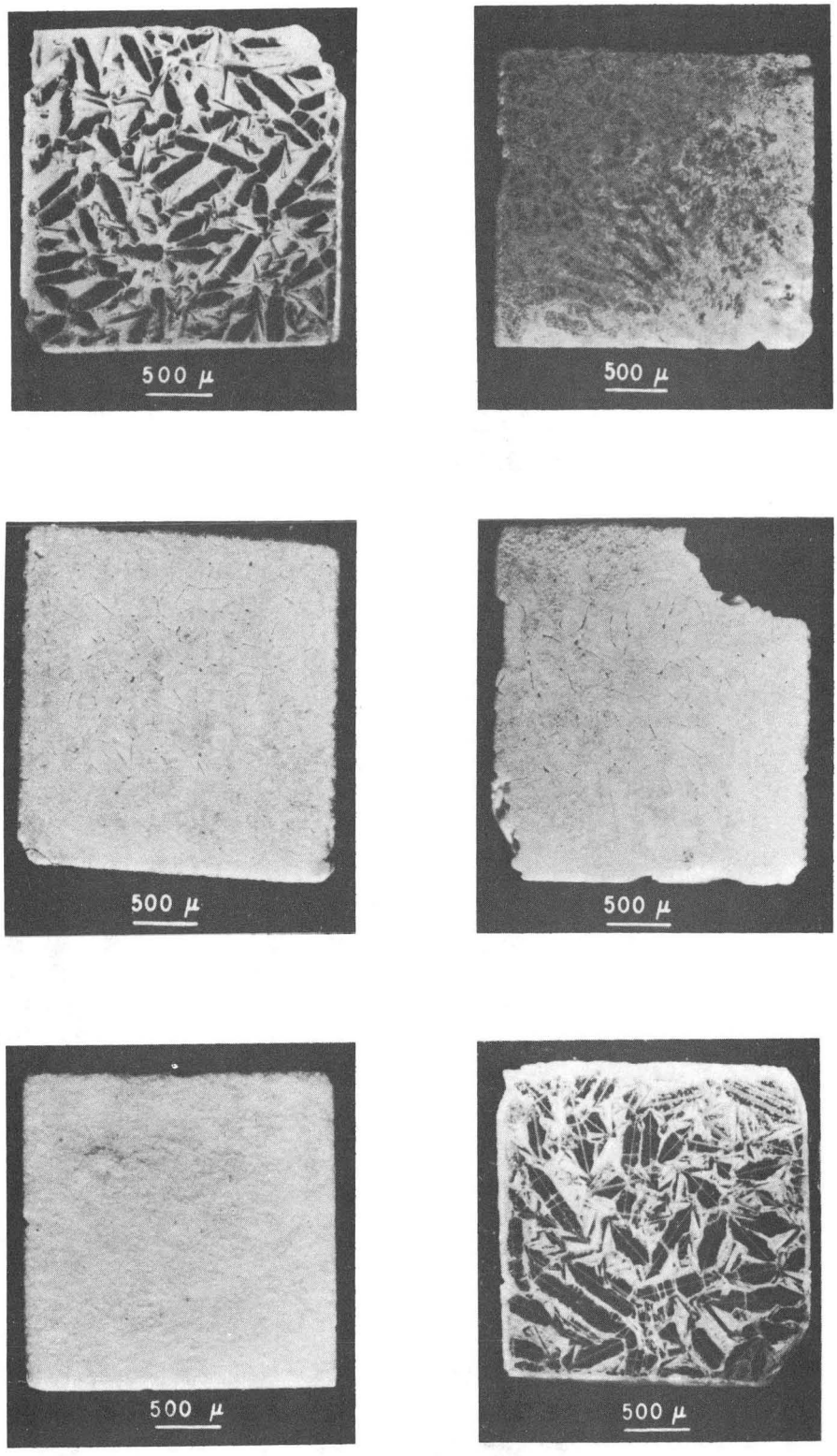

XBB707-3067

Fig. 40. Microstructure of mullite pieces fired in helium at 1750°C for (a) unfired, (b) 30 min., (c) 1 hr., (d) 3 hr., (e) 12 hr., (f) in air at 1650°C for 11 days.

$$Al_6Si_2O_{13(s)} \rightarrow 3Al_2O_{3(s)} + 2SiO_{2(g)} \qquad (A1)$$

$$SiO_{2(g)} \rightarrow 1/2\ O_{2(g)} + SiO_{(g)} \qquad (A2)$$

The decomposition is written as a two-step process, since no free silica was found in the mullite. In other words, since all the available silica is in mullite in the composition of SiO_2, it is thought that the silica leaves the mullite as a gas phase. The SiO_2 gas subsequently decomposes to SiO and O_2 to a degree governed by the SiO_2/SiO ratio or ultimately by the partial pressure of oxygen in the system.

To understand this reaction more fully, the reaction expressed by Eq. (A2) can be considered to be in equilibrium. The equation for the standard free energy of formation of SiO_2 gas can thus be expressed as*

$$\Delta F^\circ = - RT \ln \frac{P_{SiO_2}}{P_{SiO}\ P_{O_2}^{1/2}} \quad . \qquad (24)$$

The values of ΔF° were calculated from known data for this reaction[54] and used to determine $\log [P_{SiO_2}/P_{SiO}\ (P_{O_2})^{1/2}]$ for the temperature range of 1800°-2100°K as given in table XI.

---

*The author is indebted to Mr. Ilhan Aksay for suggestions concerning the thermodynamic procedures and help in the various calculations and interpretation of the results.

Table XI. ΔF° and log $P_{SiO_2}/P_{SiO} \cdot P_{O_2}^{1/2}$ values for temperature range 1800°-2100°K, determined from Eq. (A2)

Temperature (°K)	ΔF° (Kcal/mole)	Log $P_{SiO_2}/P_{SiO}P_{O_2}$
1800	- 16.988	2.07
1900	- 15.148	1.75
2000	- 13.317	1.46
2100	- 11.489	1.20

Analogous calculations were performed for the reaction described by Eq. (A1) to determine the equilibrium pressure of SiO_2. These results are given for several temperatures in Table XII and plotted against absolute temperature in Fig. (41).

Table XII. ΔF° and P_{SiO_2} values for temperature range 1800°-2100°K, determined from Eq. (A1)

Temperature (°K)	ΔF° (Kcal/mole)	P_{SiO_2} (atm)
1800	133.749	7.09×10^{-9}
1900	126.219	5.12×10^{-8}
2000	118.706	3.09×10^{-7}
2100	111.206	1.58×10^{-6}

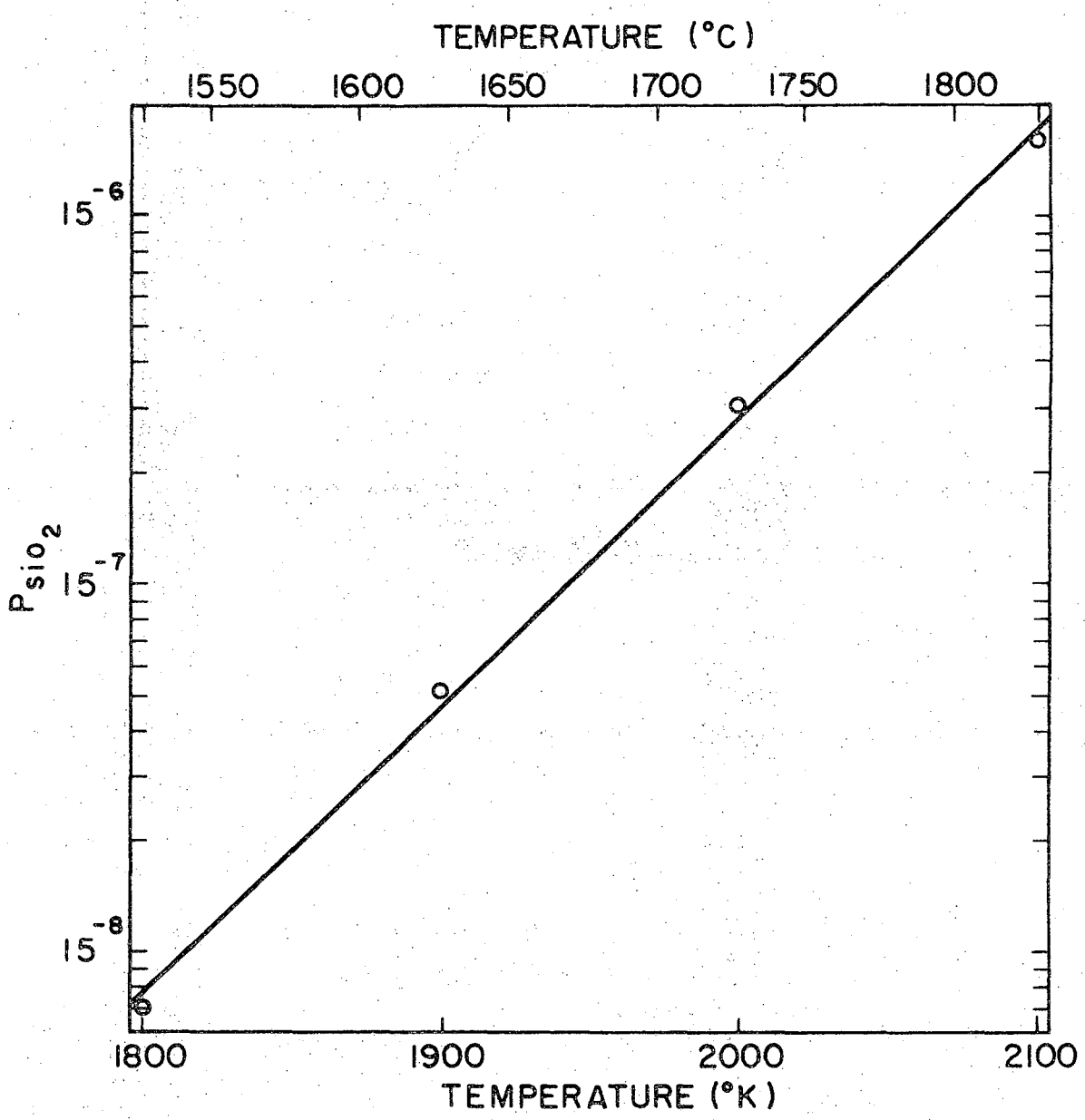

XBL 707-1529

Fig. 41. Curve of P_{SiO_2} versus absolute temperature determined for reaction (A1).

In air, the partial pressure of oxygen equals 0.20 atm; however, under nonoxidizing conditions similar to those of this research, P_{O_2} is determined by the equilibrium partial pressure of oxygen in contact with heated tantalum. The reaction between tantalum and oxygen may be written as

$$2Ta + 5/2\ O_2 \rightarrow Ta_2O_5 \quad . \qquad (A3)$$

Again, the standard free energy of formation of Ta_2O_5 may be calculated from known data,[55] and the equilibrium partial pressure of oxygen determined from these results for the temperatures of the diffusion runs, as shown in Table XIII and Fig. (42).

Table XIII. ΔF° and log P_{O_2} values for temperature range 1923°-2073°K determined for the reaction described in Eq. (A3).

Temperature (°K)	ΔF° (Kcal/mole)	Log P_{O_2} (atm)
1923	297.890	- 13.59
1973	293.318	- 13.04
2023	288.769	- 12.52
2073	284.226	- 12.03

Knowing the range of oxygen pressures for both air and helium conditions of this research, plots of log (P_{SiO_2}/P_{SiO}) versus log P_{O_2} can be constructed for each temperature by assuming values of P_{O_2} which fall within this range (Fig. 43). From these graphs, values of log (P_{SiO_2}/P_{SiO})

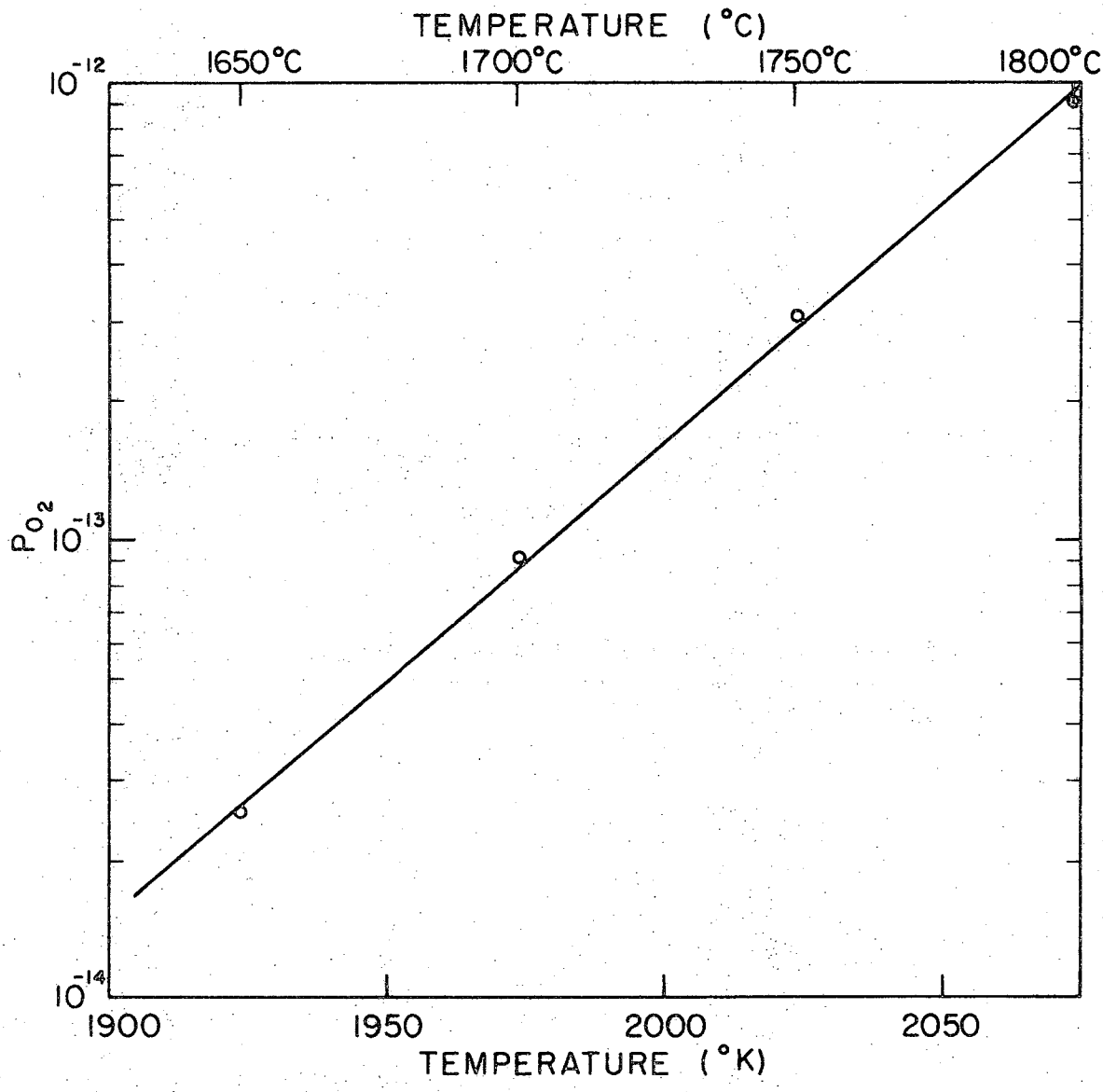

Fig. 42. Curve of equilibrium partial pressure of oxygen versus temperature of the diffusion runs for reaction (A3).

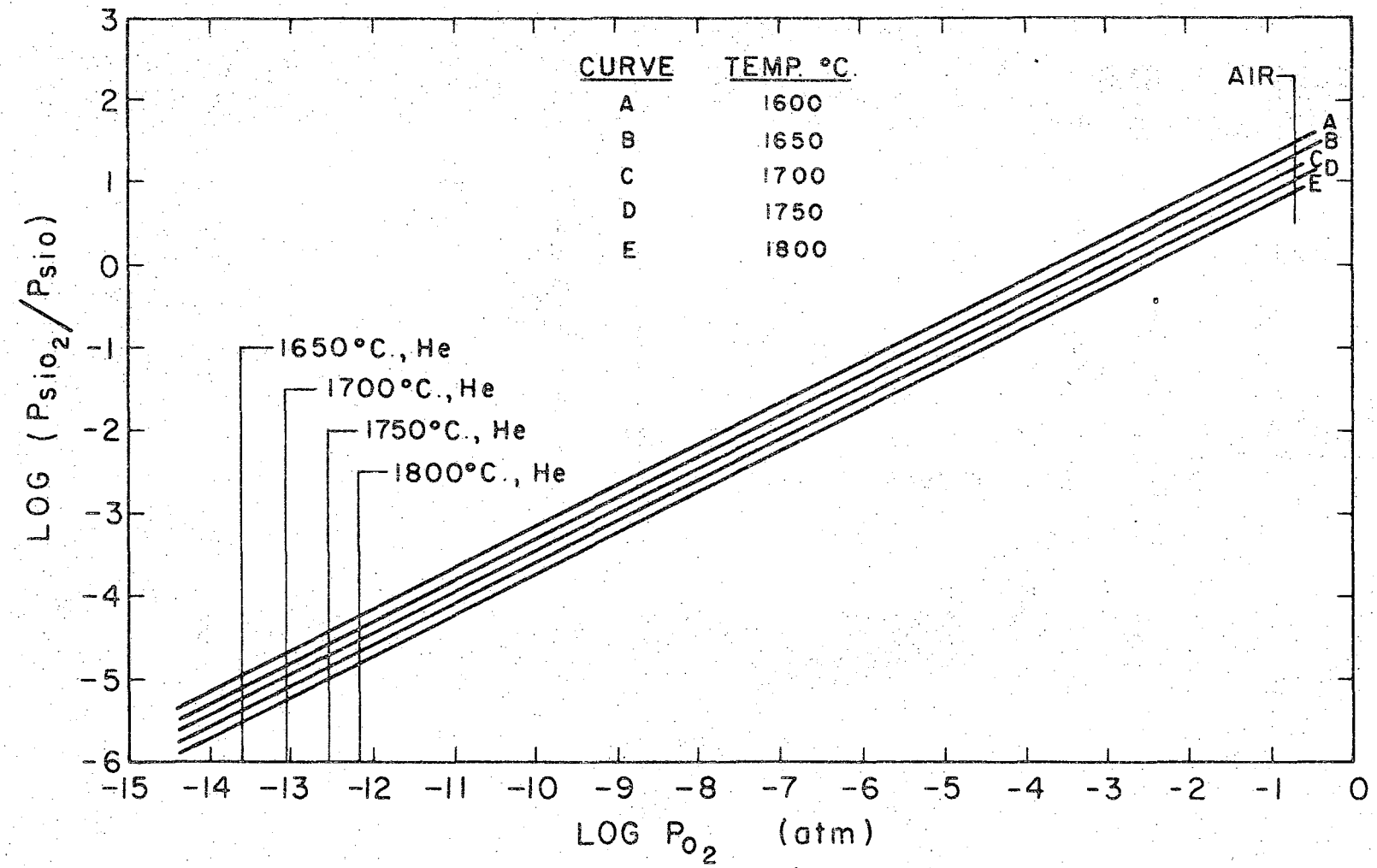

XBL 707-1528

Fig. 43. Curve of log (P_{SiO_2}/P_{SiO}) versus log P_{O_2} (atm).

can be determined at the different temperatures for the known oxygen pressures in the helium and air atmospheres as shown by the isobaric lines drawn in Fig. 43. A tabulation of these values is given in Table XIV below.

Table XIV. P_{SiO_2}/P_{SiO} values for temperature range 1650°-1800°C determined at constant oxygen pressures from Fig. 43.

Temperature (°C)	P_{SiO_2}/P_{SiO} (He)	P_{SiO_2}/P_{SiO} (air)
1650	$10^{-5.12}$	$10^{1.30}$
1700	$10^{-4.97}$	$10^{1.25}$
1750	$10^{-4.88}$	$10^{1.00}$
1800	$10^{-4.82}$	$10^{0.90}$

These ratios of P_{SiO_2}/P_{SiO} given above must be maintained to insure equilibrium in air and He for the given temperature. For example, Fig. 41 shows that at 1650°C, one must establish and maintain a pressure of 7.2×10^{-8} atm of SiO_2 to prevent further dissociation of mullite. For an air atmosphere, one finds the ratio of P_{SiO_2}/P_{SiO} to be $10^{1.30}$. Thus the corresponding SiO pressure would be $7.2 \times 10^{-9.30}$ atm. Since there is little decomposition of mullite heated in air at this temperature, the pressure of SiO_2 in the system must come relatively near the equilibrium value. As the SiO_2 is vaporized from the mullite, it will, in turn, decompose to SiO and O_2 to a degree determined by the surrounding oxygen pressure. As seen above, for an air atmosphere the P_{SiO_2}/P_{SiO} ratio is approximately 10, i.e., the partial pressure of SiO_2 is only ten times

that of SiO. This value has also been reported by Porter, et al.,[56] for the equilibrium constant for the decomposition of SiO_2 gas. Hence, under oxidizing conditions, the dioxide becomes the major species with the monoxide also a primary constituent.

In the case of a tantalum heated helium atmosphere at 1650°C, the equilibrium partial pressure for SiO_2 is still 7.2×10^{-8} atm; however, the P_{SiO_2}/P_{SiO} ratio is now $10^{-5.12}$. Thus the corresponding SiO equilibrium partial pressure increases tremendously to a value of $7.2 \times 10^{-2.88}$ atm.

This means that with the low oxygen pressure and thus the high equilibrium partial pressure of the monoxide, the SiO_2 gas readily dissociates to SiO and free oxygen. The equilibrium partial pressure of SiO_2 gas is never reached and the mullite continues to decompose. The amount of SiO present is approximately 10^5 times larger than that of gaseous SiO_2.

REFERENCES

1. E. L. Williams, Diffusion in Glass: I, Glass Industry 43, 113-17 (1962); II, ibid, 186-91; III, ibid, 257-61; IV, ibid, 394-95, 402; Appendix, ibid, 437-40 (1962).

2. R. H. Doremus, Diffusion in Noncrystalline Silicates, in Modern Aspects of the Vitreous State, Vol II, edited by J. D. Mackenzie (Butterworth & Co. Ltd., London, 1962).

3. A. E. Paladino and W. D. Kingery, Aluminum Ion Diffusion in Aluminum Oxide, J. of Chem. Phys. 37, 957 (1962).

4. Y. Oishi and W. D. Kingery, Self-Diffusion of Oxygen in Single Crystal and Polycrystalline Aluminum Oxide, J. of Chem. Phys. 33, 480 (1960).

5. E. W. Sucov, Diffusion of Oxygen in Vitreous Silica, J. Am. Ceram. Soc. 46, 14 (1963).

6. W. L. DeKeyser, Reactions at the Point of Contact Between SiO_2 and Al_2O_3, in Science of Ceramics, Vol. II, edited by G. H. Stewart (Academic Press, New York, 1963).

7. W. G. Staley, Jr., Mechanism of Reaction Between Corundum and Cristobalite in the Subsolidus Region of the System Al_2O_3-SiO_2 (Ph.Dl Thesis), Pennsylvania State University, Dec. 1968. (A portion of this thesis appeared as a paper entitled "Development of Non-Crystalline Material in Subsolidus Reactions Between Silica and Alumina" in J. Am. Ceram. Soc. 52, 616 (1969).

8. D. Y. F. Lai and R. J. Borg, Some Observations on the Effect of Surface Roughness upon Diffusion, UCRL 70289, Feb. 1967.

9. G. A. Parks, The Composition and Reaction Capability of Oxide Surfaces, Research in Mineral Proc., Prog. Rept. 65-1, Stanford Univ. June 1965.

10. M. Robinson, J. A. Pask, D. W. Fuerstenau, Surface Charge of Alumina and Magnesia in Aqueous Media, J. Am. Ceram. Soc. 47, 516 (1964).

11. R. Theisen, Quantative Electron Microprobe Analysis (Springer-Verlag, New York, 1965).

12. J. Z. Frazier, et al., Computer Programs EMX and EMX2 for Electron Microprobe Data Processing, Scripps Institute of Oceanography, University of California, La Jolla, California.

13. M. L. Huggins and K. Sun, Calculation of Density and Optical Constants of a Glass from Its Composition in Weight Percentage, J. Am. Ceram. Soc. 26, 4 (1943).

14. J. F. MacDowell and G. H. Beall, Immiscibility and Crystallization in Al_2O_3-SiO_2 Glasses, J. Am. Ceram. Soc. 52, 17 (1969).

15. S. Fugge, Encyclopedia of Physics, Volume XXX, (Springer-Verlag, Berlin, 1957).

16. E. W. White, H. A. McKinstry, and T. F. Bates, Crystal Chemical Studies by X-ray Fluorescence, in Proc. Conf. Appl. X-ray Anal., 7th Denver, 1958, Vol. 7, p. 231.

17. G. W. Brindley and H. A. McKinstry, The Kaolinite-Mullite Reaction Series: IV, The Coordination of Aluminum, J. Am. Ceram. Soc. 44, 506 (1961).

18. D. E. Day and G. E. Rindone, Properties of Soda Aluminosilicate Glasses: III, Coordination of Aluminum Ions, J. Am. Ceram. Soc. 45, 579 (1962).

19. C. G. Dodd and G. L. Glen, Chemical Bonding Studies of Silicates and Oxides by X-ray K-Emission Spectroscopy 39, 5377 (1968).

20. W. Jost, Diffusion in Solids, Liquids, and Gases (Academic Press, New York, 1931).

21. J. Crank, Mathematics of Diffusion, (Clarendon Press, Oxford, 1956).

22. P. G. Shewmon, Diffusion in Solids (McGraw-Hill, New York, 1963).

23. C. Wagner, Unpublished results in reference 20, p. 70.

24. L. Boltzmann, Zur Integration der Diffusions Gleichung bei Variabeln Diffusions Coefficienten, Ann. Physik. 53, 959 (1894).

25. C. Matano, The Relation Between the Diffusion Coefficients and Concentrations of Solid Metals (the Nickel-Copper System), Jap. J. Phys. 8, 109 (1933).

26. J. M. Short and R. Roy, Use of Interdiffusion to Determine Crystalline Solubility in Alkali Halide Systems, J. Am. Ceram. Soc. 47, 149 (1954).

27. N. Swindells, The Determination of Equilibrium Diagrams by Electron Probe Microanalysis, J. Inst. Metals 90, 167 (1962).

28. S. Aramaki and R. Roy, Revised Phase Diagram for the System Al_2O_3-SiO_2, J. Am. Ceram. Soc. 45, 299 (1962).

29. N. A. Toropov and F. Y. Galakhov, New Data for the System Al_2O_3-SiO_2, Doklady Akad. Nauk S.S.S.R. 78, 299 (1951).

30. J. Grofesik and F. Tamas, Mullite, Its Structure, Formation, and Significance (Publishing House of the Hungarian Academy of Science, Budapest, 1961).

31. F. M. Wahl, R. E. Grim, and R. B. Graf, Phase Transformations in Silica-Alumina Mixtures as Examined by Continuous X-ray Diffraction, Am. Mineralogist 46, 1064 (1961).

32. J. F. Schairer and N. L. Bowen, Melting Relations in the Systems Na_2O-Al_2O_3-SiO_2 and K_2O-Al_2O_3-SiO_2, Am. J. Sci. 245, 193 (1947).

33. L. S. Castleman and L. L. Seigle, Formation of Intermetallic Layers in Diffusion Couples, J. Met. 9, 1173 (1957).

34. G. V. Kidson, Some Aspects of the Growth of Diffusion Layers in Binary Systems, J. Nucl. Mat. 3, 21 (1961).

35. L. S. Castleman, An Analytical Approach to the Diffusion Bonding Problem, Nucl. Sci. and Eng. 4, 209 (1958).

36. A. Neuhaus and W. Richartz, "Uber die Einkristallzuchtung und Zustandsverhaltniss Von Müllit" (Growing of Single Crystals of Mullite and Their Constitution), Ber. Deut. Keram. Ges 35, 108 (1958).

37. J. O. Isard, Electrical Conduction in the Aluminosilicate Glasses, J. Soc. Glass Tech. 43, 113T (1959).

38. D. E. Day and G. E. Rindone, Properties of Soda Aluminosilicate Glasses: I, Refractive Index, Density, Molar Refractivity, and Infrared Absorption Spectra, J. Am. Ceram. Soc. 45, 489 (1962); II, Internal Friction, ibid., 496.

39. E. D. Lacy, Aluminum in Glasses and Melts, Phys. and Chem. of Glasses 4, 234 (1963).

40. R. W. Heckman, J. A. Ringlien, and E. L. Williams, Sodium Diffusion and Electrical Conductivity in Sodium-Aluminosilicate and Sodium-Calcium-Aluminosilicate Glasses, ibid. 8, 145 (1967).

41. R. Terai, Self-diffusion of Sodium Ions and Electrical Conductivity in Sodium Aluminosilicate Glasses, ibid. 10, 146 (1969).

42. R. Rossin, J. Bersan, and G. Urbain, Viscosity of Fused Silica and Slags Belonging to the SiO_2-Al_2O_3 system, Comptes Rendus 258, 562 (1964).

43. W. A. Weyl, Coloured Glasses (Society of Glass Technology, Sheffield, 1951).

44. M. F. Nazarenko, The Mechanism of the Mineralizing Effect of Additives on the Process of Mullitization, Vestnik Akad. Nauk. Kazakh. S.S.S.R. 15, 78 (1959).

45. W. D. Kingery and J. A. Lecron, Oxygen Mobility in Two Silicate Glasses, Phys. and Chem. Glasses 1, 87 (1960).

46. T. B. King and P. J. Koros, Diffusion in Liquid Silicates, in Kinetics of High Temperature Processes, edited by W. D. Kingery (John Wiley and Sons and Technological Press, New York, 1959).

47. H. Towers and J. Chipman, Diffusion of Calcium and Silicon in a Lime-Alumina-Silica Slag, Trans. AIME 203, 769 (1955).

48. L. Reed and L. R. Barrett, The Slagging of Refractories: II, The Kinetics of Corrosion, Trans. Brit. Ceram. Soc. 63, 509 (1964).

49. J. O'M. Bockris, J. A. Kitchener, S. Ignatowicz, and J. W. Tomlinson, Electric Conductance in Liquid Silicates, Trans. Faraday Soc. 48, 75 (1952).

50. B. N. Samaddar, W. D. Kingery, A. R. Cooper, Jr., Dissolution in Ceramic Systems: II, Dissolution of Alumina, Mullite, Anorthite and Silica in a Calcium-Aluminum-Silicate Slag, J. Am. Ceram. Soc. 47, 249 (1964).

51. C. O. Hulse and J. A. Pask, Analysis of Deformation of a Fireclay Refractory, J. Am. Ceram. Soc. 49, 312 (1966).

52. V. Skola, Thermal Decomposition of the Mullite Phase, Keram. Rundschau 45, 188 (1937).

53. R. E. Wright and H. I. Wolff, Refractory Problems in Production of Hydrogen by Pyrolsis of Natural Gas, J. Am. Ceram. Soc. 31, 31 (1948).

54. JANAF Interim Thermochemical Tables, Midland, Michigan (1960).

55. O. Kubaschewski, E. Li. Evans, C. B. Alcock, Metallurgical Thermochemistry, 4th ed. (Pergamon Press, New York, 1967).

56. R. F. Porter, W. A. Chupka, and M. G. Inghram, Mass-Spectrometric Study of Gaseous Species in the Si-SiO_2 System, J. Chem. Phys. 23, 1347 (1955).

TECHNICAL INFORMATION DIVISION
LAWRENCE RADIATION LABORATORY
UNIVERSITY OF CALIFORNIA
BERKELEY, CALIFORNIA 94720